INFORMATION TO USERS

This manuscript has been reproduced from the microfilm master. UMI films the text directly from the original or copy submitted. Thus, some thesis and dissertation copies are in typewriter face, while others may be from any type of computer printer.

The quality of this reproduction is dependent upon the quality of the copy submitted. Broken or indistinct print, colored or poor quality illustrations and photographs, print bleedthrough, substandard margins, and improper alignment can adversely affect reproduction.

In the unlikely event that the author did not send UMI a complete manuscript and there are missing pages, these will be noted. Also, if unauthorized copyright material had to be removed, a note will indicate the deletion.

Oversize materials (e.g., maps, drawings, charts) are reproduced by sectioning the original, beginning at the upper left-hand corner and continuing from left to right in equal sections with small overlaps. Each original is also photographed in one exposure and is included in reduced form at the back of the book.

Photographs included in the original manuscript have been reproduced xerographically in this copy. Higher quality 6" x 9" black and white photographic prints are available for any photographs or illustrations appearing in this copy for an additional charge. Contact UMI directly to order.

UMI

A Bell & Howell Information Company
300 North Zeeb Road, Ann Arbor MI 48106-1346 USA
313/761-4700 800/521-0600

Downloaded from SHAREOK. Persistent Handle URL: https://hdl.handle.net/11244/5628

NOTE TO USERS

The original manuscript received by UMI contains broken or light print. All efforts were made to acquire the highest quality manuscript from the author or school. Microfilmed as received.

This reproduction is the best copy available

UMI

THE UNIVERSITY OF OKLAHOMA

GRADUATE COLLEGE

ISB AND IVBS SEMIACTIVE CONTROL OF DYNAMIC RESPONSE FOR HIGHWAY BRIDGES

A Dissertation

SUBMITTED TO GRADUATE FACULTY

in partial fulfillment of the requirements for the

degree of

DOCTOR OF PHILOSOPHY

By

GUANGJUN LI

Norman, Oklahoma

1998

UMI Number: 9828781

UMI Microform 9828781
Copyright 1998, by UMI Company. All rights reserved.

This microform edition is protected against unauthorized
copying under Title 17, United States Code.

UMI
300 North Zeeb Road
Ann Arbor, MI 48103

© Copyright by Guangjun Li 1998

All Right Reserved.

ISB AND IVBS SEMIACTIVE CONTROL OF DYNAMIC RESPONSE FOR HIGHWAY BRIDGES

A DISSERTATION

APPROVED FOR THE SCHOOL OF AEROSPACE AND MECHANICAL ENGINEERING

BY



Dr. William Neff Patten
(Committee Chairman)

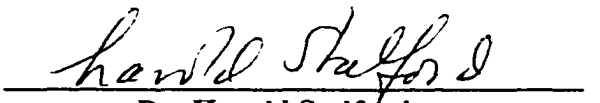

Dr. Harold Stalford

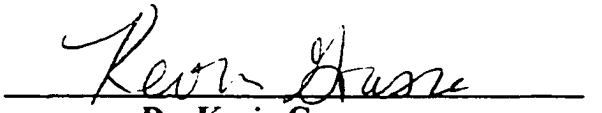

Dr. Kevin Grasse



Dr. Feng C. Lai

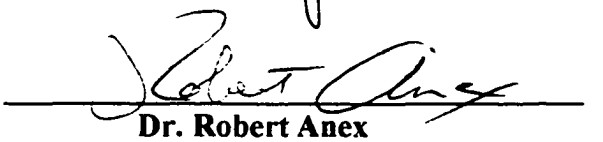

Dr. Robert Anex

Acknowledgments

The author would like to express his very sincere appreciation and gratefulness to Dr. William Neff Patten for his great ideas, guidance, patience and support through all the phase of this work, and for serving as the chairman of his advisory committee.

The author also wishes to express his thanks to Dr. Kevin Grasse, Dr. Harold Stalford, Dr. Robert Anex and Dr. Feng C. Lai for serving as committee members and for their sincere evaluation of this dissertation.

The author wishes to express his especially thanks to Dr. Sun, Dr. He and Dr. Song for their contribution and cooperation during this research work.

The author has had a great time in the Center for Structural Control at University of Oklahoma. It has been great experience for him to study and do research at this famous University. A lot of thanks go to his colleagues: to Jeff, Rongrong, Ginna, Wei and Wen.

The author would also like to thank Susan, Shilo, Annie and Eugene for their editing and contributions.

For their encouragement, sacrifice and patience, the author wishes to thank his girlfriend Hua Yang, his parents and sisters.

TABLE OF CONTENTS

ACKNOWLEDGEMENTS iii
TABLE OF CONTENTS v
NOMENCLATURE viii
LIST OF FIGURES xi
LIST OF TABLES xvi
ABSTRACT xvii

1. INTRODUCTION AND LITERATURE REVIEW 1
1.1 Introduction 1
1.2 Reviews of Literature 4
1.3 Summary of Dissertation 9

2. MODAL UPDATING AND CORRECTION OF THE WALNUT CREEK BRIDGE 12
2.1 Introduction 12
2.2 Reviews of Previous CSC Team Work 13
2.2.1 The Walnut Creek Bridge 13
2.2.2 Full Bridge FE Model 14
2.2.3 The ROM of Walnut Creek Bridge 15
2.2.4 Modal Testing of Walnut Creek Bridge 17
2.3 Modal Modification of the Bridge 18
2.3.1 Stiffness Matrix Modification by Crawl Test Data 19
2.3.2 Mass Matrix Correction 22
2.4 Implementation 24
2.4.1 Stiffness Matrix Correction by Crawl Tests 24
2.4.2 Modal Test and FE Modal Correction Results 26
Conclusions 28

3. DYNAMICS OF BRIDGE/VEHICLE INTERACTION: MODAL COUPLING AND ITS EFFECT ON IMPACT FACTORS 34
3.1 Introduction and Background 34
3.2 Modeling of the Bridge and Vehicle System 35

3.2.1 Bridge and Vehicle Modeling 37
3.2.2 Motion Equations of Coupled Bridge/Vehicle System 41
3.3 Simulation Method 45
3.4 Simulation and Test Results 49
3.4.1 Effect of Vehicle Speed 49
3.4.2 Effect of Vehicle Fundamental Frequencies 52
3.4.3 Effect of Vehicle Weight 54
3.4.4 Comparison of Simulation and Test Results 56
3.4.5 Impact Factor of Dynamic Loads 59
3.5 Summary 61

4. INTELLIGENT STIFFENER FOR MEDIUM SPAN BRIDGES (ISB) 63
4.1 Introduction 63
4.2 Bridge and Actuator Modeling 64
4.2.1 Motion Equations of the Bridge 64
4.2.2 Dynamic Equations of Hydraulic Actuator 66
4.2.3 Coupled Model 69
4.3 Semiactive Controller Design 71
4.3.1 Basic Semiactive Control Law 71
4.3.2 Modified Control Law 74
4.4 Numerical Simulation 76
4.4.1 A Simple Span Girder 78
4.4.2 A Continuous Girder 83
4.5 Safe Life Predictions 91
4.6 Conclusions and Recommendations 92

5. ROBUST STABILITY ANALYSIS OF A BRIDGE/VEHICLE COUPLED CONTROL SYSTEM 95
5.1 Introduction and Literature Review 95
5.2 Problem Statement 98
5.3 Robust Lyapunov Semiactive Controller Design 99
5.4 Perturbation of Eigenvalues and Eigenvectors 105
5.5 Simulation Results and Discussions 107
5.5.1 Robustness Semiactive Controller Design 109

5.5.2 Robustness of Closed Loop Performance 110
5.6 Conclusions and Discussions 111

6. ISB ON THE WALNUT CREEK BRIDGE: DESIGN AND TESTING 112
6.1 Introduction 112
6.2 Design of an ISB System 112
6.3 Installation 118
6.4 Control System Set Up 119
6.4.1 System Configuration 119
6.4.2 Sensors and Location 121
6.4.3 Field Test of the Controller 122
6.4.4 Simulation Results of Controlled Response 124
6.4.5 Experimental C Program for Control Field Tests 126
6.5 Semiactive Control Field Test Results 128
6.5.1 ISB Passive Performance Test 129
6.5.2 Controlled Response 131
6.6 Safe Life Predictions 137
6.7 Summary 139

7. INTELLIGENT VEHICLE/BRIDGE CONTROL SYSTEM 141
7.1 Introduction and Background 141
7.2 Prototype Design of an IVBS 142
7.2.1 Modeling of the Bridge and Vehicle 143
7.2.2 Control Design of the IVBS 144
7.3 Simulation Results 148
7.3.1 Bridge-Friendly Truck Suspension (BFTS) 149
7.3.2 The Performance of the IVBS 153
7.4 Conclusion and recommendation 154

8. CONCLUSIONS AND RECOMMENDATIONS 156
8.1 Conclusions 156
8.2 Recommendations 159

REFERENCES 161
APPENDIX I 169
APPENDIX II 170
APPENDIX III 171
APPENDIX IV 172
APPENDIX V 181

NOMENCLATURE

A	The plant matrix	
A_p	Effective piston area of actuator	m^2
A_v	Hydraulic valves orifice area	m^2
A_{vmax}	Maximum hydraulic orifice area	m^2
A_{vmin}	Minimum hydraulic orifice area	m^2
B	Control input matrix	
c_1	Damping coefficient of truck suspension	N*S/m
C_b	Bridge damping matrix	
C_d	Service valve fraction coefficient	
d(t)	Truck disturbance	N
D	Truck disturbance input matrix	N
E	Young's module	N/m^2
$g(\Delta P)$	Nonlinear damping function	
h	Height of moment arms	m
I	Inertia of the bridge girder	m^4
k2	Stiffness of suspension	N/m
K_b	Bridge stiffness matrix	
K_t	Truck stiffness matrix	
K_{tire}	Stiffness of tire N/M	
L	Span length of the bridge	m
m1	Mass of tire	kg

m2	Mass of truck body	kg
M_b	Bridge mass matrix	
M_t	Truck mass matrix	
Q	Weighing matrix of control	
v	Truck traveling speed	m/s
V	Lyapunov function	
w	Static weight of truck	kg
W	Width of moment arms	m
$\hat{x}$	State vector of bridge	m
$\hat{y}$	Generalized coordinate of bridge	
$\hat{z}$	Displacement vector of bridge	
$\dot{z}_0$	Initial velocity of truck suspension	m/s
α	Coefficient of hydraulic damper	N/m^2
β	Coefficient of hydraulic damper	N/m^2
Δ	Beam element length	m
ΔP	Differential pressure of hydraulic damper	N/m^2
v	Semiactive control force vector	
ρ	Density of hydraulic damper	N/m^3

LIST OF FIGURES

Figure 1.1 The I-35 Walnut Creek Bridge with ISB system attached 9
Figure 2.1 Full FE model of Walnut Creek Bridge 15
Figure 2.2 225 reduced order model of Walnut Creek Bridge 16
Figure 2.3 Test bridge model 17
Figure 2.4 Measured deflection of Walnut Creek Bridge 25
Figure 2.5 Simulated deflection before stiffness matrix correction 25
Figure 2.6 Simulated deflection after stiffness matrix correction 25
Figure 2.7 Comparison of transfer functions; modal test vs. ROM 27
Figure 3.1 A Bridge coupled with a quarter vehicle 36
Figure 3.2 Superstructure of the Oklahoma I-35 Walnut Creek Bridge 37
Figure 3.3 Reduced order FE mesh of Walnut-Creek Bridge 38
Figure 3.4 A quarter vehicle model 39
Figure 3.5 Dynamic model of a four axle tractor-trailer (RT) 40
Figure 3.6 Load distribution and wheel space of RT 40
Figure 3.7 Road profile at the entrance of Walnut Creek Bridge 46
Figure 3.8 First 4 modes of the bridge/vehicle system 47
Figure 3.9 Flow chart of computer program 48
Figure 3.10 Simulation of typical dynamic response of
the second span of the Bridge 49
Figure 3.11 Effect of vehicle speed on peak deflection
(a) Girder #1, (b) Girder #3, (c) Girder #5 51
Figure 3.12 Effect of vehicle speed on initial displacement
of vehicle suspension 52
Figure 3.13 Effect of vehicle natural frequency on peak deflection
(a) Girder #1, (b) Girder #3, (c) Girder #5 53

Figure 3.14 Effect of vehicle weight on peak deflection
(a) Girder #1, (b) Girder #3, (c) Girder #5 55
Figure 3.15 Frequency response of Walnut Creek Bridge and RT chassis 56
Figure 3.16 Bridge response of open loop, simulation vs. test results,
Rock Truck in right lane, a) Girder #1; b) Girder #3; c) Girder #5 58
Figure 3. 17 Transfer function obtained from the modal test at the middle of
span #1; Mode numbers are shown circled 59
Figure 3.18 Impact factor of test results, crawl test vs. dynamic test,
Rock Truck in right lane, a) Girder #1; b) Girder #3; c) Girder #5 60
Figure 4.1 Simple span bridge with moving vehicle 64
Figure 4.2 Kinematic layout of the simple span 65
Figure 4.3 Hydraulic actuator 67
Figure 4.4 Block diagram of the Lyapunov bistate controller 74
Figure 4.5 Introduction of the deadband 75
Figure 4.6 A quarter car model 77
Figure 4.7 The single span bridge FE model 79
Figure 4.8 Simulation of controlled vs. uncontrolled deflection
at Center of Simple Span, W= 12.2m, h=2.54m, L=30.48m 80
Figure 4.9 Moment time history at the Center of the simple span (bottom flange),
L=30.48m, W=12.2m, h=2.54m 80
Figure 4.10 Maximum moment distribution at each point along the girder
L=30.48m, W=12.2m, h=2.54m 81
Figure 4.11 Variation of maximum moment at each point along the girder
vs. h, L=30.48m, W=18.28m 82
Figure 4.12 Variation of maximum moment at each point along the girder
vs. W, L=30.48m, h=1.5m 82
Figure 4.13 Four span bridge with traveling vehicle 83
Figure 4.14 The four span bridge FE model 84

Figure 4.15 Deflection time history at midpoint of third span,
a. without ISB, b. with ISB (h=2.54m, W=12.2m) 85
Figure 4.16 Moment time history at the center of the third Span
(h=2.54m, W=12.2m) 85
Figure 4.17 Maximum moment time history at each point along the third span
(h=2.54m, W=12.2m) 86
Figure 4.18 Moment distribution when vehicle is at the center of the third span
(h=2.54m, W=12.2m) 86
Figure 4.19 Actuator stroke vs. control time history 87
Figure 4.20 Actuator force vs. control time history 88
Figure 4.21 Actuator force vs. relative velocity of piston 88
Figure 4.22 Time history of the kinematic and potential energy
in the bridge/vehicle system 89
Figure 4.23 Time history of $\dot{E}$ 89
Figure 4. 24 Moment distribution when the truck is at center of third span
(h=2.54m, W=12.2m) 90
Figure 5.1 The system energy flow chart 99
Figure 5.2 The first five mode natural frequencies time history
of the bridge/vehicle System 108
Figure 5.3 Eigenvalues changing with time in complex plane 108
Figure 5.4 Eigenvalues of $A^T(t)Q + QA(t)$ changing with time 109
Figure 5.5 $-\lambda_{min}$ of $A^T(t)Q + QA(t)$ changing with time 109
Figure 5.6 Control performance under different vehicle Eigenvalues 110
Figure 5.7 Control performance under different vehicle speed 110
Figure 6.1 FFT of accelerometer at girder #5 (span #4), in response
to the passage by a typical tractor-trailer traveling at 105km/h 113
Figure 6.2 Test strain pot signal; girder #3, midpoint of span #3 114

Figure 6.3 The final ISB hardware layout at the I-35 Walnut Creek Bridge 117
Figure 6.4 Design drawing of moment arm and hydraulic actuator 117
Figure 6.5 Kinematic assembly of an ISB actuator 120
Figure 6.6 Control system layout; MC=micro controller 121
Figure 6.7 12 Strain gauges and two string pots Location 122
Figure 6.8 ISB control logic 123
Figure 6.9 Simulated closed loop vs. open loop control performance,
with the RT traveling in the right lane at 105 km/h 125
Figure 6.10 Simulated ISB control force output of the center actuator 126
Figure 6.11 Flow chart of experimental control program 127
Figure 6.12 Four test trucks wheel load distribution and axle spacing 128
Figure 6.13 Stress response (1) when ISB operated as passive dampers (2)
before the ISB system was installed, (at span #3 bottom flange 130
Figure 6.14 Closed loop vs. open loop control performance, RT traveling
in the right lane at 105 km/h; a) girder #1, b) girder #3, c) girder #5 132
Figure 6.15 Closed loop vs. open loop control performance, HT traveling
in the right lane at 105 km/h; a) girder #1, b) girder #3, c) girder #5 133
Figure 6.16 Closed loop vs. open loop control performance, WT traveling
in the right lane at 105 km/h; a) girder #1, b) girder #3, c) girder #5 134
Figure 6.17 Closed loop vs. open loop control performance, DT traveling
in the right lane at 105 km/h; a) girder #1, b) girder #3, c) girder #5 135
Figure 6.18 Actuator #1 performance, RT runs over the right lane passive vs.
closed Loop, a) differential pressure, b) LVDT, c) control command 136
Figure 6.19 Comparison of control performance in frequency domain,
RT in the right lane; passive vs. closed loop control 137
Figure 6.20 Maximum stress measured at span #3 mid-section,
RT traveling in the right lane 138
Figure 7.1 The IVBS system Layout 143

Figure 7.2 Block diagram of global bridge /truck control 148
Figure 7.3 Dynamic response comparison at third span midpoint xiv 150
Figure 7.4 Moment time history at third span midpoint 150
Figure 7.5 Tire force comparison a. without control,
b. local truck chassis control, ... 151
Figure 7.6 The control logic of local truck chassis control 151
Figure 7.7 Deflection comparison between the local truck chassis
control and the global truck chassis control 152
Figure 7.8 Tire force comparison between the local truck chassis
control and the global truck chassis control 152
Figure 7.9 Actuator force comparison 153
Figure 7.10 Performance contrast a) without ISB, b) with ISB 154
Figure 7.11 Performance contrast a) without ISB, b) with IVBS 154

LIST OF TABLES

Table 2.1 Modal Frequencies 27
Table 2.2 Comparison Between Test Model and Modified FE Model 29
Table 2.3 One Section Comparison of First 9 Model Shapes 32
Table 6.1 Structural Parts for the ISB Assemblies 118
Table 6.2 Remain Safe Life of Walnut Creek Bridge from the Rock Test 138

ABSTRACT

The purpose of this dissertation is to develop a systematic methodology for semiactive control systems to suppress the stress of highway bridges induced by heavy truck traffic. A program of research has been conducted by the Center for Structural Control (CSC) at the University of Oklahoma to extend the service life of highway bridges, by retrofitting them with computer-controlled hydraulic semiactive actuators. The dissertation explores two major complimentary research areas: (1) the intelligent stiffener for bridges (ISB) and (2) the second is intelligent vehicle/bridge system (IVBS).

The dissertation describes a full scale design and implementation of an ISB system on a 122 m (400') four-spans highway bridge. An Lyapunov analysis is used to synthesize a control law. Simulations, using variable bridge models, demonstrate the advantages of the new technology. The results indicate that the ISB system can reduce maximum deflections by as much as 60%; thus, adding many years of additional service life to the bridge. The expected performance of the ISB control system is also demonstrated by a full scale control experiment on an in-service interstate bridge. The results appear promising. Finally, the analytical studies on an alternative bridge vibration suppression system (IVBS) are presented.

The application of reduced order model and modal modification techniques for dynamic analysis and semiactive control design is initiated in this dissertation. A 225

DOF bridge model which has been experimentally verified is used in the dynamic analysis and control system design. The bridge/vehicle coupled nonautonomous model is presented to investigate the dynamic characteristics of highway bridges in Chapter Three. The effect of several different parameters which significantly affect bridge dynamics are studied via simulation. Experimental data are provided to verify the simulation results. A practical control model which combined bridge dynamic equations and the coupled nonlinear hydraulic actuator dynamics is derived in Chapter Four. An Lyapunov bistate controller design for the ISB system is presented. The expected performance of the system is examined via simulation (deflection and moment). The trade-off design which is used to select a final configuration of the ISB assembly is also addressed in this chapter. The sufficient stability criterion for the nonautonomous bridge/vehicle perturbed system is next presented and the robustness of proposed Lyapunov semiactive controller is investigated in Chapter Five. Experimental results are presented in Chapter Six, and a description of the control hardware is also included. Chapter Seven provides the results of a preliminary effort to explore the feasibility of an intelligent vehicle/bridge system (IVBS). The performance of the IVBS is examined via numerical simulation. The last chapter (eight) offers conclusions and makes recommendations for future work.

CHAPTER ONE

INTRODUCTION AND LITERATURE REVIEW

1.1 Introduction

The bridge infrastructures in the United States are in need of significant remediation. A recent FHWA report (1995) on the condition of bridges paints a dismal picture. As much as 25% of bridge infrastructures are rated as structurally deficient. Many highway bridges built in the last 50 years are now reaching the end of their design life. The options to bridge owners are few. They can replace these bridges, but the estimated cost to repair and replace structurally deficient bridges is approximately 8 billion dollars per year for 25 years. Even if the funds were available, any rush to replace existing bridges would likely cause a serious disruption of commerce.

A program of research conducted at the Center for Structural Control (CSC) at the University of Oklahoma has produced a working concept for an intelligent bridge/vehicle control system. The concept envisions two major complimentary components. First, muscle-like appendages are retrofitted to the bridge superstructure. The system is referred to as an intelligent stiffener for bridges (ISB). These controllable muscles are operated to provide judicious amounts of stiffness and damping to the bridge superstructure in order to reduce peak stresses that accompany the passage of heavy trucks. Second, is the means of adjusting the suspension damping of a truck as

it passes over the bridge. This component of the system is referred to as an intelligent vehicle/bridge system (IVBS). Bridges characteristically exhibit one or more modal responses that very often correspond to the chassis vibration resonance of the trucks passing over that bridge. The object of the truck chassis suspension adjustment would be to make sure that the truck does not vibrate at the bridge resonant frequencies. The ISB and IVBS do not require line power or hydraulic pumps and use a battery to power a system of sensors and a small microcontroller that makes timely decisions about when to add stiffness and damping. If trucks are not present, the ISB system relaxes. Since every bridge is unique, the adjustable suspension on the truck must talk to the ISB control system in order to achieve the desired performance. If both ISB and IVBS are shown to be feasible, then they can increase the load capacity of a bridge, while extending its service life. The technology of ISB has been analyzed and field-tested on an in-service interstate bridge and the results are promising. The IVBS, on other hand, is still in the prototype design stage.

Control strategies based on semiactive devices appear to combine the best features of both passive and active control systems and offer the best likelihood for near-term acceptance by practitioners in the United States. According to a presently accepted definition (Housner et al., 1996 [1]), a semiactive control device is one that cannot inject mechanical energy into the controlled structure. On the other hand, the properties of the semiactive actuator can be controlled to reduce the responses of the system by storing and dissipating energy. In contrast to active control devices,

semiactive control systems do not have the potential to destablize (in the bounded input/bounded output sense) the control system.

The focus of this dissertation is to present the systematic methodology for the design of an ISB and IVBS to mitigate the vibration induced by heavy traffic loads on highway bridges. Included in the design process is the establishment of a model of the bridge and the identification of a reduced order model of the bridge for control design purposes. Next, the design, installation and field test of the ISB system is presented. Finally, the development of a prototype IVBS is introduced and the performance of the control strategy is verified by simulations.

The subjects that have been examined during the course of this project are very complex. The dissertation first introduces the modal reduction and modification technique of the structure, which can be used to build a suitable control model. Next, a time-varying bridge/vehicle coupled model is proposed to accurately estimate dynamic behavior of bridge/vehicle interaction characteristics. The development of a Lyapunov based feedback control law is then presented. A design trade-off analysis that was used to select a final configuration of the components used in the assembly is discussed in some detail. Next, a discussion of the robustness of the semiactive design against model uncertainties is presented. The experimental results of the performance of the ISB system are displayed. Finally, the IVBS modeling and design strategies are introduced and simulation results are given to indicate the performance of the proposed IVBS for future field test.

1.2 Review of Literature

The subject of bridge vibration control has received much attention in the archival literature over the last century, and has been recognized as one of the most challenging and significant areas of research in the field of structural engineering in recent years (Housner et al., 1996 [1]; Kobori, 1996 [2]). Through the application of a control system, a bridge can potentially reduce peak stresses by modifying its stiffness and damping during dynamic loading in order to add many additional years of service life to the bridge.

Bridge/Vehicle Interaction: A review of the bridge vibration literature dates back to the work of Jeffcott [3] in 1929. In his studies, the vehicle was modelled as a travelling static load. In 1995, Biggs, Suer and Louw [4] discussed the action of a signal mass/spring system to a simple supported bridge. In their study, only the fundamental frequency of the bridge was considered. A more recent and comprehensive dynamic analysis of the bridge/truck interaction problem was presented by Veletsos and Huang (1970) [5] in which he incorporated the effects of several significant variables including bridge damping, road roughness, and suspension friction. Timoshenko, et al. [6] developed an analytical solution for the motion of a beam/bridge subjected to a moving pulsating load. The stability of a vehicle on a multispan simply supported guideway was investigated by Chung and Genin [7]. The stability analysis of the system was examined in terms of the parameters and frequency content of the disturbing load. Schilling in 1984 [8] proposed an analytical method to develop design values for the number of

stress cycles caused by the passage of a truck across various span types of steel highway bridges. More recently, work done by Hwang and Nowak in 1991 [9] , Kou and Dewolf in 1997 [10] focused on the influence that span length, gross vehicle weight, vehicle speed and axle spacing have on bridge vibration. Veletsos and Huang [11] presented a numerical method developed for the computation of dynamic response of highway bridges. Tiedman, et. al [12] presented some analytical and experimental work on bridge dynamics. They concluded that the finite element method (FEM) should be involved to predict stresses, moments and deflection of a two-span continuous test bridge subjected to axle loading on single and multiple lanes. Yang and Fonder [13], Senthilvasan, et al. in 1991 [14] presented some iterative solution methods to simulate the dynamic response of the bridge/vehicle system. In their studies, the bridge/vehicle system was divided into two subsystems at the interface; their compatibility at the interface is achieved by an iterative procedure with under-relaxation or with Aitken acceleration.

Structural Control: The number of works that explore the possibility of applying an automatically adjustable (active, semiactive) actuator to achieve bridge motion mitigation are few. Yao [15] was among the first investigators to suggest the concept of active control of civil engineering structures in 1972. Yang and Giannopoulos [16] [17] explored the possibility of applying an active control system to regulate the tension forces in the supporting cables of a cable-stayed bridge, and they developed a rational basis for the stiffness control of the cables. More recently, Achkire and Preumont

(1996) [18] described a laboratory-scale experiment to demonstrate the effectiveness of using active control to regulate the tension in a loaded bridge tendon. The paper suggests that the control should be designed to detune or decouple the resonance vibration of the bridge structure from the resonance vibrations of the cables.

The potential benefit gained by applying active control to long-span truss bridges was recently examined by Adeli and Saleh (1997) [19]. Using simulations, they examined the question of how many actuators were needed and where they should be positioned on the structure. They concluded that sensors and actuators should be co-located, and they developed a parallel processing algorithm, which was used on a supercomputer to determine the response of various bridges to wind, vehicular and seismic inputs.

The typical highway bridge is constructed with girders and a composite deck. The active control of bending vibrations of a girder was considered by Abdel-Rohman, et al. (1980) [20]. They suggested a bridge attachment of a moment-producing actuator assembly to reduce maximum deflections. They simulated the response of the girder to a moving load and determined that the suggested mechanism could provide a significant reduction of the vibration amplitude. The authors noted that the moving load creates a nonautonomous control problem. They proposed a feedback control, where the feedback gain is obtained at each time step by solving a time-varying Riccatti Equation. While the approach is elegant, there is little possibility of accomplishing the computational effort required in real time. A more recent paper by Lin and Trethewey

(1993) [21] re-examines the girder vibration problem essentially using the same kinematic (active) control assembly used in the preceding reference. They also utilized an optimal tracking control, where they assumed a knowledge of the magnitude and velocity of the moving load. Their control also required the solution of a time-varying Riccatti Equation. Shelley, et al. (1993) [22] reported recent results of an experimental effort to demonstrate the effectiveness of active control when applied to a decommissioned 76.2m (250') steel through-truss highway bridge in Ohio. They employed a electro-hydraulic reaction mass to dampen plane vibrations of the structure. The device was capable of 0.81m (32") of stroke and used a 68 kg (150 lb) reaction mass, making it possible to develop a force output of 454 kg (1000 lb). The authors employed an adaptive modal filter approach to synthesize a modal controller. The experiment produced an order of magnitude reduction of the fundamental mode of the bridge. Wu and Soong (1996) [23] proposed a modified bang-bang control law for response control of civil engineering structures. The control law is based on the optimal bang-bang control principle.

Das and Dey (1992) [24] discussed the potential of applying tuned mass dampers in reducing random response of simple bridges. They suggested that optimum tuning parameters could be found to achieve reduction of random response.

Semiactive Control: The application of semiactive (SA) control to structures remains an uncharted area of research. A semiactive control system requires no line power or pumps, as opposed to a fully-active control system. Semiactive control systems are

especially attractive because they can provide performance nearly equivalent to that afforded by a fully-active system (if designed properly). A major advantage of SA control is that the possibility of an unstable operation, which is a serious consideration when using active control, can be effectively eliminated. The issue of the stability of a semiactive system was recently discussed by Leitmam (1994) [25]. Karnopp [26] is credited with having first introduced the concept of semiactive control, and his work was aimed at the development of suspension systems for automobiles. A number of authors have done paper studies on the effectiveness of a SA system when applied to structures under seismic loads (Soong, 1993 [27]; Spencer, 1995 [28]; Symans and Constantinuou, 1994 [29]). These works show that semiactive control can be used to mitigate the vibration of a dynamic system. Feng and Shinozuk [30] outlined a strategy for the implementation of continuously variable semiactive dampers and suggested that a bang-bang controller based on optimization may provide a control logic for semiactive dampers. Hrovat, Barak and Rabins [31] utilized a clipped optimal design to examine the efficiency of the semiactive structural control design. Their simulation studies showed the proposed system was superior to the conventional design. Hatada and Smith in 1997 [32] proposed a nonlinear controller which utilized variable damping devices for civil structure under seismic loads. The control algorithm was formulated based on Lyapunov's stability theorem and performance index. In 1994, Patten et al. [33][34] first proposed to apply a semiactive control system to mitigate the bending vibrations of a bridge, employing a clipped optimal control policy. Based on that

approach, an "on-off" control algorithm was proposed. A field experiment, using a small bridge, confirmed the effectiveness of the proposed system. More recently, the ISB system was developed and field-tested on an in-service interstate bridge (The Walnut Creek Bridge, see Figure 1.1) in the US [35][36][37]. The experimental results indicated that the ISB system can add decades of service life to an existing bridge. The work done by the CSC team is considered as the first successful demonstration of the ISB technology on a full scale semiactive control system for highway bridges in the US.



Figure 1.1 The I-35 Walnut Creek Bridge with ISB System Attached

1.3 Summary of Dissertation

In Chapter Two, the modal reduction and modal test techniques are reviewed. A quasi-static modal modification method is developed and applied to correct the analytical model of the Walnut Creek Bridge. An accurate and reduced order model is

developed for bridge/vehicle dynamic analysis and control design purpose.

The dynamic response of highway bridges is studied in Chapter Three, The bridge/vehicle coupled model is presented to investigate the dynamic characteristics of highway bridges. The time-varying general dynamic bridge/vehicle model is formulated. The effect of several different parameters which significantly affect bridge dynamic characteristics are studied via numerical simulation. Experimental data is provided to verify the simulation results.

The mathematical model of an ISB system is derived in Chapter Four. A practical control model which combines bridge dynamic equations and a coupled nonlinear hydraulic actuator dynamics is first derived. Then, an Lyapunov-based feedback controller design for the ISB system is presented. The expected performance of the system is examined via simulation. The chapter addresses various design trade-off issues that must be treated prior to selecting a final configuration of the components used in the assembly. The chapter also provides evidence that confirms that the ISB system is more desirable than the alternative: a dumb (fixed) stiffener.

The sufficient stability criterion for the bridge/vehicle perturbed model is next presented and the robustness of proposed Lyapunov semiactive controller is investigated in Chapter Five. Lyapunov's second method and a matrix inequality method are used to achieve this purpose. Internal stability of the bridge/vehicle coupled system is then verified by a modified frozen-coefficient method. Finally, the simulation results are carried out to verify the above criterion.

Chapter Six offers particulars of the design, and an in depth description of the Walnut Creek Bridge, on which the ISB was mounted and field tested. A description of the control hardware is also included. The proposed Lyapunov semiactive control law is applied to the control field test. Finally, experimental results of the performance of the ISB system are presented.

Chapter Seven provides the results of a preliminary effort to explore the feasibility of an intelligent vehicle/bridge system (IVBS). The general bridge/vehicle/actuators model is derived, and a general IVBS controller is then described based on the analysis of Chapter Four. Two control schemes including a smart truck suspension and a combined vehicle/bridge control scheme are proposed. The performance of the IVBS system is examined via numerical simulations. The last chapter (eight) offers conclusions on the research and makes recommendations on future work.

CHAPTER TWO

MODAL UPDATING AND CORRECTION OF THE WALNUT CREEK BRIDGE

2.1 Introduction

The focus of this chapter is the development of a bridge finite element model (FEM) for dynamic system analysis and semiactive control system design. The previous modal analysis and modal tests conducted by CSC team are reviewed first. Based on these works, a practical modal correction method is proposed and applied to modal updating of the Walnut Creek Bridge, which considers both analytical stiffness and mass matrices which need to be corrected. The procedure includes modifying the stiffness matrix by the quasi-static (Crawl) test data, followed by a correction of the mass matrix by the modal test data.

A principal goal of the modal updating is to determine an analytical model of a bridge which can be verified by an actual test and applied in numerical simulations. The synthesis of a control system requires a model that can simulate the dynamic response of the bridge under moving vehicle loads. The use of a full bridge FEM is impractical for dynamic and control simulations. A modal reduction procedure is needed to produce a reduced order model (ROM) of the bridge that has a minimal

number of generalized coordinates. The reduced order model must also be able to accommodate control inputs, control outputs, and the effects caused by a moving vehicle disturbance. The ROM must mimic at a minimum eigenvalues and eigenshapes of the principle modes of the full bridge model. Before a ROM can be developed, the full model itself must be tuned to provide a high fidelity match with the actual bridge. Consequently, a modal modification procedure must be employed to adjust the analytical ROM model to provide the desired degree of correspondence between simulated and measured data. The error between the analytical model and the test data can be corrected by modal modification techniques. The information obtained by modal test are then used to tune the ROM model. The corrected ROM model is then used to establish a working concept of the bridge.

2.2 Review of Previous CSC Team Work

In order to develop a semiactive control system capable of mitigating the vibration of a highway bridge, the CSC first took steps to develop a rigorous FE bridge model. The experimental modal analysis and related modal reduction are part of the principal investigations for a semiactive control system design.

2.2.1 The Walnut Creek Bridge

The Walnut Creek Bridge (see Figure 1.1) is located on Interstate 35 in the vicinity of Purcell, Oklahoma. I-35 originates at the Mexican border (at Loredo, TX) and terminates at the Canadian border (at Duluth, MN). The study was restricted to the

bridge carrying the two north-bound lanes of traffic. The bridge was originally constructed in 1971 and was opened to traffic in 1972. Periodic traffic counts indicate that the northbound bridge carries just over 18,000 vehicles per day, including approximately 3,100 heavy trucks. The largest number of trucks are typically 5-axle, 4.3 m (42') wheel base tractor-trailers.

The superstructure consists of five 122 m (400') long continuous girders weighing 196.5 kg/m (125 lbs./ft.), with a 1.37 m (54") deep web and 0.36 m (14") wide flanges. The concrete deck is 0.19 m (7 1/2 ") thick reinforced concrete. The bridge, which has a skew of 45°, is supported by three intermediate concrete piers at 30.5 m (100') intervals. The superstructure includes diaphragms constructed of lightweight elements located at 20' intervals along the span.

2.2.2 Full Bridge FE Model

The full FE model of the Walnut Creek Bridge is shown in Figure 2.1. The I-DEAS® FEM software (marketed by Structural Dynamics Research Corporation) was selected for the analysis because of its excellent modal analysis capabilities. In addition, I-DEAS® has a state-of-the-art graphics support module, which makes it especially easy to illustrate the system. The full bridge model consists of 410 thin shell elements, 620 beam elements (including "I", "T", and angle), 316 rigid bars and 74 solid elements. The base model includes 811 nodes, requiring 4,800 coupled equations of motion. Boundary conditions at the support piers are included in a routine manner.

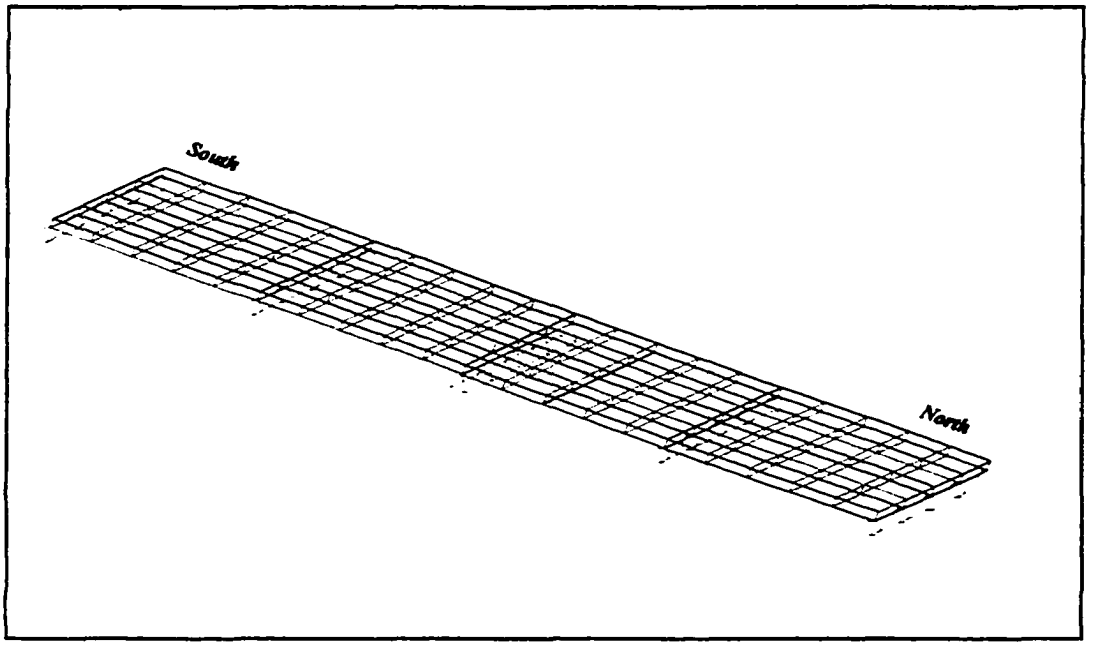

Figure 2.1 Full FE model of the Walnut Creek Bridge

The initial full bridge modal analysis shows that the fundamental natural frequency is about 2.5 Hz. The natural frequencies of the first 10 bridge modes are less than 5.0 Hz and the first 20 bridge modes are less than 10 Hz. The most mode shapes of the first 10 modes are bending, torsion or bending with torsion. These results provide a working base for the Walnut Creek Bridge modal analysis and modal correction effort.

2.2.3 The ROM of Walnut Creek Bridge

The work presented in the above section provides a highly accurate full FEM of

the bridge. Next, a reduced order model of the bridge is constructed that consists of 120 beam elements (see Figure 2.2). The model is assembled, and the boundary conditions are accounted for, then a 225 DOF's system results. The ROM is configured to allow control inputs (moments) along the girder. This model also provides a setting format for the design of a suitable controller, but the course mesh provides a poor estimate of the stresses that result from the simulation. When accurate estimates of the local stress are needed, then additional nodes must be added in the vicinity of the location where the stress is being examined. That approach is presented in conjunction with the work described in Chapter Four.

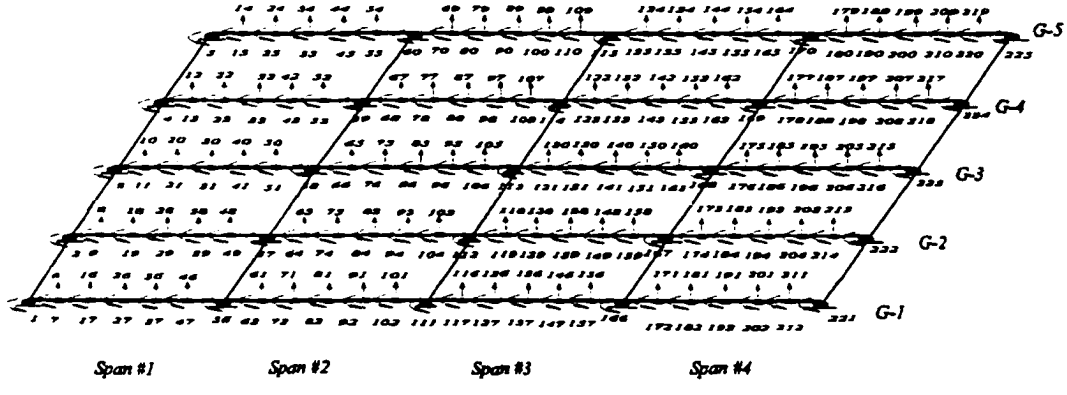

Figure 2.2 225 Reduced order model of the Walnut Creek Bridge

The methods used to achieve the reduced order model for the bridge have been presented in an earlier publication (Pang [38], Patten, et. al [39], Sun, et. al [40]) and

will not be repeated.

2.2.4 Modal Test of the Walnut Creek Bridge

The modal testing, full FEM and the ROM (225 DOF) development of the Walnut Creek Bridge were previously reported by Pang [38] and Sun et al. [40]. The following offers an overview of that original work.

In order to validate the ROM bridge analytical model, modal testing of the bridge was conducted by installing a densely packed system of sensors that were utilized to record the response of the bridge to ambient (truck) loads as well as modal excitation loads. A system of 36 piezo-resistive accelerometers were installed at the location which was shown in Figure 2.3. All accelerometers were rated for a 2g output. Also installed were strain gauges to measure the strain at 12 different critical locations. The original modal test data was then used to adjust the parameters in the ROM (225 DOF), which was provided from the full FE bridge model by Guyan or IRS modal reduction method (Pang [38], Guyan [41], O' Callahan [42], Pilkey, et. al [43]).

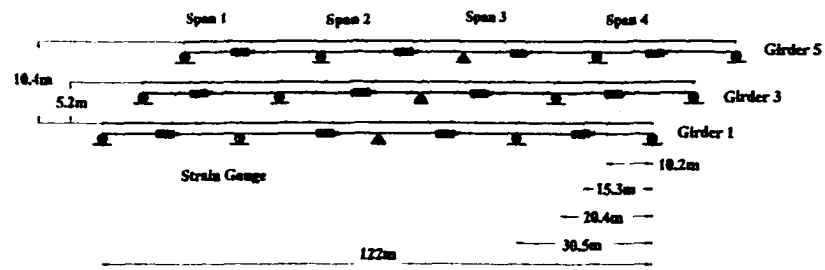

Figure 2.3 Test Bridge Model

The modal tests and ambient load tests made it clear that modes beyond 10 Hz contain only a small percentage of the system's response energy. The correspondence between the modal frequencies was acceptable, while the error in modal shapes was large in the originally reported results.

2.3 Modal Modification of the Bridge

As a general observation, there are three different ways to correct the analytical model: (1) assume the mass matrix is correct and tune the stiffness matrix to match the test data; (2) assume stiffness matrix is correct and tune the mass matrix to achieve the same propose, and (3) turn both mass and stiffness matrices to correct the model. Based on previous observations, there are three sets of data: an analytical mass matrix, an analytical stiffness matrix, and an incomplete set of measured modes. It is apparent that, if any one of these sets is assumed to be exact, it is possible to correct the other two to achieve a modified model which is completely compatible with measured data (Berman [44], Wei [45] and Collins [46]). In previous modal correcting task of CSC team, Pang [38] applied a matrix perturbation method to improve the ROM analytical model via the testing frequencies and modal shapes for the Walnut Creek Bridge.

Test data and analytical modeling accuracies are both important considerations in modal modification procedures. The observations indicate that the modal deflection (mode shape) measurement is not accuracy as frequency measurement (Sanayei) [47] especially in large complex structures. Use of the mode shape data in the correction of

the measurement data is problematic due to errors in the modal test data. The methods used to correct the original property values should conform to those observed in the test. The modification procedure depends on test data and modeling accuracies, and it also depends on problem type and the experience of the analyst. On the other hand, a static parameter estimation scheme can provide high accuracy . It is reasonable to apply both static and modal test data in FEM updating and model correction procedures. For example, Hajela and Soeiro (1990) [48] compared the use of incomplete static and dynamic data. Their results showed that static displacements were lower in computational cost and provided greater insight into damage assessment of bridges than dynamic measurements.

The work here describes an alternative approach to modal model updating that relies initially on the quasi static (crawl) test response of the bridge. The crawl test is accomplished by traveling the bridge at a slow speed (e.g., 5 km/h). The strain gauge outputs can be used to establish a corrected stiffness characteristic for the bridge.

2.3.1 Stiffness Matrix Modification by Crawl Test Data

The equations of motion of the bridge have the following form:

$$M_b \{\ddot{x}\} + C_b \{\dot{x}\} + K_b \{x\} = \{F(t)\} \tag{2.1}$$

where

M_b = Analytical mass matrix;

C_b = Analytical proportional damping matrix;

K_b = Analytical stiffness matrix;

{F(t)} = exogenous force vector;

The stiffness matrix modification method is based on measured deformation induced by crawl test such as a very slow moving truck on the bridge. When traveling at a low speed, the dynamic loads induced by truck suspension can be neglected, and $\ddot{x}$, $\dot{x}$ can be neglected as well. As a result, Equation (2.1) can be rewritten as:

$$K_b \{x(t_i)\} = \{F(t_i)\} \qquad (i = 1,2,3,.....s) \tag{2.2}$$

s is number of time steps; if {x(t)} and {F(t)} can be measured or estimated at each time step, then K_b can be estimated uniquely by Equation (2.2). Rewrite K_b as: $K_b = [K_1, K_2, ..., K_n]^T$. Every column K_m can be rewritten as the following equations

$$\begin{aligned}
&K_{m1}X_1(t_1) + K_{m2}X_2(t_1) + ... + K_{mn}X_n(t_1) = f_m(t_1)\\
&K_{m1}X_1(t_2) + K_{m2}X_2(t_2) + ... + K_{mn}X_n(t_2) = f_m(t_2)\\
&K_{m1}X_1(t_3) + K_{m2}X_2(t_3) + ... + K_{mn}X_n(t_3) = f_m(t_3)\\
&\vdots \qquad\qquad \vdots \qquad\qquad \vdots \qquad\qquad \vdots\\
&K_{m1}X_1(t_s) + K_{m2}X_2(t_s) + ... + K_{mn}X_n(t_s) = f_m(t_s)
\end{aligned} \tag{2.3}$$

Equation (2.3) is a over-determined set of equations (s > n) which can be rewritten as:

$$[x]_{sxn} \; K_m{}^T_{nx1} = f_{m_{sx1}} \qquad (s > n) \tag{2.4}$$

[x] are test deflection data matrix, and f_m is exteral force vector which acting on m th DOF. K_m is m th row of real stiffness matrix, which needs to be corrected. Next, define

an error vector, ε, in the following way:

$$\{\epsilon\} = [x]\, K_m^T - f_m \tag{2.5}$$

A quadratic function is then posed:

$$J = \{\epsilon\}^T \{\epsilon\} \tag{2.6}$$

Combining Equation (2.5) and Equation (2.6) and minimizing J with respect to $\{K_m\}$ yields:

$$\frac{\partial J}{\partial K_m} = 2\,[x]^T [x]\, K_m^T - 2[x]^T f_m = 0 \tag{2.7}$$

Solving for $\{K_m\}$ yields:

$$\{K_m\} = ([x]^T [x])^{-1} [x]^T f_m \tag{2.8}$$

which is a least squares solution [49]. The stiffness matrix K_b is:

$$K_b = \sum_{m=1}^{n} ([x]^T [x])^{-1} [x]^T f_m \tag{2.9}$$

Equation (2.9) was used to determine a bridge stiffness matrix.

2.3.2 Mass Matrix Correction

Suppose M_0, K_0 are (n x n) analytical mass and stiffness matrices, Φ_0 is an (n x n) analytical modal shape matrix, $\Lambda_0 = [\lambda_r]$ where λ_r is r th natural frequency of analytical model and M, Λ, Φ, correspond to the corrected analytical system parameters. The stiffness matrix has already been adjusted using the above quasi-static test results. The next step is to adjust the mass matrix to match the modal test data. The difference between the analytical model and the experiential data can be expressed by Δ ; the following equations are utilized:

$$\begin{aligned} \Lambda &= \Lambda_0 + \Delta\Lambda \\ K &= K_0 \\ \Phi &= \Phi_0 + \Delta\Phi \\ M &= M_0 + \Delta M \end{aligned} \tag{2.10}$$

where, in each case, the expression on the left is the adjusted values at each iteration of the matrix/vector quantity. Both the experimental model and the analytical model must satisfy orthogonality.

$$\begin{aligned} \Phi^T K \Phi &= [K_d] \\ \Phi^T M \Phi &= [M_d] \end{aligned} \tag{2.11}$$

The model will satisfy the characteristic equation

$$\boldsymbol{K}\Phi = \boldsymbol{M}\Phi\Lambda \tag{2.12}$$

Combining Equation (2.12) with the above, then:

$$\Lambda = (\Phi^T \boldsymbol{M}\ \Phi)^{-1}\ \Phi^T \boldsymbol{K}\ \Phi \tag{2.13}$$

Combining Equation (2.13) with Equation (2.11), then:

$$\Lambda = (\Phi^T (\boldsymbol{M} - \Delta \boldsymbol{M})\ \Phi)^{-1}\ \Phi^T \boldsymbol{K}\ \Phi \tag{2.14}$$

or combining Equation (2.13) with Equation (2.14), then:

$$\Delta \boldsymbol{M} = \Phi^{-T} (\Phi^T \boldsymbol{K}\ \Phi\ (\Lambda^{-1} - \Lambda_0^{-1}))\ \Phi^{-1} \tag{2.15}$$

Equation (2.15) provides a means of adjusting the analytical mass matrix to fit the test data, and the eigenvalues of the test data are used to accomplish that goal.

2.4 Implementation

The method developed in the preceding section of this chapter was applied to the modal updating of the ROM of the Walnut Creek Bridge.

2.4.1 Stiffness Matrix Correction by Quasi-Static Tests

A series of crawl tests were conducted on the Walnut Creek Bridge using four types of trucks. Each of the vehicles traveled across the bridge at 5 km/hr which established the crawl response of the bridge. The test is referred to as a quasi-static test.

The experimental deflections are compared with the simulation results before modifying the analytical stiffness matrix. Figure 2.4 depicts the output of the four strain gauges fixed to the bottom of the flange of the central girder (G-3) at the midpoint of each span, when the 24.5 ton (54 klb) Dump Truck is traveled across the bridge. Figure 2.5 depicts the simulated output of the four strain gauges at the bottom of the flange of the central (G-3) girder at the midpoint of each span. The differences of the response at the center of the girder (G-3) bottom flange in each span are obvious.

After the analytical stiffness matrix was corrected using the crawl test with the proposed quasi static modification method outlined above, the simulation was repeated and plotted in Figure 2.6. The results show that the modified stiffness matrix matches the test data to within 5%. The second and third span realize 30% more deflection because the bottom flange of the girder in those spans is thinner (3/4" vs. 1/4") than the flange on the girders in the first and fourth spans.

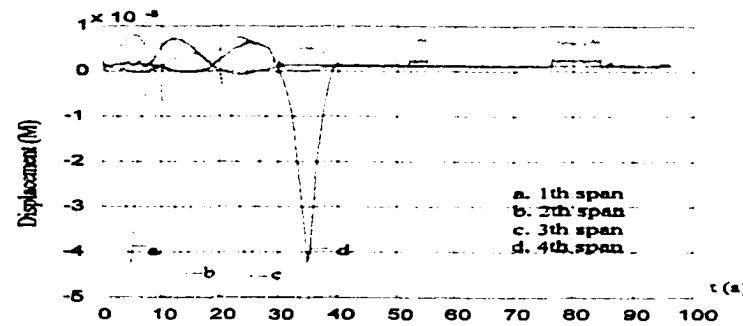

Figure 2.4 Measured Deflection of Walnut Creek Bridge

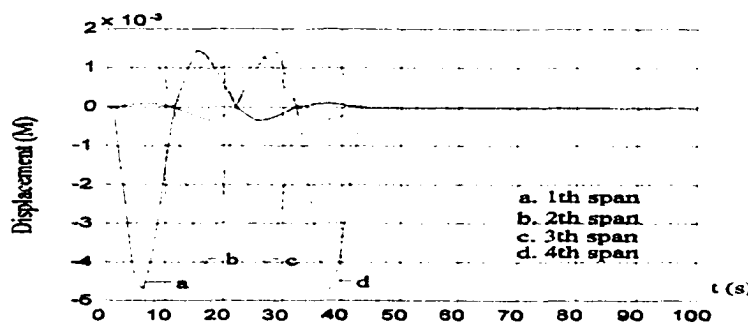

Figure 2.5 Simulated Deflection before Stiffness Matrix Correction

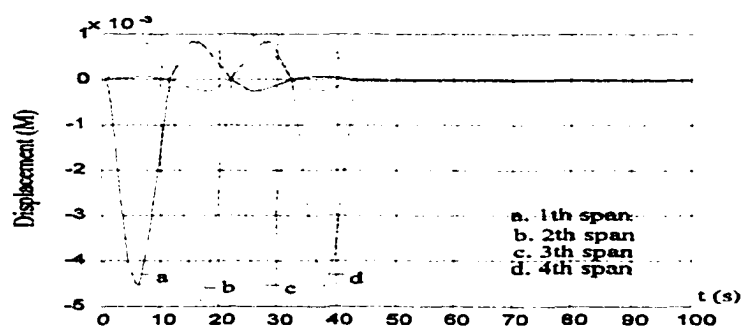

Figure 2.6 Simulated Deflection after Stiffness Matrix Correction

2.4.2 Modal Test and FE Modal Correction Results

As mentioned previously, 36 channels of accelerometer output and one channel of load cell signal (input) were recorded during each modal test [38,39]. The input and output signals were analyzed by using PC MATLAB™. In MATLAB™, transfer functions, mode shapes and modal parameters were obtained using the modal analysis package. The simulations of modal analysis were also conducted in MATLAB™ for comparison.

The mass matrix correction procedure is carried out after the stiffness matrix has been corrected. Modal test data was employed to correct mass matrix. The transfer function obtained from the corrected FEM and the test data are shown in Figure 2.7. Table 2.1 lists the modal frequencies of the first nine modes obtained from the test data and the original ROM and the corrected ROM. Table 2.2 lists the modal shapes of the first nine vibrating modes obtained using the test data, the original ROM and the corrected ROM of the bridge. Table 2.3 depicts the variation of mode shape produced by the modification process. The graphs show these correspond to mode shapes along the girder (G-3).

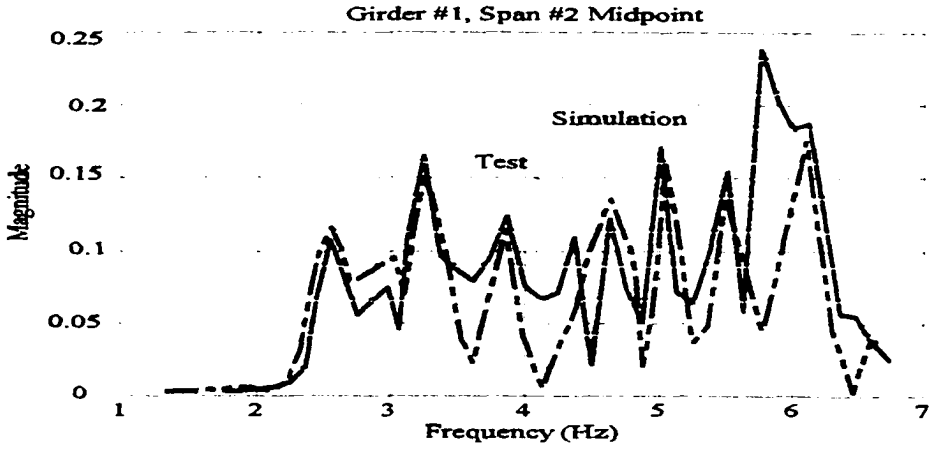

Figure 2.7 Comparison of Transfer Functions; Modal Test vs. ROM

Table 2.1 Modal Frequencies

Mode No.	Test (Hz)	ROM (% error) (Hz)	Modified FEM (Hz)
1	2.56	2.696 (-5.3%)	2.55 (0.39%)
2	3.01	3.171 (-5.35%)	3.02 (-0.15%)
3	3.25	3.412 (-4.98%)	3.27 (-0.62%)
4	3.63	3.887 (-7.11%)	3.64 (-0.28%)
5	3.88	4.065 (-4.77%)	3.87 (0.26%)
6	4.25	4.111 (3.27%)	4.25 (0.01%)
7	4.56	4.565 (0.11%)	4.57 (0.42%)
8	4.78	4.792 (-0.28)	4.75 (0.63%)
9	5.00	5.12 (-2.4%)	5.05 (-1.0%)

Table 2.2 Mode Shape Comparison Between Test Model and Modified FE Model

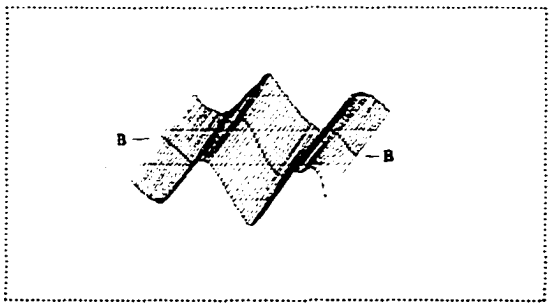

1st Test Model 2.56 Hz

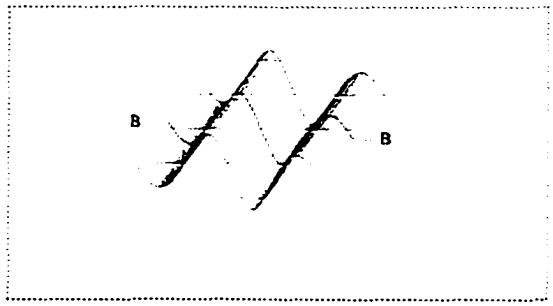

1st Modified FE Model 2.55 Hz

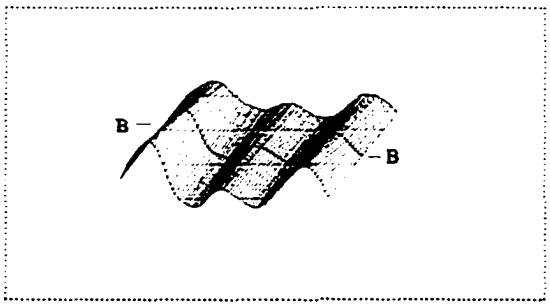

2 nd Test Model 3.01 Hz

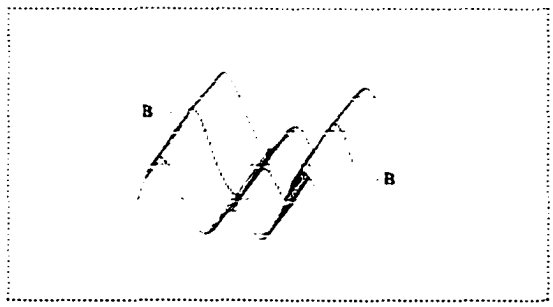

2 nd Modified FE Model 3.12 Hz

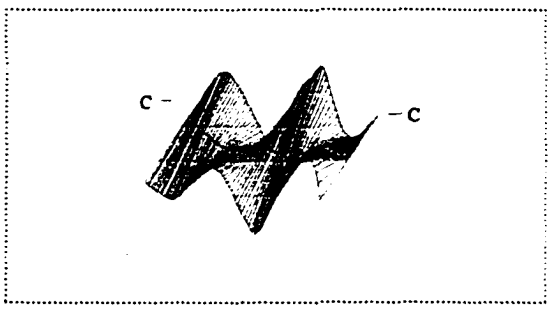

3 rd Test Model 3.25 Hz

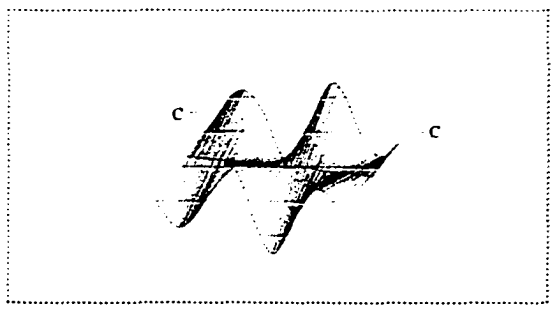

3 rd Modified FE Model 3.27 Hz

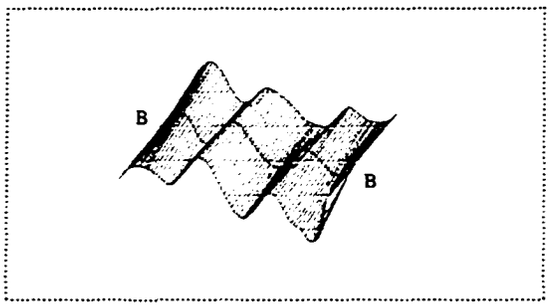

4 th Test Model 3.63 Hz

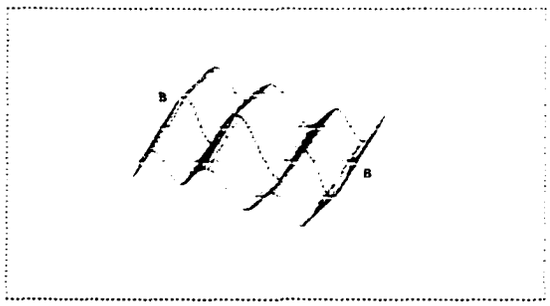

4 th Modified FE Model 3.64 Hz

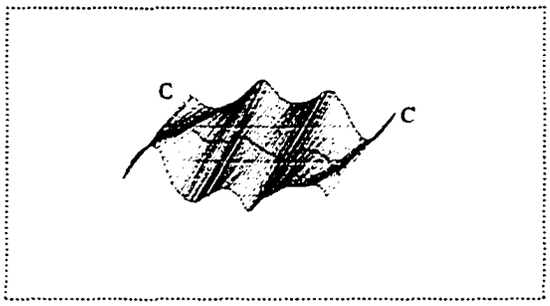

5 th Test Model 3.88 Hz

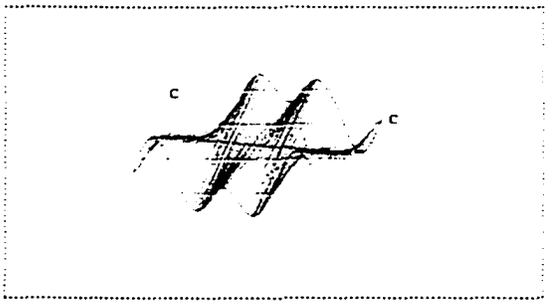

5 th Modified FE Model 3.87 Hz

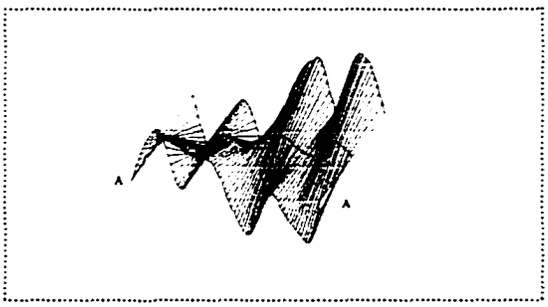

6 th Test Model 4.25 Hz

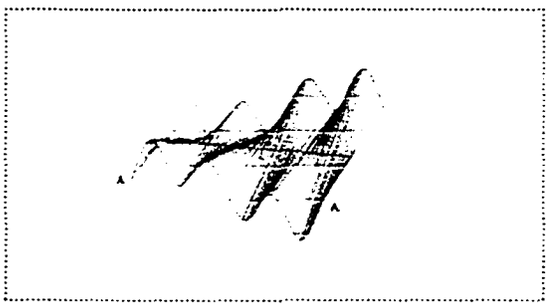

6 th Modified FE Model 4.25 Hz

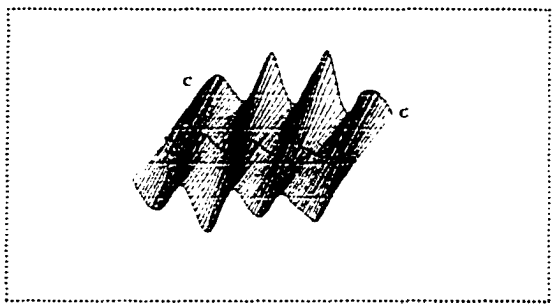

7 th Test Model 4.56 Hz

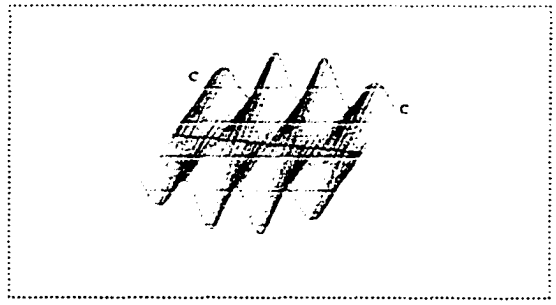

7 th Modified FE Model 4.37 Hz

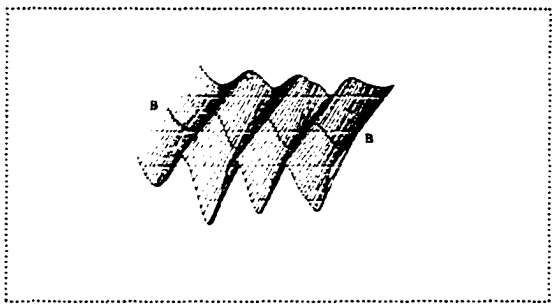

8 th Test Model 4.78 Hz

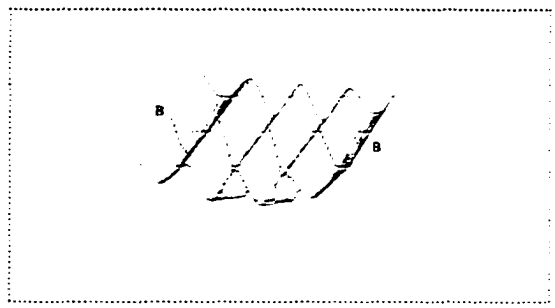

8 th Modified FE Model 4.75 Hz

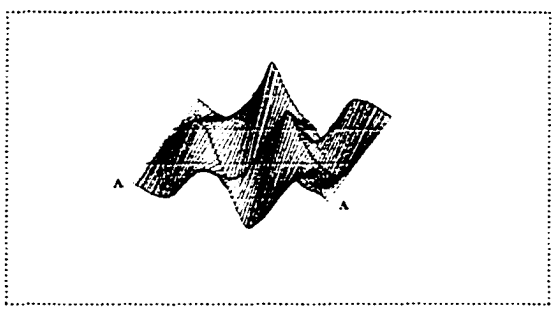

9 th Test Model 5.14 Hz

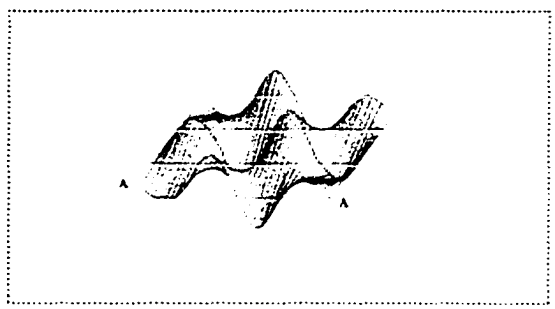

9 th Modified FE Model 5.13 Hz

Table 2.3 One Section Comparison of 9 Mode Shapes.

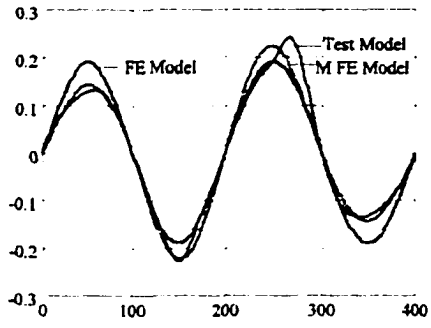

1st mode B-B Section

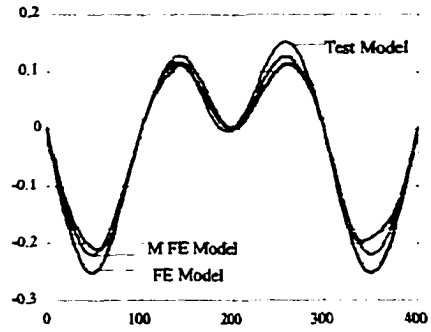

2 nd mode B-B Section

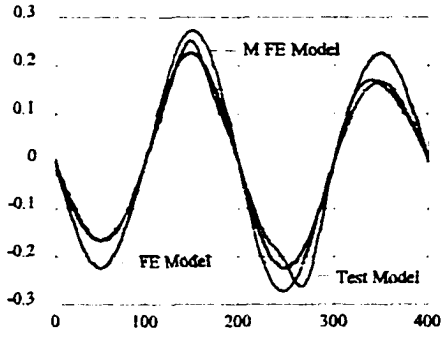

3 rd mode C-C Section

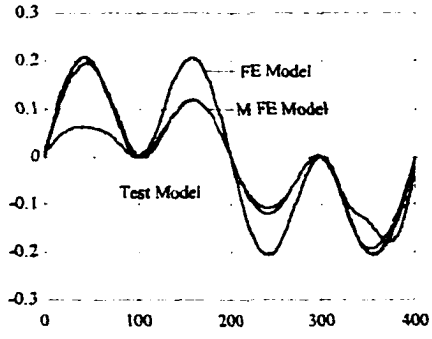

4 th mode B-B Section

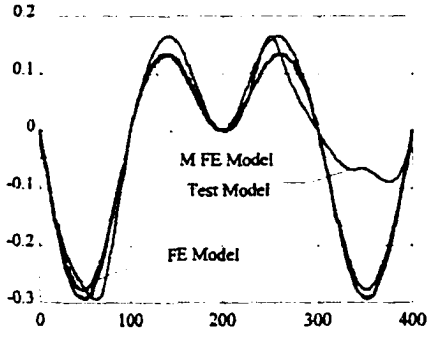

5 th mode C-C Section

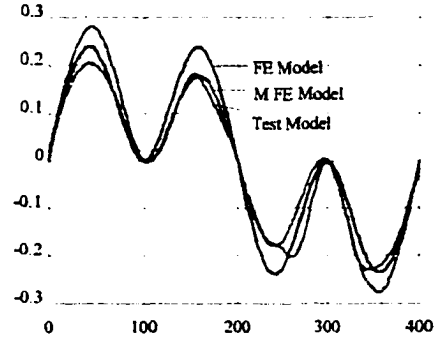

6 th mode A-A Section

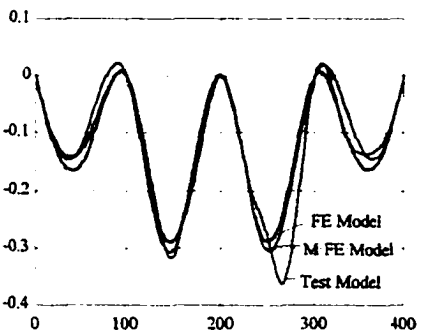

7th Mode C-C Section

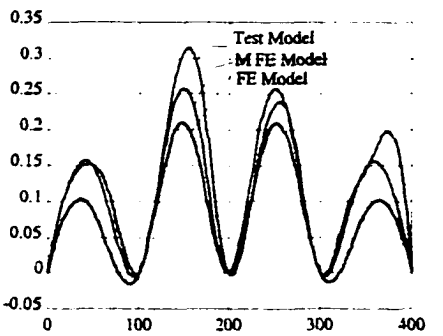

8th Mode B-B Section

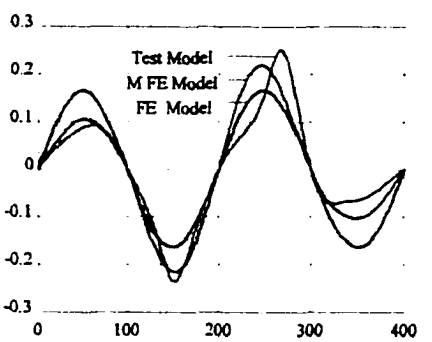

9th Mode A-A Section

2.5 Conclusions

This chapter describes the results of an effort to develop an accurate mathematical model of the two lane, four span Walnut Creek Bridge (north bound) on I-35. The procedures used to construct a full FEM and a ROM of the bridge were

reviewed. Modal modification techniques were introduced to improve the correspondence between the test data and the analytical model.

CHAPTER THREE

DYNAMICS OF BRIDGE/VEHICLE INTERACTION: MODAL COUPLING AND ITS EFFECT ON IMPACT FACTORS

3.1 Introduction and Background

The objective of this chapter is to present the results of various analytical and experimental studies on the effect that trucks have on the dynamic behavior of the Walnut Creek Bridge. This chapter provides a description of the methods employed to model the bridge dynamics and the interaction of vehicles with the bridge. A time-varying bridge/vehicle coupled model is first derived. Parametric studies are then presented to demonstrate the influence different parameters have on the dynamic response of the bridge. Finally, field measurements are compared to the predicted model-based response.

Many methods have been presented to predict the dynamic behavior of bridges subjected to various kinds of heavy truck loads. The earliest research treated vehicles as a travelling static load. Later works included models of trucks outfitted with compliant suspensions to develop a more exact prediction of a bridge's dynamic response to vehicle traffic. In order to exactly predict the characteristic of a

bridge/vehicle system for the design of a control system, it is necessary to consider the bridge and the vehicle as a dynamically coupled system, because (as the work here will demonstrate) bridge/vehicle dynamic behavior is dramatically affected by bridge/vehicle interaction forces. In order to develop an improved simulation scheme for bridge /vehicle interaction dynamics, the bridge and vehicle are treated as two different substructures that interface at the surface of the bridge. This makes it possible to derive a compact system of motion equations.

There are three factors that must be taken into account when the dynamic analysis of the bridge/vehicle interaction is examined: (1) most of the heavy trucks that cross the bridge have chassis modes in the range of 1.5 Hz to 4 Hz; (2) a large number of medium span length bridges (20 m - 40 m) exhibit fundamental frequencies in the same domain (1.5 Hz to 4 Hz); and (3) when a truck passes over a bridge, if the truck's chassis vibration modes correspond closely with the bridge's fundamental vibration modes, then the bridge and truck interact to cause a resonance condition. That resonance coupling typically brings about a corresponding magnification of moments, shears and stresses in bridge girders. The increase due to the dynamic component is normally treated at the design stage as an impact factor, which is defined as the difference between the dynamic and static value (the dynamic value divided by the static value). Normally, an increase of the deflection will cause an increase of the stress levels, which over time shortens the useful life of bridges. (Kou and Dewolf [10])

3.2 Modeling of the Bridge/Vehicle System

Figure 3.1 shows the general bridge/vehicle interaction problem. As the vehicle moves along the bridge, vibration of vehicle suspension deformation produces a dynamic tire force to the bridge deck. The bridge girders deflect in response to the moving, unsteady suspension tire forces. The dynamic deflection of the bridge deck couples with the truck suspension at the contact point; thus, producing a reaction force back to the suspension which excites suspension vibration. The bridge dynamics are easily characterized using a finite element model of the structure.

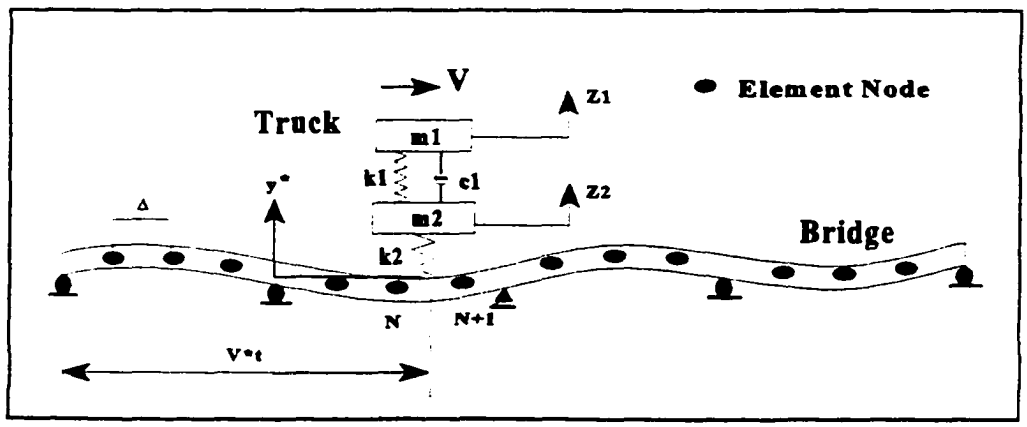

Figure 3.1 A bridge coupled with a quarter vehicle

The dynamic interaction force is characterized by the force in the tire. The tire force is simply the product of the stiffness of the tire by the relative displacement of the tire and bridge at the interface ($z_2 - y^*$) as shown in Figure 3.1. The bridge deflection at the contact point can be determined by proportioning the total deflection of

neighboring nodes of the FEM in a linear fashion. If, for example, the tire is at the 2/3 point along an element, then total deflection consists of 1/3 of the deflection of the farthest node and 2/3 of the deflection of the nearest node (Veletsos and Huang [5]).

3.2.1 Bridge and Vehicle Modeling

The Walnut Creek Bridge superstructure with natural fundamental frequency 2.5 Hz is shown in Figure 3.2. It consists of four spans and five continuous girders. The supports for the main girders are pinned with rollers at all but the center support, which has a fixed shoe arrangement. The bridge structure is discretized into elements, with the girders modeled as beam elements and the concrete deck modeled as plate elements.

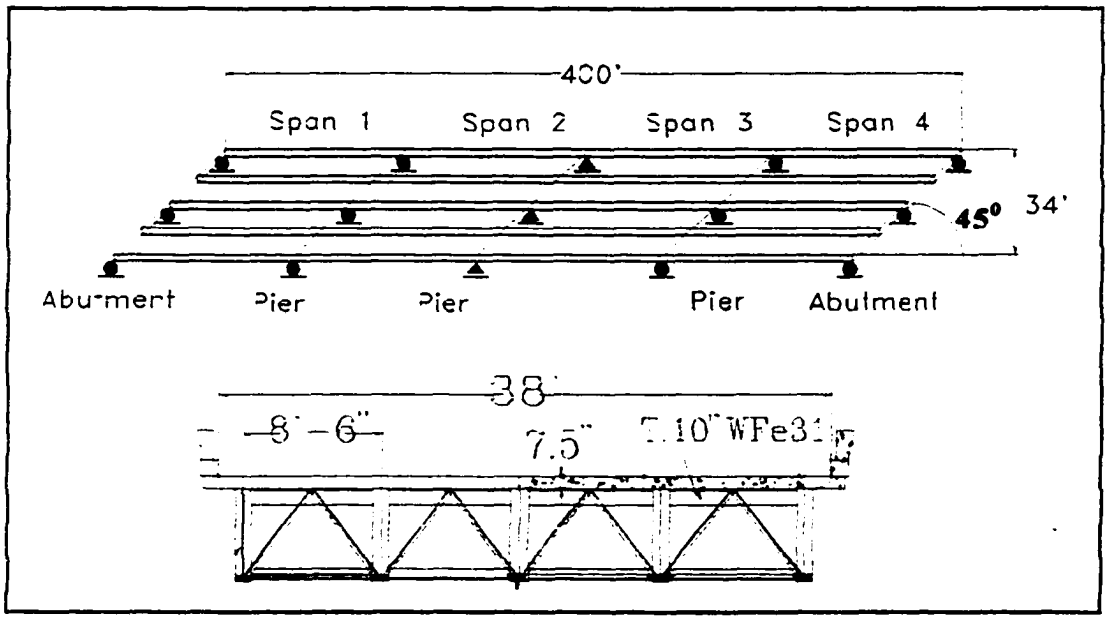

Figure 3.2 Superstructure of the Oklahoma I-35 Walnut Creek Bridge

Figure 3.3 shows a reduced order FE model (ROM) of the Walnut Creek Bridge

which is employed throughout this dissertation for bridge/vehicle interaction dynamic analysis. This ROM consists of a total of 225 DOFs, which assumes that the motion consists of planer displacements and rotation with only 2 DOFs for each node. This is in contrast to the full FEM of the bridge developed for modal analysis purposes which consists of 4,800 DOFs. In spite of the pronounced skew of the bridge, the modal analysis of the field test data indicates that the maximum out-of-plane motions are less than 5 % of the maximum in-plane motion; thus, justifying the assumption that out of plane dynamics can be neglected.

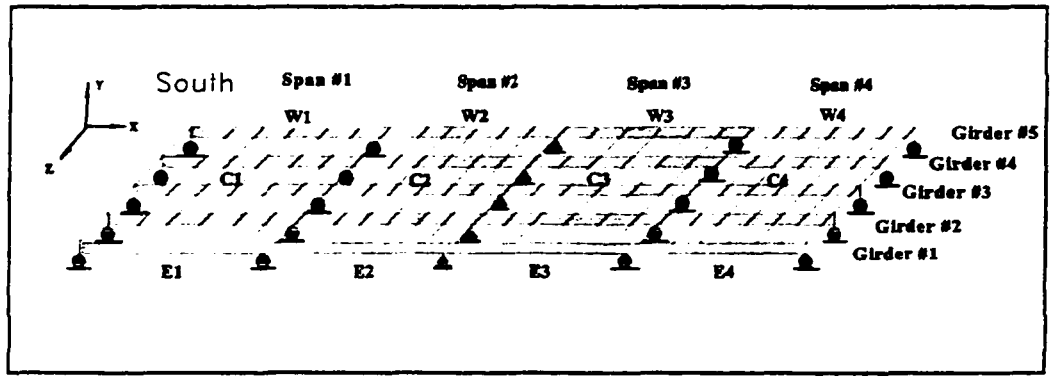

Figure 3.3 Reduced order FE mesh of the Walnut Creek Bridge

The test vehicle was a five-axle tractor-trailer owned by Cleveland County. In order to conduct parameter study, two vehicle models were used for the analysis presented below. A quarter vehicle model, which is a simplified tractor-trailer, is shown in Figure 3.4. The spring, K_2, in the diagram represents a tire spring, and the

upper spring, K_1, represents a suspension spring. Both springs in this model are considered to be linear. The damped natural frequencies of the quarter vehicle model are: sprung mass (2.12 Hz) and truck unsprung mass (10.25 Hz). The selection of parameter values is guided by testing and experience. The parameters of the quarter vehicle used in dynamic simulation are listed in Appendix I.

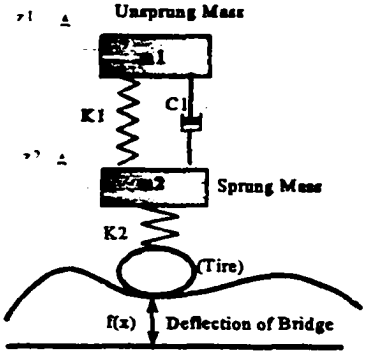

Figure 3.4 A quarter vehicle model

Figure 3.5 shows the detailed features of the representation of a Rock Truck (RT) tractor-trailer that was used extensively in the research reported here. Lee, a fellow research associate at the CSC, has derived a model of the truck dynamics that was used in this subsequent analysis [40]. The load disturbution and wheel space of RT are represented in Figure 3.6. Various tests were conducted to verify the model of the loaded truck. The test truck used in the experimental study was analytically modeled with the same features. The selection of parameter values was guided by published data on the truck's chassis components and by testing. The parameters that were found to

provide a best fit to test data are listed in Appendix II. The damped natural frequencies of the various inertial components are: (1) steering axle 13.45 Hz; (2) tractor tandem axle #1 10.29 Hz; (3) tractor tandem axle #2 9.92 Hz; (4) rear tandem axle 9.51 Hz; (5) pitch mode, tractor 2.26 Hz; (6) pitch mode, trailer 1.52 Hz; and (7) heavy mode entire truck 2.68 Hz.

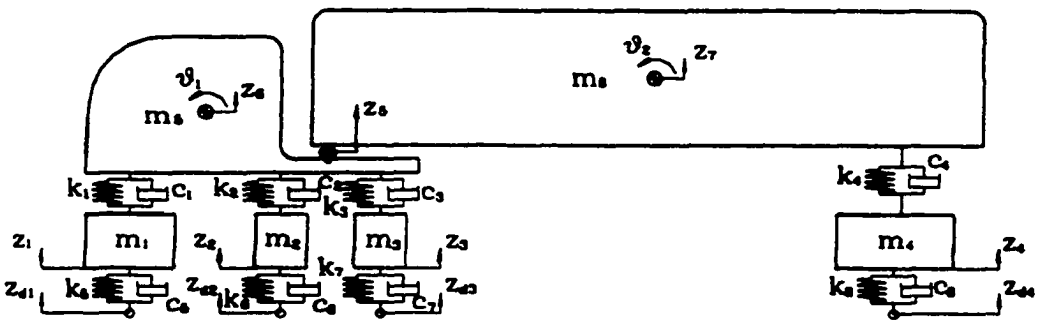

Figure 3.5 Dynamic model of four axle tractor-trailer (RT)

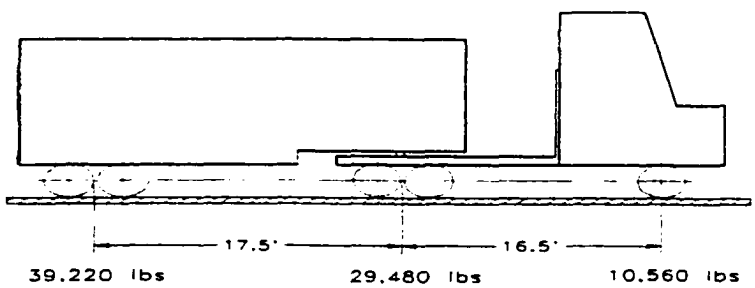

Figure 3.6 Load distribution and wheel space of Rock Truck

3.2.2 Motion Equations of Coupled Bridge/Vehicle System

The ROM of the bridge is defined by a vector of generalized coordinates as $\hat{y} = [\xi^T, \xi'^T]$, in which ξ is the vector of global nodal displacements and ξ' is a vector of the slopes at each nodal point (the prime indicates differentiation with respect to the length of the beam). The FEM of the bridge takes the form:

$$M_b \hat{\ddot{y}} + C_b \hat{\dot{y}} + K_b \hat{y} = \hat{d}(t) \; ; \quad \hat{y} \in R^m \tag{3.1}$$

The matrices, M_b, C_b and K_b, represent the consistent mass, the proportional damping and the stiffness matrix of the discretized girder, respectively. The proportional damping matrix can be estimated from the test data. The term $\hat{d}(t)$, on the right-hand side of Equation (3.1), represents the tire force imposed by the moving vehicle. While it is well known that the response of the system is dependent on the speed of the vehicle(Timoshenko [6]), the vehicles traveling on roadway bridges typically move at or near the posted speed (i.e., the speed of the vehicle is constant). The work here assumes that the vertical tire force is distributed to the local nodes in the vicinity of the tire contact point. The force at each node is determined by proportioning the total load in a linear fashion. For example, if the actual load is at the 2/3 point along an element, then 1/3 of the load is appointed to the farthest node, and 2/3 of the load is applied to the nearest node which is same as the assumption of proportioning the total deflection in the previous section. This particular formulation disregards the influence of the road

roughness on the dynamics. This is reasonable when the dynamic response of the bridge and vehicle are coupled at a near resonance condition, because the coupling response is many times larger than the response due to the rough texture of the bridge deck surface.

A quarter vehicle model was adopted to represent the truck. The equations of motion of the quarter vehicle are:

$$\begin{aligned} m_1 \ddot{z} &= k_1 (z_2 - z_1) + c_1 (\dot{z}_2 - \dot{z}_1) \\ m_2 \ddot{z}_2 &= -k_1 (z_2 - z_1) - c_1 (\dot{z}_2 - \dot{z}_1) + K_{tire} [(\hat{\varphi}(t), \hat{y}) - z_2] \end{aligned} \tag{3.2}$$

where $\hat{\varphi}(t)$ is a vector that maps the beam nodal coordinates into the current position of the truck tire. When the truck tire is between any two adjacent nodal points, φ_N and φ_{N-1}, then $\hat{\varphi}(t)$ has the following form:

$$\hat{\varphi}(t) = [0, 0, \ldots, \varphi_N, \varphi_{N-1}, 0, \ldots 0] \tag{3.3}$$

where

$$\varphi_N = 1 - \frac{x - x_N}{\Delta}, \quad \varphi_{N-1} = \frac{x - x_N}{\Delta} \tag{3.4}$$

which Δ is the element length.

The disturbance input to the bridge is then:

$$\hat{d}(t) = K_{tire}\hat{\varphi}(t)\,[z_2 - (\hat{\varphi}(t), \hat{y})] \tag{3.5}$$

Equations (3.1), (3.2) and (3.5) define the coupled bridge/vehicle system. Equation (3.2) can also be written as:

$$M_t\hat{\ddot{z}} + C_t\hat{\dot{z}} + K_t\hat{z} = K_{tire}\Phi\,(\Phi^T\hat{z} - \hat{\varphi}(t)^T\hat{y}) \tag{3.6}$$

in which $\hat{z} = [z_1, z_2]^T$ and

$$M_t = \begin{bmatrix} m_1 & 0 \\ 0 & m_2 \end{bmatrix}, \quad C_t = \begin{bmatrix} c_1 & -c_1 \\ -c_1 & c_1 \end{bmatrix} \quad K_t = \begin{bmatrix} k_1 & -k_1 \\ -k_1 & k_1 \end{bmatrix} \tag{3.7}$$

$\Phi = [0, 1]^T$ is a vector which maps z_2 to $\hat{z}$. Thus, the bridge dynamic equations can be rewritten as:

$$M_b\hat{\ddot{y}} + C_b\hat{\dot{y}} + K_b\hat{y} = K_{tire}\hat{\varphi}(t)(\Phi^T\hat{z} - \hat{\varphi}(t)^T\hat{y}) \tag{3.8}$$

Combining Equation (3.6) and (3.8), The general equations of system (bridge/vehicle) can then be written as:

$$M\ddot{\hat{\zeta}} + C\dot{\hat{\zeta}} + K(t)\hat{\zeta} = 0 \quad ; \quad \hat{\zeta} \in R^{m+n} \tag{3.9}$$

where $\hat{\zeta} = [\hat{y}, \hat{z}]^T$, and

$$M = \begin{bmatrix} M_b & 0 \\ 0 & M_t \end{bmatrix} \quad C = \begin{bmatrix} C_b & 0 \\ 0 & C_t \end{bmatrix} \quad K = \begin{bmatrix} K_b + k_{tire}\varphi(t)\varphi(t)^T & -k_{tire}\varphi(t)\Phi(t)^T \\ -k_{tire}\Phi\,\varphi(t)^T & K_t + k_{tire}\Phi\,\Phi^T \end{bmatrix} \tag{3.10}$$

Defining the state vector, $r = [\hat{\zeta}, \dot{\hat{\zeta}}]^T$, then the uncontrolled state space form of the bridge/vehicle model can be expressed as:

$$\dot{r} = A(t)r; \qquad r(t_0) = r_0 \tag{3.11}$$

where

$$A(t) = \begin{bmatrix} [0] & [I] \\ [-M^{-1}K(t)] & [-M^{-1}C] \end{bmatrix} \tag{3.12}$$

Equation (3.11), which combines two subsystems together with a constraint equation at the interface of the bridge and vehicle, completely specifies the behavior of the bridge/vehicle system. By a suitable extension, the axle loads can be expanded to multiple axle loads and the number of vehicle on the bridge can be selected arbitrary

in numerical simulation.

3.3 Simulation Method

Once the coupled bridge/vehicle model was derived, then a C++ numerical simulation program was developed for the coupled dynamic analysis of medium span bridges subjected to moving vehicles. The analysis was carried out by solving the state space bridge/vehicle dynamic Equation (3.11). The program is designed to handle up to 500 DOFs bridge model on a PC.

The matrix, **K(t),** varies according to the position of the vehicle on the bridge and therefore the matrix must be updated at each time step in the simulation. The time-varying vector, $\hat{\varphi}(t)$, is determined in accordance with the vehicle's location on the bridge. The general stiffness matrix must be recomputed at each time step while the mass and damping matrices remain constant. The general equations are solved simultaneously with a 4th order Runge-Kutta method with a fixed integration time step.

Assumptions: The following assumptions were made for the bridge/vehicle interaction problem in numerical simulation results presented here:

(1) The vehicle travels with a constant speed during the motion;

(2) Wheels are always in contact with the bridge deck;

(3) The bridge riding surface is a reinforced concrete deck and the surface roughness is neglected;

(4) It is assumed that 10 % of the total weight of the vehicle (RT) is loaded on the front axle, 30% of the total weight is loaded on the middle axle, 60% on the real axle and

65% of the total wheel load is loaded on the center girder, 25% of the total weight is loaded on the east girder when the vehicle is traveling in the right lane;

(5) The impact factor is defined as the maximum dynamic deflection range divided by the maximum static deflection range (or stress range) at midpoints of each span;

(6) The vehicle is excited by the road profile just before it enters the bridge. The actual entrance profile at the test bridge is shown in Figure 3.7. It was assumed that the vehicle was at equilibrium prior to encountering the bridge entrance;

(7) Vehicle damping is considered to be viscous, which neglects the interleaf friction in the suspension springs; and

(8) The bridge damping ratio were found via modal testing.

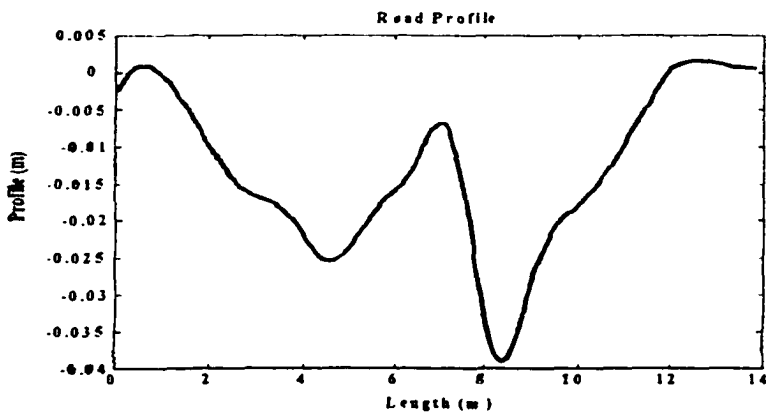

Figure 3.7. Road profile at the entrance of the Walnut Creek Bridge

Figure 3.8 shows the time history of first three eigenvalues of the bridge/vehicle

system. The truck travels at 105 km/h. There is a 6.5% variation of the natural frequencies of the bridge.

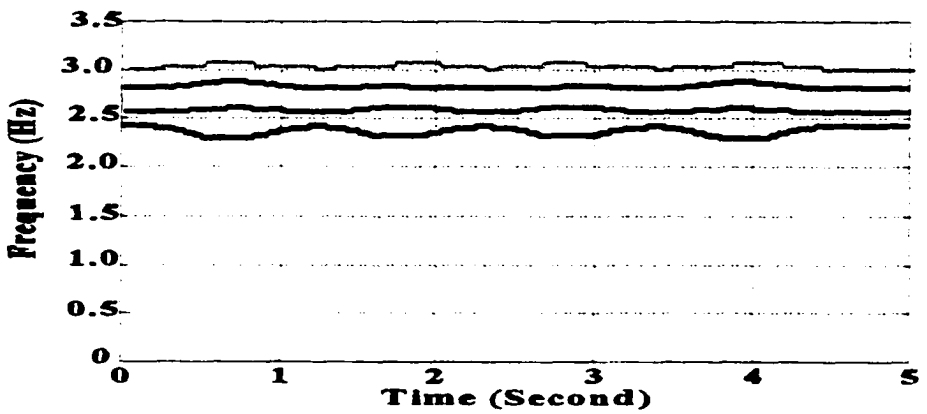

Figure 3.8 First 4 modes of the bridge/vehicle system

The evaluated response includes the deflection, velocity and acceleration at several selected points along the bridge.

The flow chart of the simulation algorithm is shown in Figure 3.9. The simulation algorithm starts at the beginning of the bridge profile start point. The bridge and the truck suspension are at an equilibrium, t=0, when the truck reaches the starting point of the bridge and the computer program starts to calculate time-varying vector, $\hat{\varphi}(t)$, according to the vehicle's location on the bridge. The matrix, **A(t)**, is reassembled at each step. The general bridge/vehicle state space equation is then solved simultaneously using a 4th order Runge-Kutta numerical method.

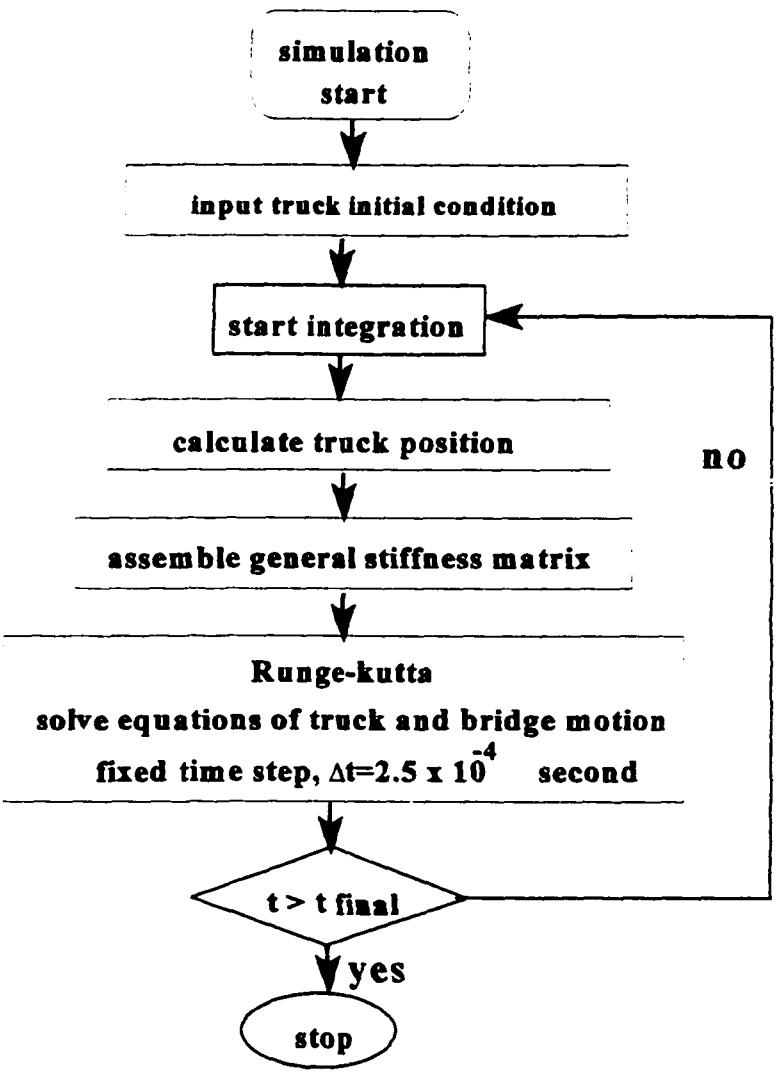

Figure 3.9 Flow chart of the computer program

3.4 Simulation and Test Results

Figure 3.10 depicts the displacement at the center of the bottom flange of three of the five girders in span #2 of the four span bridge as the RT traverses in the right lane at a speed of 105 km/h (65 mph). The results indicate that the maximum deflection occurs at the center girder #3. The peak value of girder #5 is relatively small.

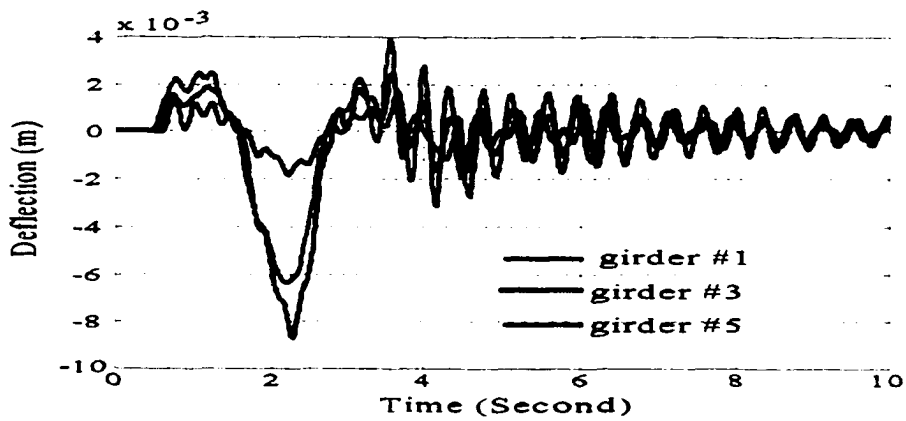

Figure 3.10 Simulation of typical dynamic response of displacement for the Second Span with RT passing over

Many factors influence the dynamic behavior of the bridge. The next section examines the influence on the bridge response of vehicle speed.

3.4.1 Effect of Vehicle Speed

A substantial magnification of the dynamic load effect can occur for a continuous span girder when a vehicle travels across the bridge at a speed approaching

the bridge's fundamental natural frequency. The vehicle velocity mode is defined as $\omega_v = V/2l$, where V is the velocity of the vehicle and l is the span length. As ω_v approaches the first mode (ω_1) of the bridge, the amplification of the bridge dynamics becomes more evident. If the vehicle was actually traveling at such speed that $\omega_v \approx \omega_1$, then the dynamics of the bridge could (theoretically) approach resonance condition (Chung and Genin [7]). The vehicle would have to be traveling at about five times the post speed limit to achieve that resonance condition. The effect of vehicle speed on maximum deflection was simulated using a quarter vehicle to represent a typical truck. Figure 3.11 shows the effect of vehicle speed on the maximum deflection when the quarter vehicle travels the bridge in the right lane at different speeds.

The maximum deflection of girder #5 increases up to four times when the vehicle speed increases from 56.4 km/h (35 m/h) to 136.85 km/h (85 m/h). The center girder (#3) realizes the largest absolute deflection for all speeds tested and, for the range of speeds tested, appears that as the speed doubles, the peak deflection increases 150%.

This result is reasonable since the increasing vehicle speed will increase the resonance between the bridge and vehicle. The other important reason is that the increase of the vehicle speed will cause the increase of the initial vibration of the vehicle suspension at the entrance of the bridge. Figure 3.12 depicts the effect of vehicle speed on the maximum amplitude of suspension vibration when the quarter vehicle travels the bridge in the right lane at different speeds.

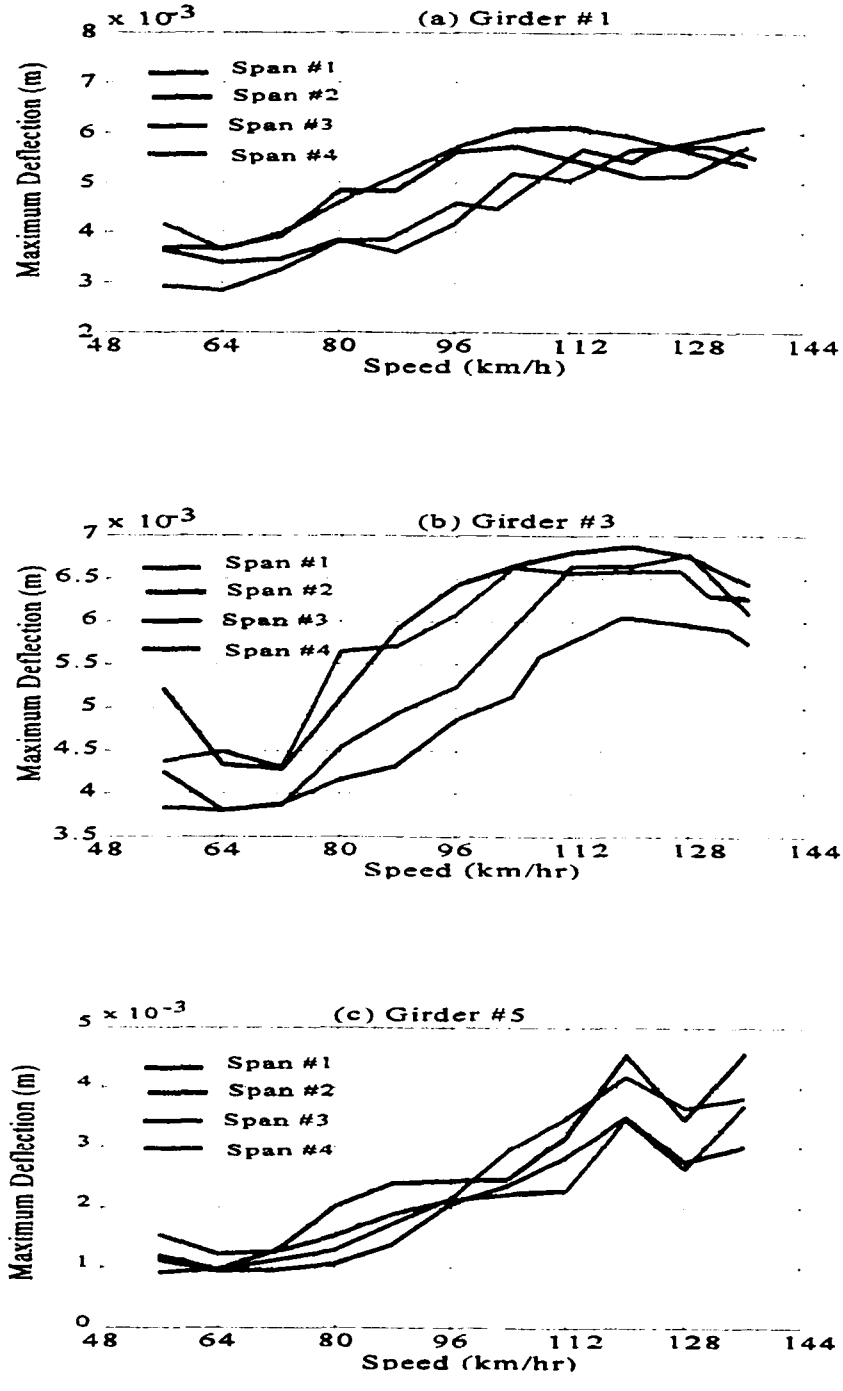

Figure 3.11 Effect of vehicle speed on peak deflection of the bridge (a) girder #1, (b) girder #3, (c) girder #5

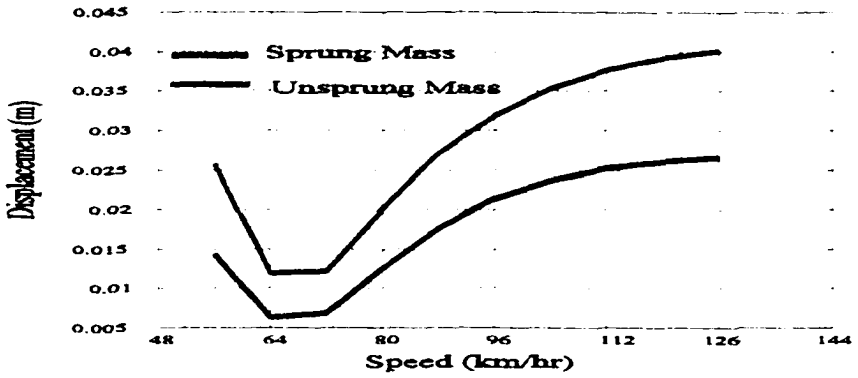

Figure 3.12 Effect of vehicle speed on initial displacement of the vehicle suspension

It indicates that the maximum vibration of unsprung mass and sprung mass increases up to four times when the vehicle speed increases from 56.4 km/h (35 m/h) to 136.85 km/h (85 m/h). This will also increase the peak deflection of the bridge.

3.4.2 Effect of Vehicle Fundamental Frequencies

Previous studies have indicated that resonance of vehicle and bridge fundamental frequencies will result in a greater dynamic response of the bridge (Chung and Genin [7]). Figure 3.13 depicts the variation of peak deflection as the vehicle sprung mass frequency is changed. The quarter vehicle travels at the posted speed limit (105 km/h) in the right lane in the simulation.

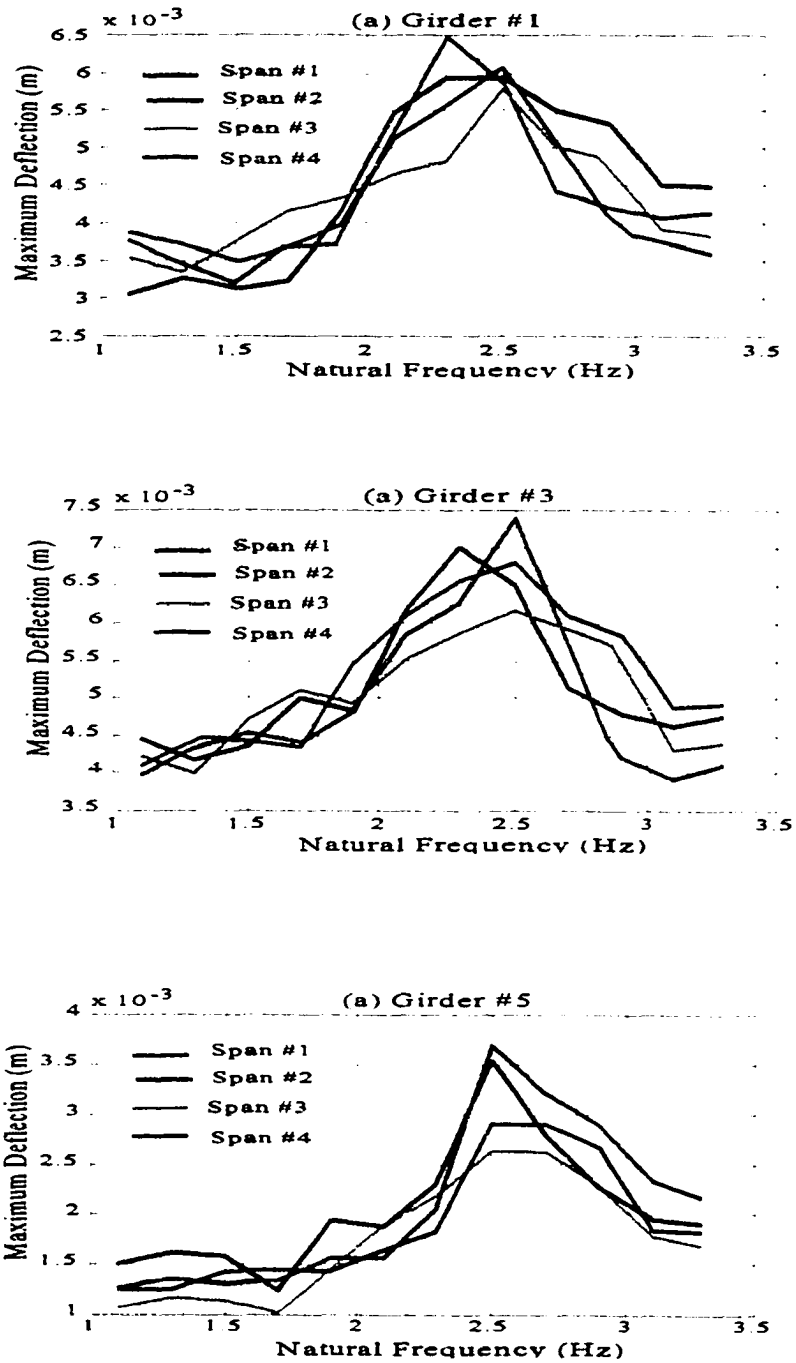

Figure 3.13 Effect of vehicle natural frequency on peak deflection of the bridge (a) Girder #1, (b) Girder #3, (c) Girder #5

The dynamic response of the bridge is found to reach the peak values when the fundamental frequency of the truck is close to 2.5 Hz, which is also the fundamental frequency of the bridge. The magnification of deflection of girder #3, which realizes the largest absolute deflection at the bridge fundamental frequency, is approximetly two times larger than the response when the fundamental frequency of the truck is close to 1.0 Hz.

3.4.3 Effect of Vehicle Static Weight

Figure 3.14 shows what the variation of static wheel load of the quarter vehicle has on the maximum displacement of the bridge when the quarter vehicle traverses in the right lane. The natural frequencies of the vehicle are fixed in order to eliminate the eigenvalues influence on the dynamic response of the bridge. The maximum deflection increases about three times when the static vehicle weight increases three times for the girder #3. The relationship between peak deflection and static weight of the vehicle is a linear patten. The maximum dynamic response was found to uniformly increase with the increased vehicle weight.

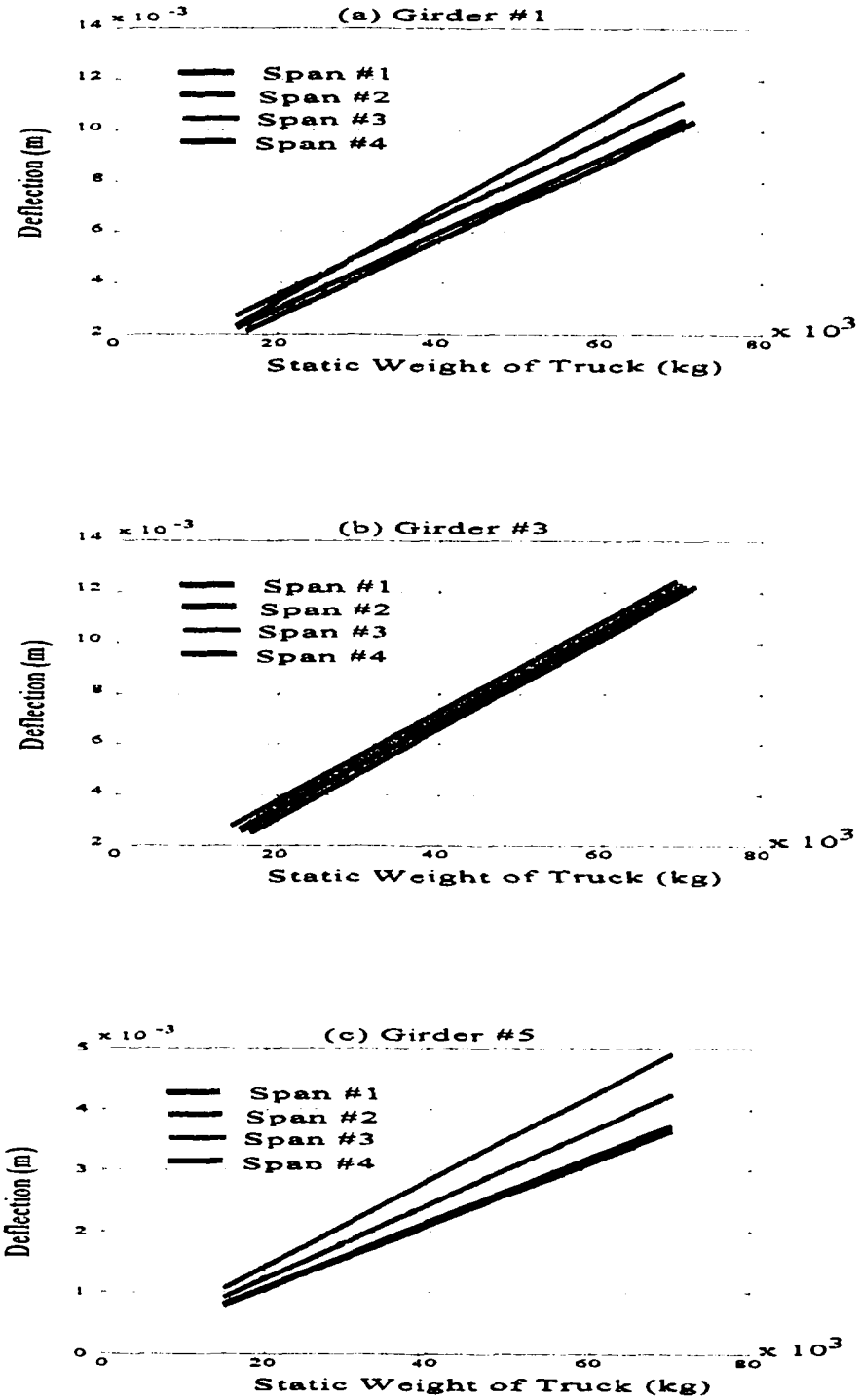

Figure 3.14 Effect of the vehicle static weight

3.4.4 Comparison of Simulation and Test Results

In order to verify the analytical model, experiments were conducted to identify the Walnut Creek Bridge dynamic behavior. A 80 klb four-axle Rock Truck with a 32 foot wheel base equipped with vibration sensors was employed in the field test. The frequency domain responses of the bridge and vehicle suspension when the truck is on the bridge are shown in Figure 3.15. It indicates that the fundamental frequencies of vehicle suspension are very close to fundamental frequencies of the bridge.

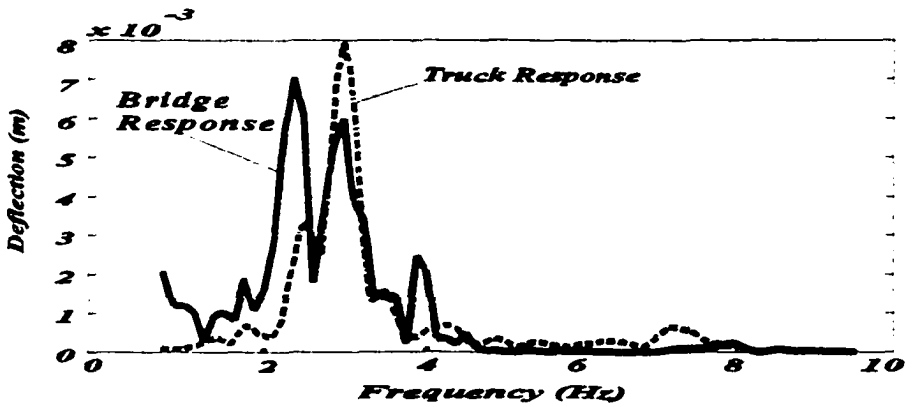

Figure 3.15 Frequency response of the Walnut Creek Bridge and RT chassis

The simulation versus the measured response of the bridge at the bottom center of the girders #1, #3 and #5 of third span of the bridge when the test truck passed over the bridge in the right lane are shown in Figure 3.16. The close correspondence between the measured and simulated response exhibited by this and several other tests made it clear that the 225 DOF FEM of the bridge provides a high fidelity replication of the

bridges dynamic response. It also verifies that the bridge/vehicle coupled model can predict the bridge/vehicle interaction behavior with high accuracy.

The data also indicates that, when the truck is in the right lane, girder #1 realizes peak deflection approximately the same magnitude as the center girder #3. The reason for this is that the bridge torsion and bending modes frequencies are very close in value which suggests that the net deflection of girder #1 is the composite of two modes of motion, while the center girder #3 deflection is essentially due to bending. A careful inspection of the dynamic response indicates that the east and west girders are moving down under the static weight of the truck, but are also vibrating out of phase - a clear indicatior of the torsion effect. Figure 3.17 depicts the frequency response of two accelerometers as the RT passed over the bridge. The 3rd and 4th modes represent torsion modes which are the most important reason of dynamic pattern of the Walnut Creek Bridge.

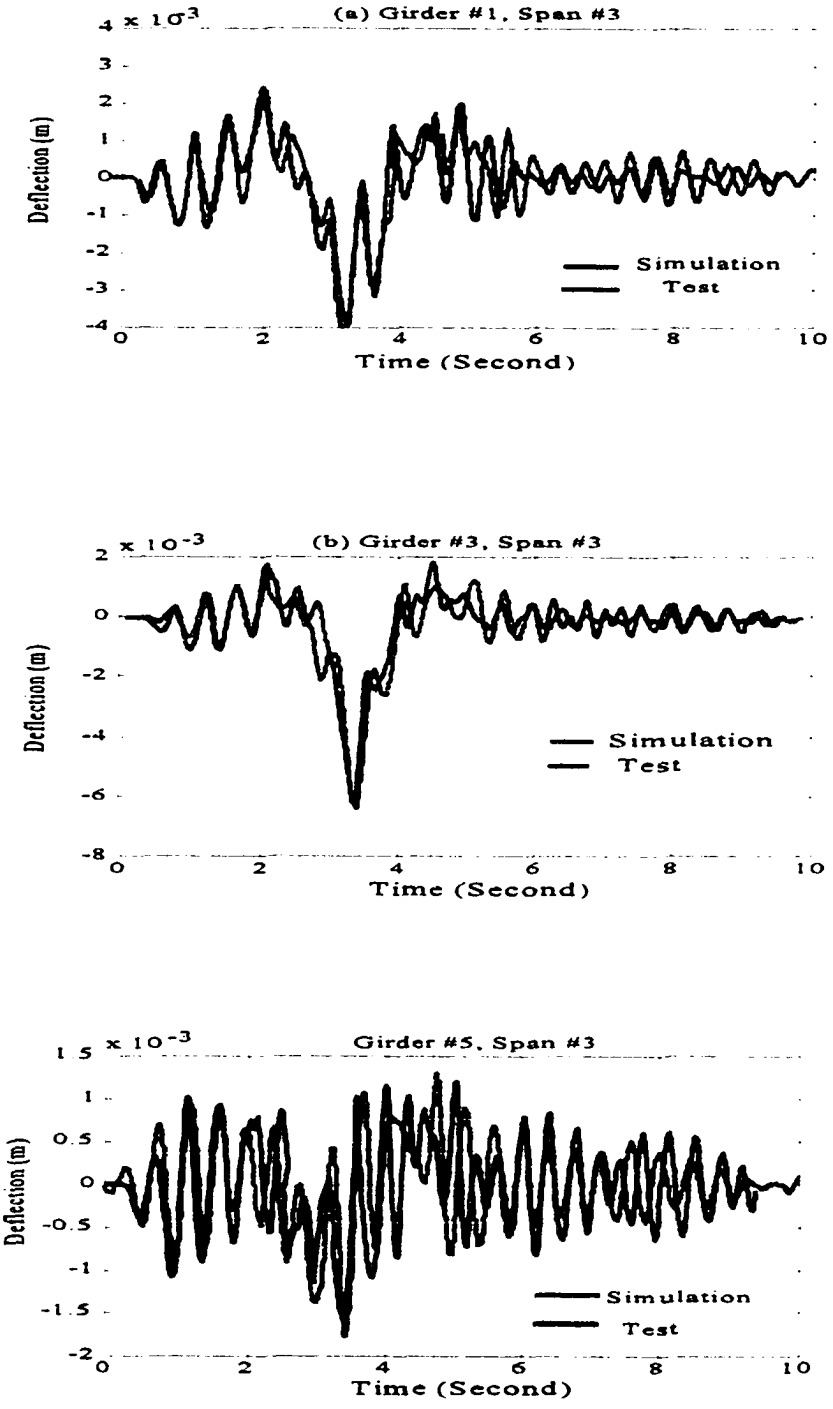

Figure 3.16 Bridge response of open loop, simulation vs. test results, rock truck in right lane, a) girder #1; b) girder #3; c) girder #5

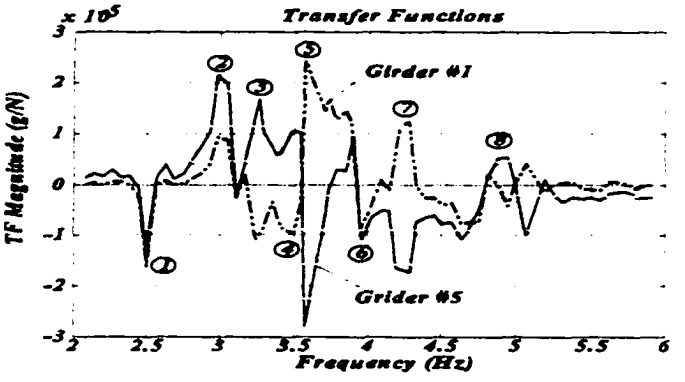

Figure 3.17 Transfer function obtained from the modal test at the middle of span #1; mode numbers are shown circled

3.4.5 Impact Factor of Dynamic Loads

In order to understand the dynamic interaction of the bridge and truck, it is necessary to provide an estimation of the impact factor for the bridge. A crawl test was conducted first. In this case, the test truck traveled at approximately 2 km/h in the right lane. Once the crawl test was finished, a dynamic response test was established while test trucks passed over the bridge at 105 km/h (65 mph) in the right lane. The impact factor is obtained by dividing the maximum dynamic deflection range by the maximum static deflection range (or stress range) at midpoints of each span. Results from the crawl test are used here to establish the static deflection. Figure 3.18 depicts the strain comparison between crawl test and dynamic response test.

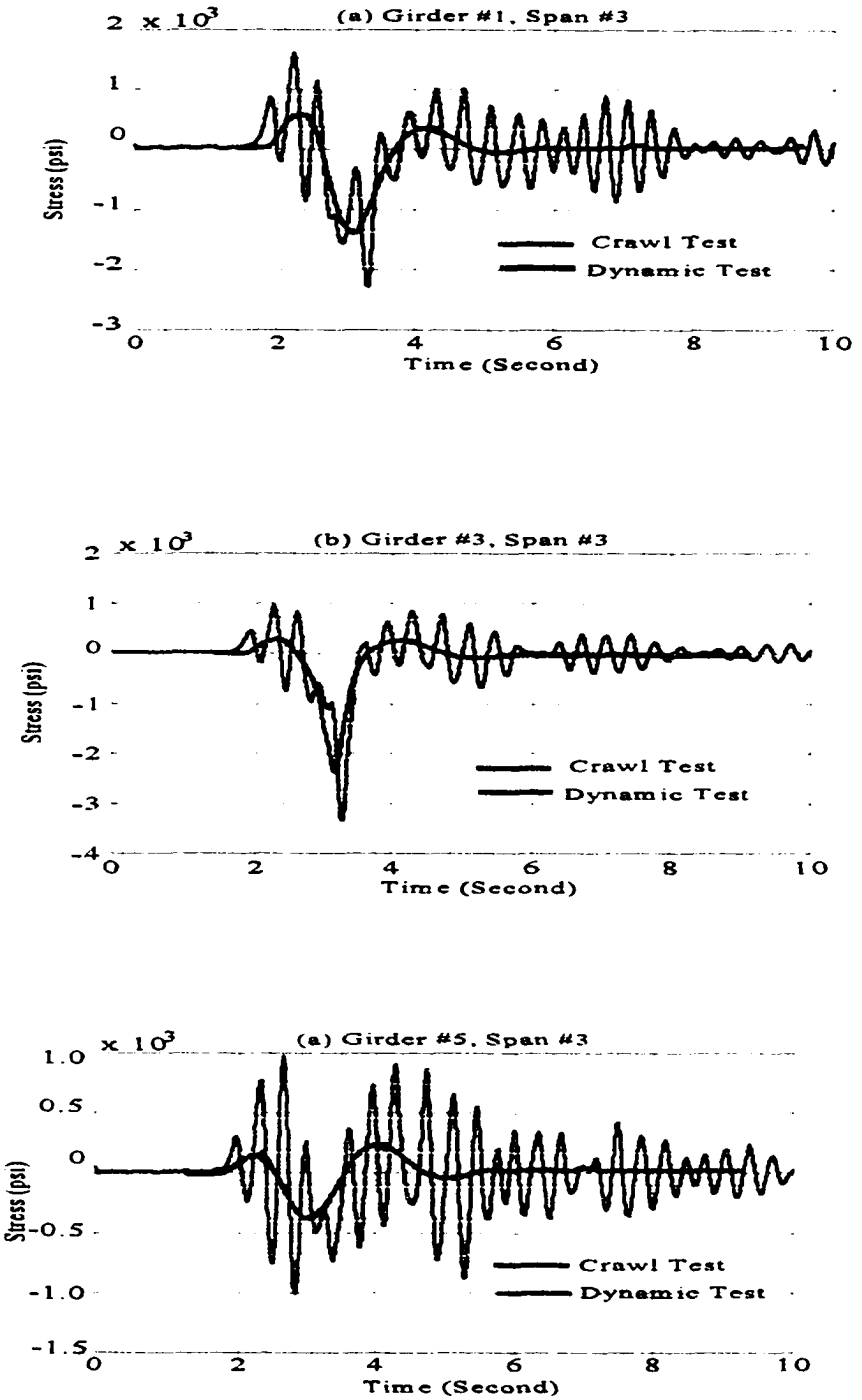

Figure 3.18 Impact factor of test results, crawl test vs. dynamic test, Rock Truck in right lane, a) girder #1; b) girder #3; c) girder #5

The RT moving in the right lane results in an impact factor of 1.45, which is within the expected limits assumed by NCHRP 299. Ascend measure of impact that is more consistent with the need to assess the effect that dynamics have on the service life of bridges is based on stress range. That is I_s = ***Stress range dynamic / Stress range static***. The maximum impact factor using that equation is 1.7 (Figure 3.18c). The impact factors at the east and west girders are much higher than the NCHRP 299 guidelines suggested 1.3.

3.5 Summary

This chapter presents the simulation and test results of the dynamic response of a four span continuous girder highway bridge. A quarter vehicle model and a Rock Truck (RT) tractor-trailer model were also formulated for simulation studies. The time-varying bridge/vehicle interaction model had been derived and applied to evaluate the influence that various parameters have on the dynamic behavior of the bridge/vehicle system. The simulation and experimental results presented in this chapter indicate the following:

(1) In studies to determine the maximum deflection (or impact factor), it was shown that the vehicle natural frequency had the greatest effect on impact factor. The vehicle weight as well as the vehicle speed can also affect the maximum deflection of the bridge. The quarter vehicle model represents the largest class of heavy truck suspension, which often exhibit modal frequencies that are similar to the fundamental

modes of many highway bridges. The near resonance between the vehicle and bridge result in a larger contact load at the bridge/tire interface.

(2) The comparison between simulation and test results indicates that the modified 225 DOF bridge model provides a high fidelity replication of the bridges dynamic response. The RT model, coupled with the ROM of the bridge, provides excellent correspondence with measured data.

(3) The observations made above suggest that control hardware should be retrofitted to the truck chassis to mitigate the vibration of the truck while it is on the bridge. A semiactive suspension system can be employed to achieve this purpose. A discussion of that proposed system is offered in Chapter Seven.

CHAPTER FOUR

INTELLIGENT STIFFENER FOR MEDIUM SPAN BRIDGES (ISB)

4.1 Introduction

The semiactive control of structures has been recognized as one of the most challenging and potentially rewarding areas of research in structural engineering in recent years. Semiactive motion mitigation systems provide a low power means of instantaneously changing a structure's passive compliance characteristics, stiffness and damping in order to reduce stresses, deflections and accelerations that occur in response to an external disturbance. The intelligent bridge system utilizes a semiactive control design. This chapter describes the methods used to design and analyze an ISB system.

This chapter commences with the development of the equations of motion of the vehicle/bridge system. This development also includes a presentation of the important actuator dynamics. The development of a Lyapunov feedback controller for ISB system is then presented, and the performance of the control design is then examined via simulation. This chapter also describes various design trade-off issues that must be addressed prior to selecting a final configuration of the components used in the assembly. This chapter closes with an estimate, based on simulation of the increased safe life of the bridge.

4.2 Bridge and Actuator Modeling

The system is comprised of three subsystems: (1) the bridge superstructure, including girders and deck (the object to be controlled); (2) the truck (the exogenous disturbance), and (3) an ISB assembly (the control actuator). Figure 4.1, which depicts a simplified version of the system, issued to discuss the various components of the system.

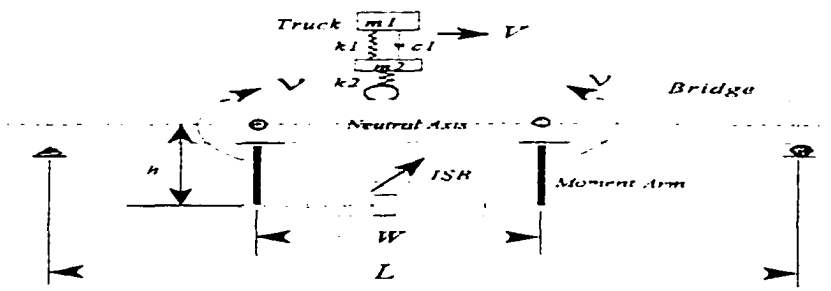

Figure 4.1 Simple span bridge with moving vehicle

4.2.1 Dynamic Equations of the Bridge

The principles that underlie the bridge control system design are best described in terms of the control of a simple pin-pin bridge girder with a quarter vehicle representation of a truck passing over the bridge. Figure 4.2 depicts a moment control apparatus affixed to the girder at points A and B.

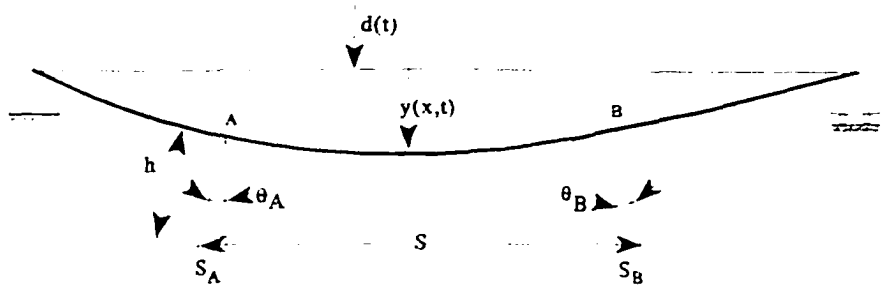

Figure 4.2 Kinematic layout of the simple span

This analysis assumes that each moment arm is attached to the girder at one point. A finite element model (FEM) of the span is first established, using beam elements (Zienkiewicz [50]).

The domain is discretized and a vector of generalized coordinates is defined as $\hat{y} = [z^T, z'^T]$. where vector, **z**, is a vector of global nodal displacements and z' is a vector of the slopes at each nodal point (the prime indicates differentiation with respect to the length of the beam). The FEM of the bridge takes the form

$$M_b \hat{\ddot{y}} + C_b \hat{\dot{y}} + K_b \hat{y} = \Gamma v + \hat{d}(t) ; \quad \hat{y} \in R^m \tag{4.1}$$

The matrices, M_b, C_b, and K_b, represent the consistent mass, the proportional damping and the stiffness of the discretized bridge superstructure. The first term, on the

right-hand side of Equation (4.1) represents the input moments to the girder produced by the ISB assembly. The matrix, Γ_{ISB}, is a Boolean matrix that provides a mapping between the global nodal unknowns and inputs. The analysis assumes that the left and right control moments, υ, provided by the ISB are equal in magnitude and of opposite sign. The disturbance input vector, $\hat{d}(t)$, represents the tire force imposed by the moving vehicle. The work here assumes that the vertical tire force is distributed to the nodes of neighboring elements, with the relative size of the input at each node determined by disturbing the total load in a linear fashion (Veletsos [5]).

4.2.2 Dynamic Equations of Hydraulic Actuator

The layout of the ISB actuator is shown in Figure 4.3. The actuator consists of a double rod hydraulic cylinder with associated plumbing. A high bandwidth flow control valve with a small battery-powered DC motor is used to regulate the orifice. The coordinate **S** represents the stroke of the piston rod which corresponds to the relative displacement between the two moment arms.

The hydraulic analysis presented here is based on an abbreviation of a recent article on the subject (Patten and Mo [52]). The analysis here assumes that the compressibility of the hydraulic fluid plays an important role in the dynamics of the actuator.

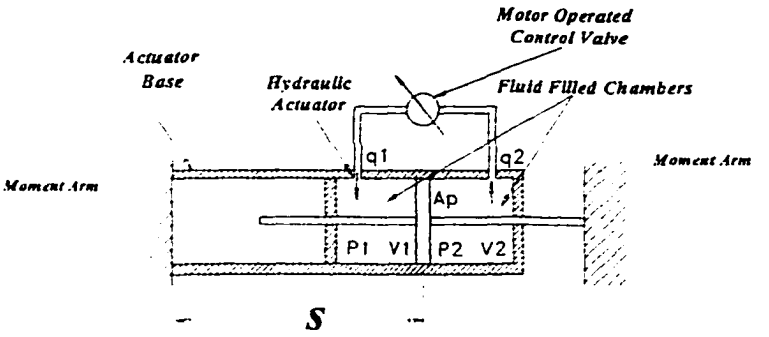

Fig. 4.3 A hydraulic actuator

The ISB dynamics can be expressed as

$$\Delta \dot{P} = -\alpha \beta (A_p \dot{S} - C_d A_v g(\Delta P)) \tag{4.2}$$

The valve orifice area, A_v, is bounded

$$0 \le A_v \le A_{VMAX} \tag{4.3}$$

The nonlinear expression, $g(\Delta P)$, has the following form:

$$g(\Delta P) \triangleq sign(\Delta P)\left(\frac{2}{\rho}|\Delta P|\right)^q \tag{4.4}$$

where the exponent **q** is 0.5 for turbulent flow through the valve. When the flow through the valve is laminar, the exponent **q** is approximately one. The transition from laminar to turbulent flow in a valve occurs when the Reynolds number is approximately 270

(Dulay [52]).

The parameter, α, represents the change in the volumetric ratio:

$$\alpha = \frac{4\ V_A V_B}{V_A + V_b} \tag{4.5}$$

where V_A and V_B represent the instantaneous volumes of each of the actuator chambers. and β represents the bulk modules of the fluid-air mix in the actuator. If β is extremely large, then the fluid-air mix is essentially incompressible. In the case of a nearly incompressible fluid, the division of both sides of Equation (4.2) by β indicates that the right-hand side of the expression is zero, leading to the simpler Bernoulli energy balance.

The work here assumes the mechanical model given in Equation (4.2), adequately portrays the hydrodynamics of the ISB actuator. A more rigorous analysis that includes the variation of density ($\dot{\rho}$) with respect to time is sometimes necessary when very large pressures are treated (Mohler [53]).

The relative velocity across the actuator is:

$$\dot{S} = \dot{S}_A - \dot{S}_B = h(\dot{\theta}_A - \dot{\theta}_B) \triangleq h(\hat{R}, \hat{y}) \tag{4.6}$$

where $\hat{R}$ is an appropriately defined Boolean vector. Substitution of Equation (4.6) in

Equation (4.2) yields:

$$\Delta \dot{P} = -\alpha \beta \{ A_p h(\hat{R}, \hat{y}) - g(\Delta P) C_d A_v \} \tag{4.7}$$

Equation (4.7) makes it clear that the actuator dynamics couple with the dynamics of the bridge. It is also evident that the two terms in the bracket on the right-hand side of Equation (4.7) represent a combination of stiffening and damping. If the valve is closed, ($A_v = 0$), then the stiffness effect dominates. On the other hand, if the valve is open, ($0 < A_v < A_{vMAX}$), then the change in pressure is due impart to the elastic deformation of the fluid and, in part, to the pressure drop across the valve.

4.2.3 Coupled Model

The coupled system Equations (4.1) and (4.7) are combined here in a more compact form. Defining:

$$\hat{x} = \{ \hat{y}^T, \hat{\dot{y}}^T, \Delta P \} \tag{4.8}$$

and noting that the applied moment in Equation (4.1) produced by the actuator is represented as:

$$v = h A_p \Delta P \tag{4.9}$$

then the following state space model is adopted:

$$\dot{\hat{x}} = A\hat{x} + Bg(\Delta P)A_v + D \tag{4.10}$$

where

$$A_{rxr} = \begin{bmatrix} [0]_{mxm} & [I]_{mxm} & [0]_{mxl} \\ [-M_b^{-1}K_b]_{mxm} & [-M_b^{-1}C_b]_{mxm} & [h\,A_p M_b^{-1}\Gamma]_{mxl} \\ [0]_{lxm} & [-\alpha\,\beta A_p \hat{R}^T]_{lxm} & [0]_{lxl} \end{bmatrix} \tag{4.11}$$

and

$$B = \begin{bmatrix} [0]_{mxl} \\ [0]_{mxl} \\ [-\alpha\,\beta\,C_d A_p] \end{bmatrix}, \qquad D = \begin{bmatrix} [0]_{mxl} \\ [d(t)]_{mxl} \\ [0]_{lxl} \end{bmatrix}$$

where l is the number of actuators, **m** is the order of the beam model, and **r=2m+l**. Equation (4.10) provides the setting for a control design study. Two observations are made here. First, the eigenvalues of **A** all have negative real parts, except one, which is zero. It could be argued that leakage around the piston eliminates the zero eigenvalue. An alternative argument that more readily assures the stability of the system is made by linearizing $g(\Delta P)$. That step will always produce a negative coefficient in the $a(r,r)$

entry, even at $\Delta P = 0$, because the index q is 1 at $\Delta P = 0$. The local asymptotic stability of the plant is therefore assured. The global asymptotic stability is not assured, as a consequence of the following observation. Given some initial condition and assuming the disturbance is 0, then in order to return the system to its original state, the valve would have to be left open beyond some finite point in time. If the valve was closed prematurely and remained closed, then the elastic energy trapped in the hydraulic fluid would never theoretically dissipate. In that case, the actuator would prevent the girder from returning to its original equilibrium position. It is also noted that if β is very large, then the matrix A becomes ill-conditioned; thus, leading to a so-called stiff system of equations. Care must therefore be exercised when simulating the combined system in order to avoid numerical instabilities.

4.3 Semiactive Controller Design

An inspection of the system (Equation 4.10) indicates that the variation of the valve orifice area is the only direct means of altering the performance of the system. The inherent (local) stability of the system suggests that any control rule will ultimately produce quiescence (for a bounded input with finite duration). For example, by simply fixing the valve at its maximum opening ($A_{I_{MAX}}$), the ISB becomes a fixed (nonlinear) damper. In that case, the structural and fluid damping will eventually dissipate any energy imparted to the system by the disturbance.

4.3.1 Basic Semiactive Control Law

The nonlinear form of the system's equations makes the controller design problematic. One direct approach to the problem, that produces a sub-optimal control, is referred to as a clipped optimal design (Patten [54]). That procedure uses feedback linearization to eliminate the nonlinear characteristic of the valve. A linear valve process model is substituted instead, and a linear quadratic controller is employed which produces a full-state feedback control. Clipping is necessary when the commanded force output is nondissipative. In that case, the valve is closed. The approach works, but the design fails to capitalize on the full effectiveness of the actuator.

The work presented here relies on a classic Lyapunov formulation that produces a direct control decision, which seeks to achieve a sequence of control actions that maximize the rate of dissipation of the system. A design approach that has been utilized many times in the past to design a regulation or for a nonlinear plant with saturation limits on the control variable, is adopted here (Hatada and Smith [32]).

The design first poses a scaler measure of the equivalent energy of the system (the Lyapunov function):

$$V = \frac{1}{2}(\hat{x}^T, Q\hat{x}) \tag{4.12}$$

Here, the existence of a positive semi-definite **Q** matrix is assumed. The dissipation of

the equivalent energy is obtained by differentiation of V.

$$\dot{V} = \hat{\dot{x}}^T Q \hat{x} + \hat{x}^T Q \hat{\dot{x}} \tag{4.13}$$

Substituting Equation (4.10) into Equation (4.13), the control is achieved by finding:

$$\max\{-\dot{V}\} \tag{4.14}$$

where

$$\dot{V} = \hat{x}^T (A^T Q + Q A) \hat{x} + \hat{x}^T Q B g(X) C_d A_v + \hat{x}^T Q D \tag{4.15}$$

It is assumed that a **Q** exists and that $A^T Q + Q A$ can be selected negative semi-definite. The last expression on the right-hand side of Equation (4.15) is disregarded, because there is nothing that can be done to affect the dissipativeness of that term. Writing **Q** as a matrix of column vectors:

$$Q = [\hat{q}_1, \hat{q}_2, \ldots\ldots \hat{q}_r] \tag{4.16}$$

and noting that the only nonzero entry in **B** is the last element ($b_n = h A_p$), then, the selection of an appropriate value of A_v is governed by the following rule:

$$x^T \hat{q}_r \, sign(\Delta P) \begin{cases} \geq 0, & A_v = A_{vmin} \\ < 0, & A_v = A_{vmax} \end{cases} \tag{4.17}$$

Here the reduction of the nodal displacement amplitude at the center of the bridge is the objective of the control action. The control is referred to as a bistate or Bang-Bang control. The vector $\hat{q}_r$ provides a means of weighing the different states to emphasize a particular control objective. The emphasis of this design here was the reduction of the nodal displacement amplitude at the center of the bridge. The elements of $\hat{q}_r$ were selected without regard to the definiteness of the **Q** matrix in the Lyapunov formulation. Recall that any control must stabilize the plant. The particular form of **Q** is of no consequence. If the effort is made to discover a **Q** matrix that does satisfy the Lyapunov equation, then the last column of **Q** can provide a means of establishing the feedback gains. The block diagram of the Lyapunov bisatate controller is shown in Figure 4.4.

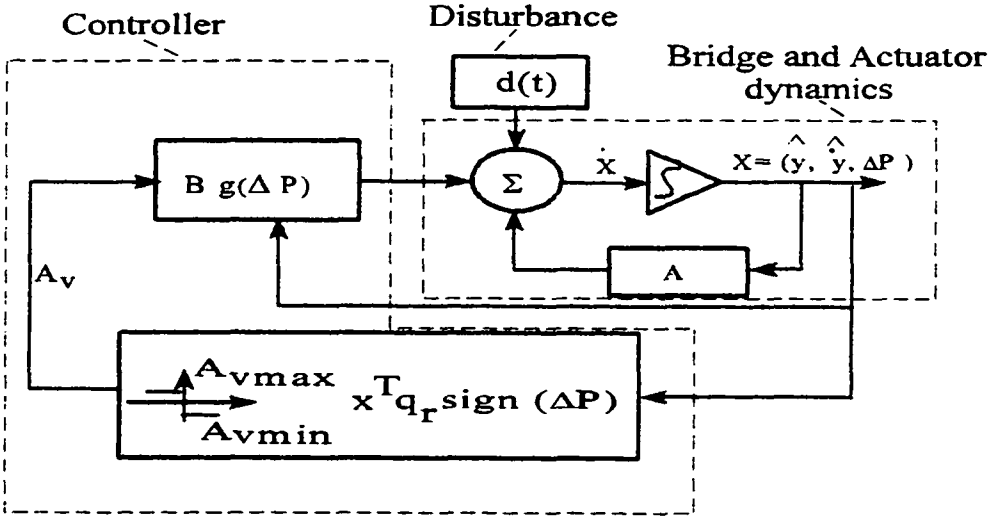

Fig. 4.4 Block diagram of the Lyapunov bistate controller

4.3.2 Modified Control Law

In an actual implementation of the proposed nonlinear controller, the effect of discontinuities across the singular switching points ($x^T q_r sign(\Delta P) = 0$) has to be considered. This feature leads to chattering due to a high-frequency switching. The degree of this effect depends on the size of the dead-zone and the maximum control force. This effect is undesirable in practice, since it involves the high-speed switching of the DC motor.

To eliminate this undesirable effect and make the controller perform properly, a deadband is introduced into the basic control law. This modification is achieved by smoothing out the control discontinuity in a thin boundary neighboring the switching points. The boundary layer is defined as:

$$\| x^T q_r sign(\Delta P) \| \le C_L, \quad C_L > 0 \tag{4.18}$$

As shown in Figure 4.5, when the left hand side of the inequality is less then C_L, the control variable A_v is not changed.

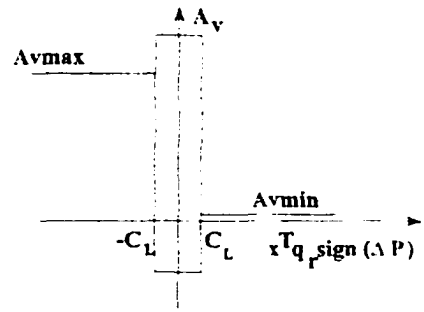

Figure 4.5 Introduction of the deadband

The control law (Equation 4.17) is therefore modified in actual practice in the following way:

$$x^T \hat{q}_r \, sign(\Delta P) \begin{cases} \geq 0, & A_v = A_{vmin} \\ < 0, & A_v = A_{vmax} \end{cases}, \qquad |x^T \hat{q}_r \, sign(\Delta P)| \geq C_L$$

$$A_v(n-1) = A_v(n), \qquad |x^T \hat{q}_r \, sign(\Delta P)| < C_L \tag{4.19}$$

The modified control law (Equation 4.19) is in the form of bang-bang controller with deadband, This modification eliminates the high-frequency switching or chatter.

4.4 Numerical Simulation

The derivation of the control law, in the above section, relied on a model of the system that treated the forces imparted by the truck's tire as an exogenous input. In order to assess the performance of the control, a simulation study is conducted that uses a quarter car model to represent the vehicular input. The parameters of this model reflect a generic truck. It is important to use a compliant model of the truck because a large majority of heavy trucks on the road today are equipped with suspensions that resonate at frequencies that correspond closely with one or more of the fundamental modes of the bridge. The coupling between the truck and bridge is realized via the force in the tire which is a direct function of the relative deflection between the bridge deck and the truck axle. That coupling gives rise to a nonautonomous bridge/truck dynamic model (see Chapter Three).

The kinematics of the truck model are depicted in Figure 4.6. The equations of motion of the quarter car are:

$$\begin{aligned} m_1 \ddot{z} &= k_1(z_2 - z_1) + c_1(\dot{z}_2 - \dot{z}_1) \\ m_2 \ddot{z}_2 &= -k_1(z_2 - z_1) - c_1(\dot{z}_2 - \dot{z}_1) + K_{tire}[(\hat{\varphi}(t), \hat{y}) - z_2] \end{aligned} \tag{4.20}$$

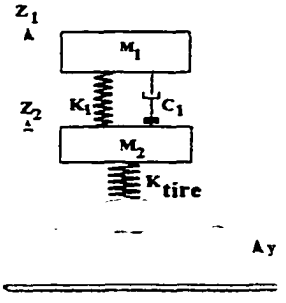

Figure 4.6 Quarter vehicle model

$\hat{\varphi}(t)$ is a vector that maps the beam nodal coordinates into the current position of the truck tire. When the truck tire is between any two adjacent nodal points, N and N+1, then $\hat{\varphi}(t)$ has the following form:

$$\hat{\varphi}(t) = [0, 0, ...,\varphi_N, \varphi_{N-1}, 0,.....0] \tag{4.21}$$

where

$$\varphi_N = 1 - \frac{x - x_N}{\Delta}, \quad \varphi_{N-1} = \frac{x - x_N}{\Delta} \tag{4.22}$$

and where Δ is the element length. The disturbance input to the bridge is then:

$$\hat{d}(t) = \hat{\varphi} K_{tire} [z_2 - (\varphi, \hat{y})] \tag{4.23}$$

Equations 4.10, 4.20 and 4.23 define the coupled bridge truck system. This particular formulation disregards the influence of the road roughness on dynamics. This is reasonable when the dynamic response of the bridge and vehicle are coupled at near resonance conditions. In that case, the response due to the coupling is many times larger than the response due to the rough texture of the bridge deck surface.

4.4.1 A Simple Span Girder

In order to demonstrate the performance of the system, a simplified beam model of a bridge is utilized first. A 30.48 m simply-supported girder with properties corresponding to the actual girder of the bridge is used. The girder is discretized into 40 uniform beam elements [55] (Figure 4.7). Noting the boundary conditions ($y(0,t) = y(L,t) = 0$), then there are 78 degrees of freedom (DOF); 40 nodal rotations and 38 nodal displacements. The significant features of the simulation are the static weight of the quarter vehicle (W=25 ton), the forward speed (V=105 km/h), and the initial conditions of the vehicle are defined as follow: ($Z_1(0) = 0.0$, $\dot{Z}_1 = 0.0$, $Z_2(0) = -0.34m$, $\dot{Z}_2 = -0.09m/s$). The nonzero values are presumed to reflect the typical excitation imparted to a truck's suspension when the entrance approach is uneven.

The parameters used in the simulation were as follows: the bridge girder... $E = 1.96 \times 10^{11} (N/m^2)$, $I = 0.048\ (m^4)$, $A = 0.084\ m^2$; the moment arm... $W = 12.2\ m$, $h = 2.54\ m$; the truck..., $v = 28.88\ m/s$, $w = 1.91 \times 10^5\ kg$, $m_1 = 1.6 \times 10^4\ kg$, $m_2 = 1.75 \times 10^5\ kg$, $k_1 = 4.7 \times 10^5\ N/m$, $k_2 = 6.33 \times 10^5\ N/m$, $c_1 = 1.7 \times 10^4\ N \cdot s/m$; and the actuator... $A_p = 4.013 \times 10^{-2}\ m^2$, $A_{vmax} = 1.394 \times 10^{-5}\ m^2$, $A_{vmin} = 0$, $C_d = 0.82\ (0.52)$, $\alpha = 1.14 \times 10^{11}\ N/m$, $\beta = 8.7 \times 10^7\ N/m$, $\rho = 8.83 \times 10^2\ kg/m^3$.

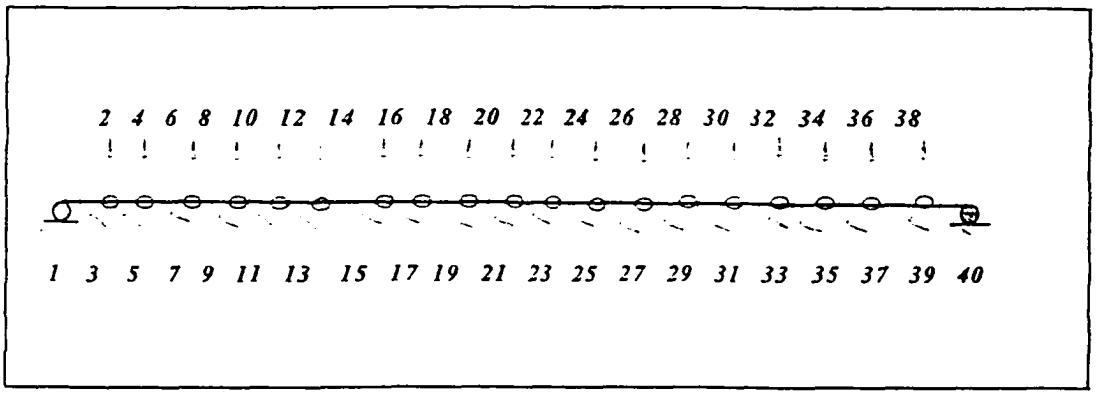

Figure 4.7 The single span analytical bridge FE model

Figure 4.8 depicts the deflection of midpoint of the girder versus time. The peak and RMS value of the deflection have been reduced by 61% and 52%, respectively.

In order to extract creditable moment information from the FEM, a fine mesh about the points where the moment acts on the girder is used. This is necessary, because the moment is proportional to the second derivative of the displacement with respect to the length of the girder. The beam element used in this work provides only a poor

estimate of that second derivative information. It is also possible to increase the accuracy of the second derivative by using higher order elements. The moment-time history at the center of the beam is shown in Figure 4.9.

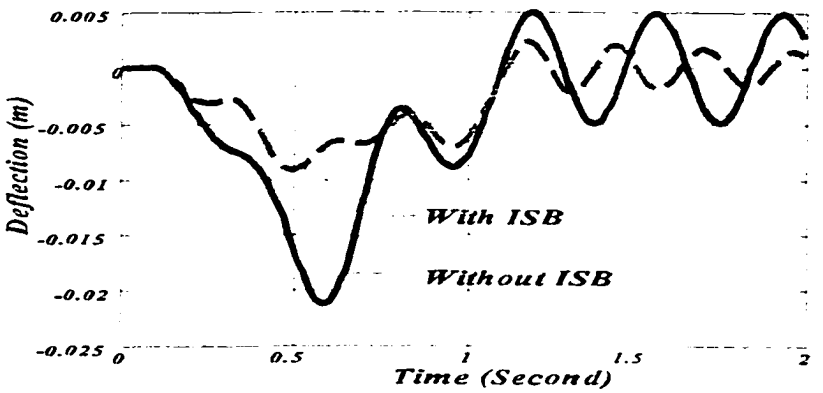

Figure 4.8 Simulation of controlled vs. uncontrolled deflection at center of the simple span, W= 12.2 m, h=2.54 m, L=30.48 m

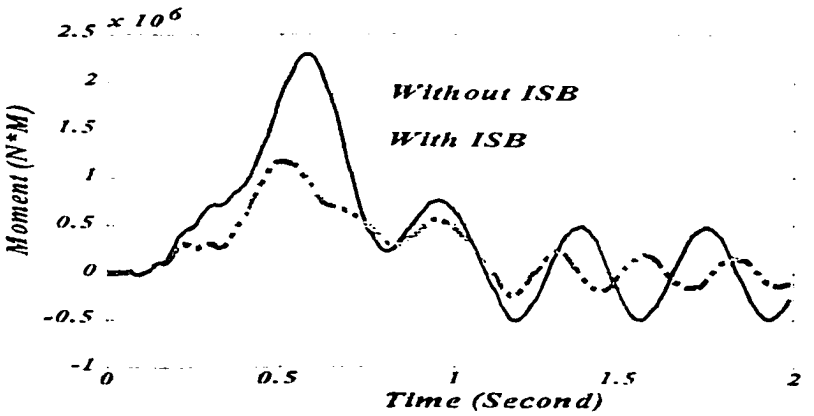

Figure 4.9 Moment time history at the center of the simple span (bottom flange): L=30.48 m, W=12.2 m, h=2.54 m

The maximum moment is reduced 52% when the control is applied. A plot of the

maximum moment over all time, at each point along the girder, is displayed in Figure 4.10.

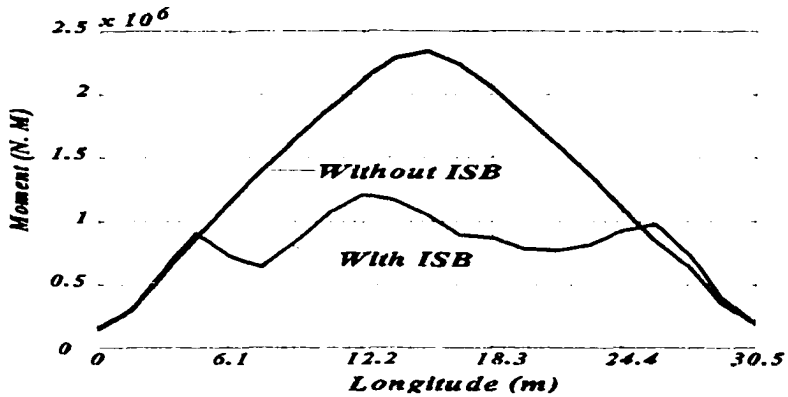

Figure 4.10 Maximum moment distribution at each point along the girder L=30.48 m, W=12.2 m, h=2.54m

This plot indicates that, at the points where the actuator assembly is attached, the moment is less than anticipated. The clear indication is that the ISB system flattens out the moment curve; thus, reducing the net strain almost every where along the girder.

The selection of an appropriate ISB system arrangement requires a trade off analysis. Various configurations and parameter values are possible, including the cylinder size of the actuator, the bulk modules of the fluid, the distance between moment arms and the moment arm height **h** from nutural axis of the bridge girder. Figure 4.11 depicts the effect that a change in **h** has on the reduction of peak moment. The decrease in effectiveness is approximately linear with the decrease in **h**.

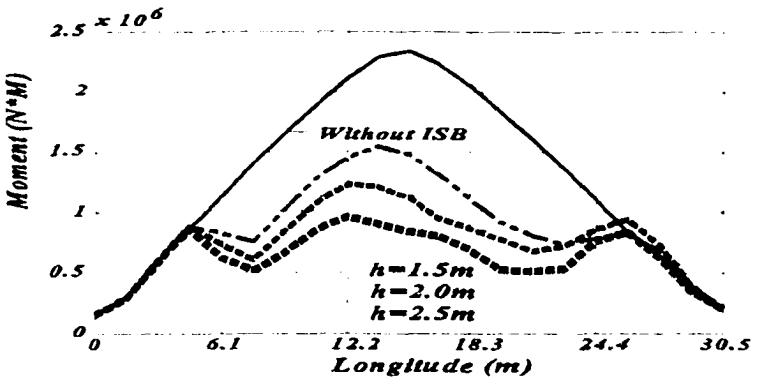

Figure 4.11 Variation of maximum moment at each point along the girder vs. h, L=30.48 m, W=18.28 m

The sensitivity of the maximum moment to the variation of the distance between moment arms (at a fixed **h**) is shown in Figure 4.12, and the result indicates that the maximum moment is insensitive to charges in **W** for **h=1.5m**. The results of the trade-off analysis are strongly effected by the boundary conditions and height of the moment arms.

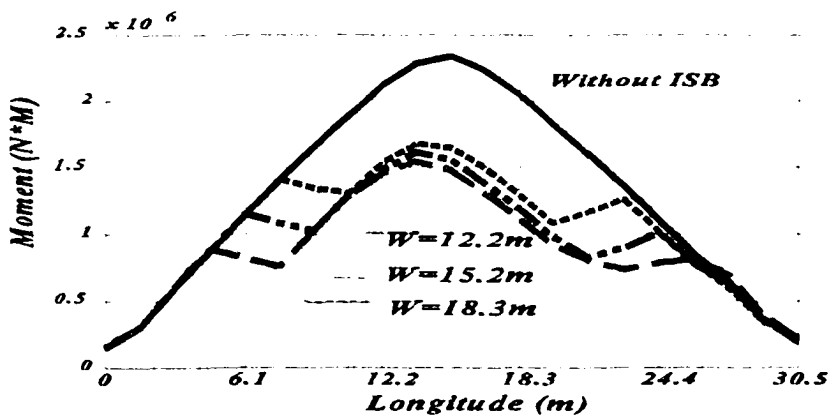

Figure 4.12 Variation of maximum moment at each point along the girder vs. W, L=30.48 m, h=1.5m

It is also noted that the local stress concertation at the points of attachment of the moment arms is sensitive to charges in **W.** This factor has to be taken into account in design of a ISB assembly.

4.4.2 A Continuous Girder

The work reported in this section reflects a preliminary analysis of the design of a ISB system that has been installed on an in-service interstate highway bridge. The Walnut Creek Bridge on I-35 in Oklahoma is a two-lane structure, consisting of five 122m (400') long continuous girders supported by intermediate piers at 30.48 m (100') intervals and by abutments at either end. The girders are supported by a fixed shoe at the center pier and ball/roller shoes at the other support points. A single girder model of the bridge is used here to demonstrate the extension of the analysis to a multi-span system. As in the actual field experiment, the ISB system is assumed to be attached to the girders in the third span only (Figure 4.13).

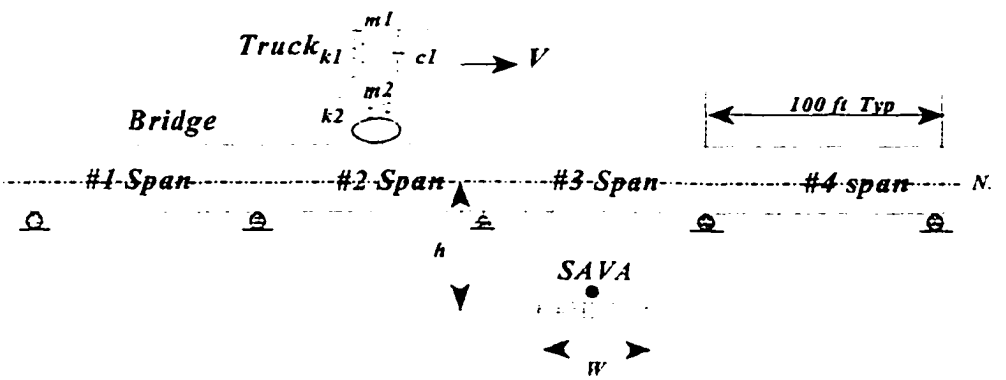

Figure 4.13 Four span bridge with traveling vehicle

The four span single girder bridge FE model is shown in Figure 4.14.

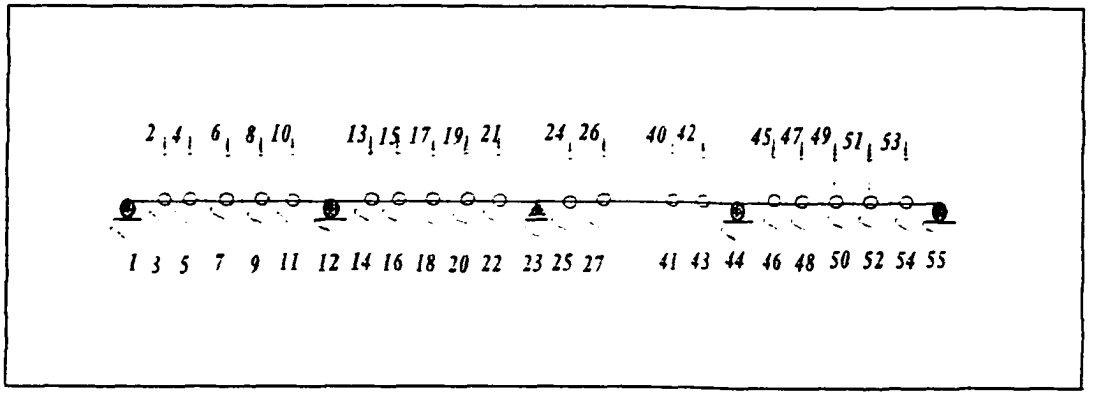

Figure 4.14 The four span bridge FE model

The quarter vehicle model, used in the simulation of the 30.48 m single span, is also used in this simulation. The ISB system is bolted to the girder with the moment arms located 4.57m (15') each way from the center line of the girder. The distance between the neutral axis of the girder and the line of action of the ISB actuator is **h=2.54m**, The speed of the vehicle is assumed to be 65 mph. The form of $\hat{q}_r$ used in this study is given in the Appendix I. The deflection time history of the midpoint of span # 3 is shown in Figure 4.15. The ISB reduces the peak defection by 75% and the RMS deflection by 50%.

The simulation makes it obvious that the truck suspension couples strongly with the bridge, and that the ISB has a significant mitigating effect for the entire time that

the vehicle is on the bridge.

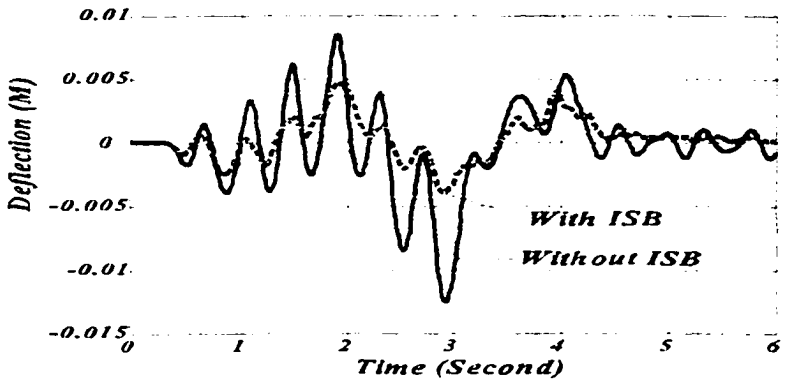

Figure 4.15 Deflection time history at midpoint of third span, a. without ISB, b. with ISB (h=2.54m, W=12.2 m)

The moment time history of the third span is shown in Figure 4.16. The ISB produces a 50% reduction in the maximum moment and a 50% RMS reduction of the entire time history of the moment. The peak (maximum) moment at each point along the third span is plotted in Figure 4.17. The figure once again confirms that the ISB tends to reduce the moment along the entire span and not just at the middle of the span.

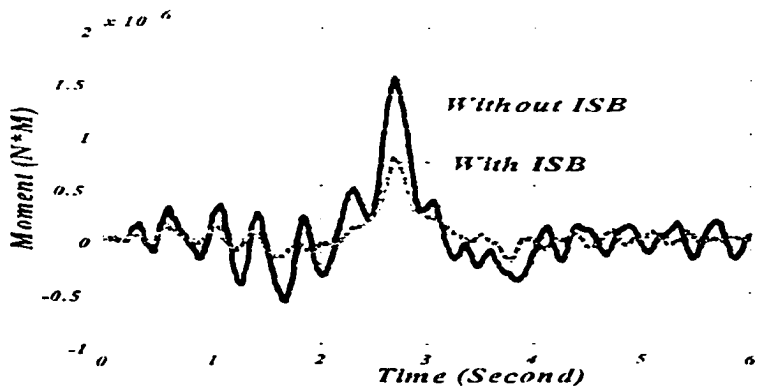

Figure 4.16 Moment time history at the center of the third span (h=2.54m, W=12.2 m)

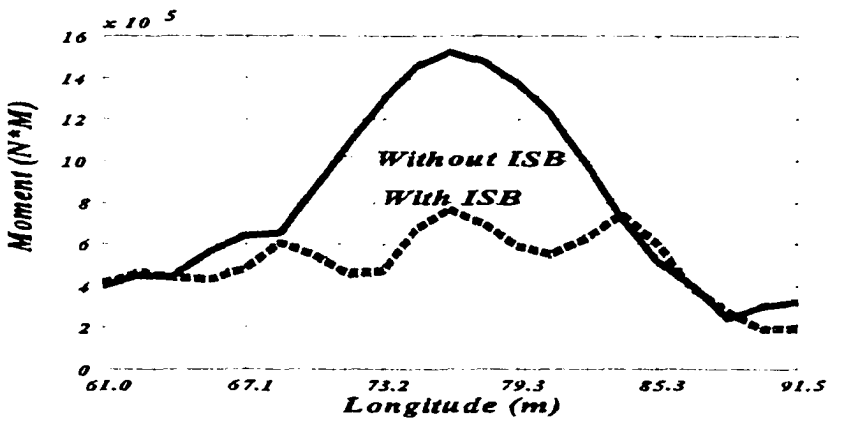

Figure 4.17 Maximum moment time history at each point along the third span (h=2.54m, W=12.2 m)

A snapshot of the moment along the entire girder, when the vehicle is at the center of span # 3, is shown in Figure 4.18. That figure suggests that, while the dominate effect of the ISB is experienced in the span it is mounted on, it also provides some mitigation of the moment in the remaining spans.

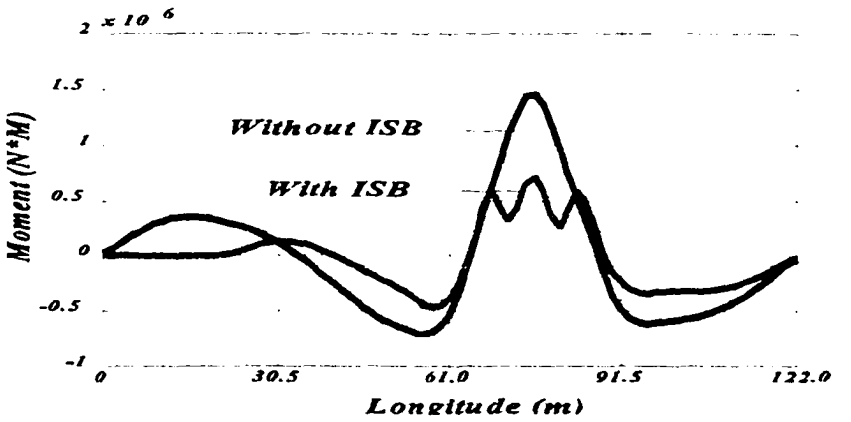

Figure 4.18 Moment distribution when the vehicle is at the center of the third span (h=2.54m, W=12.2 m)

An important consideration in the design of the ISB actuator is the amount of stroke that is expected to occur. The stroke and the stroke velocity, along with the pressure and piston area of the actuator, are used to select appropriately sized plumbing and valving for the ISB. The stroke of the actuator, with the control time history superimposed on it is shown in Figure 4.19. The force output of the actuator, with the time history of the control, is shown in Figure 4.20. Both the stroke and the force output are considerably larger in practice, because the most aggressive loads and deflections are produced by multi-truck loadings.

One indicator of the degree of dissipativeness, is the plot of the force output of the ISB versus the relative velocity across the actuator (Figure 4.21). A completely dissipative device produced a trace that lies in quadrants 2 and 3 only. The occasional storage of elastic energy in the ISB fluid results is some nondissipative action. That stored energy is used to resist the motion of the girder.

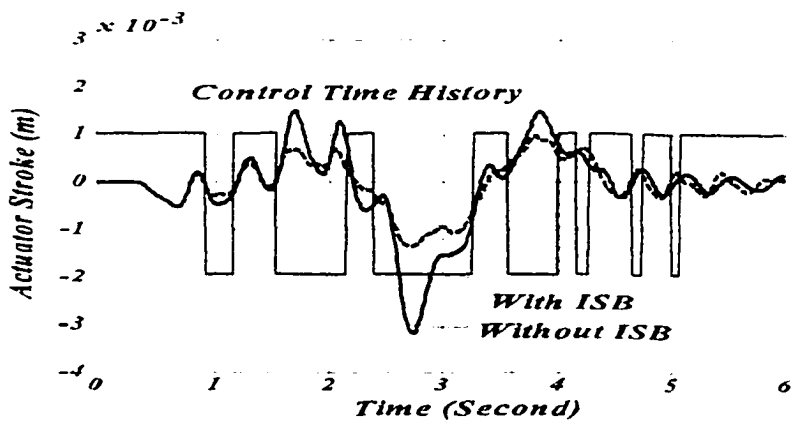

Figure 4.19 Actuator stroke and control time history

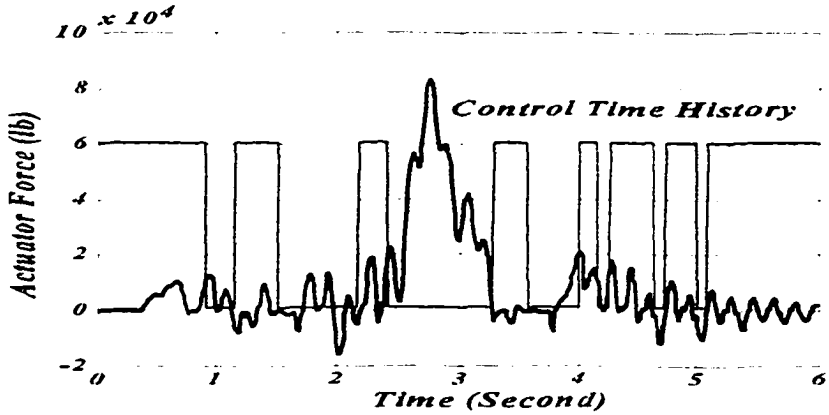

Figure 4.20 simulated actuator force and control time history

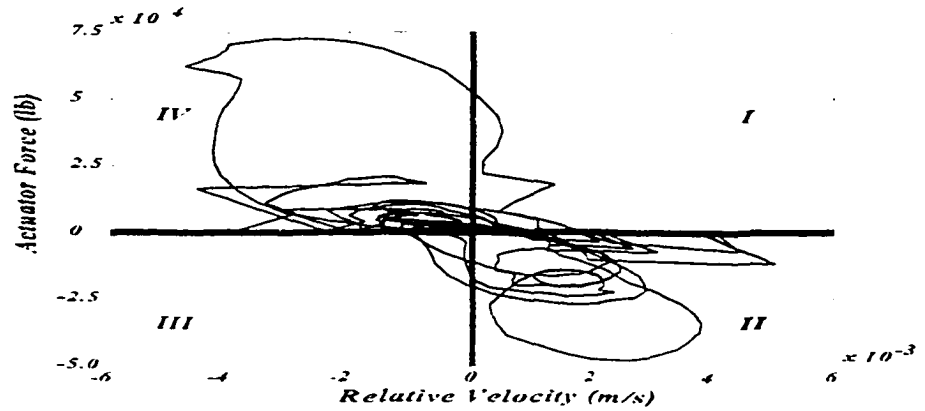

Figure 4.21 Actuator force vs. relative velocity of piston

It is also useful to track the system energy and its dissipation. **E** is the total kinematic and potential energy of the bridge and the ISB actuator. The time history of **E** and $\dot{E}$ are shown in Figures 4.22 and 4.23. It is clear that the ISB effects a significant

reduction of the system energy when the truck is in span = 3. These two figures confirm that the energy is (as expected) positive semi-definite. While the sign of the dissipativeness $\dot{E}$ is effected by the disturbance, obviously once the truck has left the bridge, the vibration diminishes to 0.

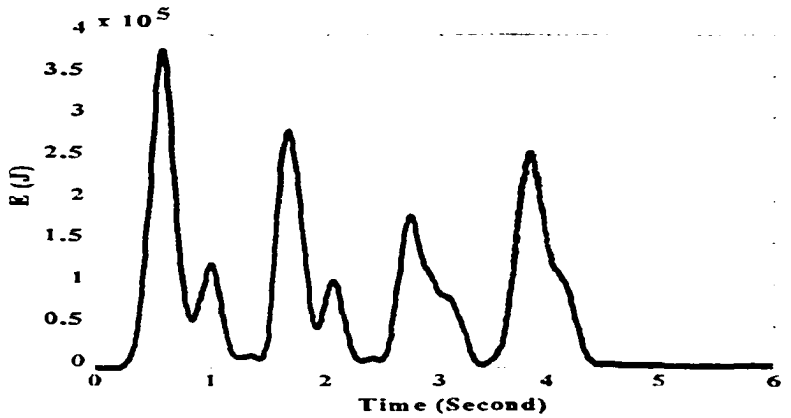

Figure 4.22 Time history of the kinematic and potential energy in the bridge/vehicle system

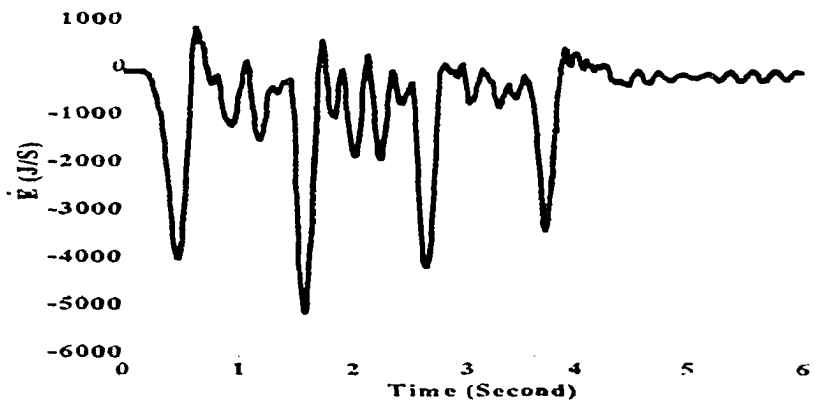

Figure 4.23 Time history of $\dot{E}$

As a closure to this section, the following question raised by many engineers is addressed, " why not simply install a stiffener?" A simulation of the moment response of the bridge, when the hydraulic actuator is removed from the moment assembly and replaced with a steel element, is shown in Figure 4.24. This result is compared to the ISB performance. The maximum moment produced by the fixed stiffener is evidently larger. The most important issue is, however, that the stiffener will produce an increased moment for all loadings. The ISB system is equipped with intelligence, and it simply relaxes for most of the vehicular traffic. When that occasional heavy truck crosses the bridge, then the ISB becomes active. The passive strut will therefore realize many more fatigue cycles than the ISB system.

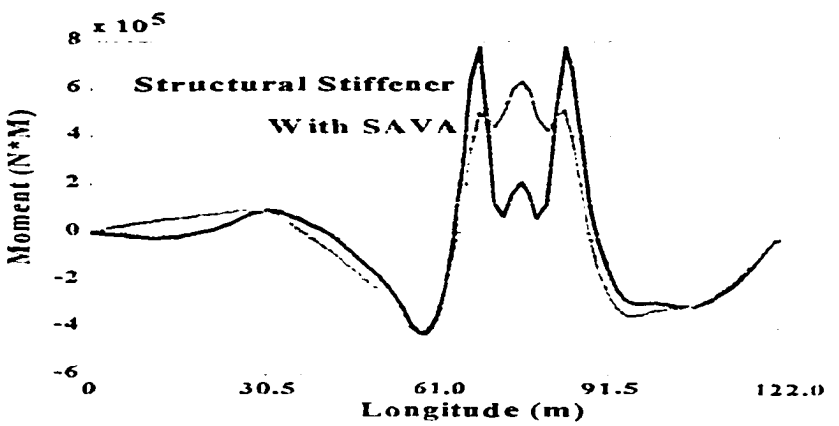

Figure 4. 24 Moment distribution when the truck is at center of third span (h=2.54 m, W=12.2 m)

4.5 Safe Life Predictions

The purpose of the ISB is to afford a means of extending the service life of a bridge. It does that by reducing the stress range that is a consequence of the passage of a heavy vehicle. A Federal study (NCHRP 299) established a means of assessing the remaining fatigue life of a steel bridge. The relationship, which is based on Miner's Rule, is applied here to the simple girder that was used in the above analysis. The remaining safe life, y_F, is determined using:

$$Y_F = \frac{f K 10^6}{T_a C (R_S \cdot S_{RC})^3} \quad a \tag{4.24}$$

We assume values of the parameters that are consistent with the actual bridge that is being retrofitted with the ISB actuators: f=1 (for safe life), **K** is a detailed constant taken here to be 12, $R_S = 1.35$ is a reliability factor, C=1 is the number of cycles of stress reversal (which can be determined via rainfall counting). $T_A = 3000$ is the estimated life time average truck volume and,. $a = 25$, is the present age of a bridge.

Noting that $E = 1.96 \times 10^{11} (N/m^2)$, $I = 0.048 (m^4)$, $\frac{1}{2} d = 0.7 (m)$ for the girder, and the maximum moment without control was $2.34 \times 10^6 (N.m)$, then the maximum stress is:

$$S_{max} = \frac{M_{max} \cdot y}{I} = 3.4125 \times 10^7 \, N/m^2 \tag{4.25}$$

The remaining safe life without the control system is then:

$$Y_{F_{NC}} = \frac{1565}{(4.9)^3} - 25 = 11.7 \tag{4.26}$$

Recall that the maximum stress was reduced **55%** with the control. The remaining safe life with the control system attached is

$$Y_{F_C} = \frac{1565}{(0.55)^3 \times (4.9)^3} - 25 = 55 \textit{ years} \tag{4.27}$$

The ISB, therefore, extends life of the bridge by approximately **65** years.

4.6 Conclusions and Recommendations

This chapter presented a tutorial on the methods used to design an ISB system for application to bridges. The control synthesis was accomplished assuming the vehicle loads to be exogenous. A Lyapunov criteria was utilized to discover a feedback control rule. The limit(s) on the valve orifice area coupled with the objective to maximize the negativity of the dissipation ($\dot{V}$) produces a bistate control logic.

The effectiveness of the design was tested (via simulation) by reforming the system model to include the chassis dynamics of a truck. The model preserves the coupling between the bridge and truck. The full model, which is nonautonomous, was then used to simulate the controlled response. The truck model represents the largest class of heavy truck suspensions, that very often exhibit modal frequencies that are

similar to the fundamental modes of many highway bridges. The near resonance between the truck and bridge result in large impact loads. The simulation does not address the effects due to deck roughness, because those effects are almost negligible when compared to the resonance effects. On the other hand, the analysis and design of ISB for short span bridges (less than 15.25 m) may require more attention to surface roughness, because the resonance effect is less an issue with short span bridges.

The analysis relies on a nonlinear model of the ISB hydrodynamics that couple the actuator to the bridge girder. The magnitude of the pressures (forces) produced by the ISB are relatively small, which made it possible to neglect the sometimes important effect produced by variations with pressure of the bulk modules. The model also assumed that the flow through the valve is incompressible, which is usually an acceptable assumption when studying the short term performance of the ISB system.

The control design was shown to be straightforward. The task was made particularly simple by the observation that the bistate control is stabilizing, no matter what criteria is adopted to facilitate a decision on when to make a switch. A simple control rule was adopted and simulations with a 30.48 m pin-pin span were conducted. The control law used in the simulation represents a least cost (for hardware) solution in that only two sensors collocated with the actuator in the vicinity of the center of the span are needed. A strain gauge on the girder, or a displacement transducer that measures the stroke of the cylinder, would be necessary to determine the displacement of the girder at its center. A differential pressure sensor is also required at the ISB

actuator. A trade off analysis between the height of the ISB moment arms and the length of the ISB, was also included. The results indicate that the controlling design variable is the height of the moment arms. An ISB system was also demonstrated for a continuous four-span girder bridge. The results indicate that the system achieves more than a 70% reduction of deflection and a reduction of peak moment range (or stress range) of approximately 60%.

While other alternative kinematic arrangements of the ISB assembly are possible, this chapter did not explore that topic.

CHAPTER FIVE

ROBUST STABILITY OF A BRIDGE/VEHICLE COUPLED CONTROL SYSTEM

5.1 Introduction and Literature Review

The assessment of the stability robustness of control systems has been the focus of much research since the early 1980's. As a consequence of that research, major progress has been made in the development of tools for the design of robust stabilizing feedback control systems. Much of the current interest in robust control system design is focused on those techniques which utilize the variable structure control method and Lyapunov's second method. Variable structure control methods include: (a) sliding mode controllers; (b) direct and indirect adaptive controllers; and (c) robust design and analysis via linear matrix inequalities. Lyapunov's second method is the most general approach used to assess the stability of dynamic systems, because it provides both local and global results that can be applied to time-varying and nonlinear problems. The application of Lyapunov's second method involves two key components: (1) finding functions that bound the magnitude (or Euclidean norm) of uncertainties and (2) searching for a robust Lyapunov function and then determining a stabilizing control that coincedently guarantees stability. The principal idea behind the Lyapunov second method is reflected in the following statement: if the rate of change of the energy of an isolated physical

system is negative for every possible state (except for the equilibrium state), then the energy will continually decrease until it finally reached its minimum value. In other words, a dissipative system perturbed from its equilibrium state will always return to it.

The objective of this chapter is to present the methodogy for the design of a robust semiactive controller. The control objective of the ISB system is to mitigate the vibrations of a bridge which are induced by moving vehicles. The model uncertainties caused by bridge/vehicle coupled dynamics have the potential to degrade the performance of an otherwise well designed control system. It is common knowledge that if a control system is powered (active control system), then a non-robust control design could result in the distabilization of the system. There is no other evidence that a semiactive system (unpowered) can be destabilized because the control design far to be robust. On the other hand, there are no guarantees that a non robust design for a semiactive system is robust. The work here examines the robustness of the Lyapunov controller that was presented in the preceding chapter. recall that a bridge/vehicle coupled model was presented in Chapter Three. It was shown that the coupled model evidenced a 6.5% variation of the bridge modal frequencies. It is then apparent that the control design based on the uncoupled bridge truck model must be capable of stabilizing the bridge in spite of an inexact model of the system. The material presented in the following paragraphs demonstrates that the bridge control design is robust to model uncertainties.

The robust stability analysis of uncertain systems with unknown, time-varying, but bounded uncertainties, has received much attention in the recent literature. Numerous

criteria have been devised that, if satisfied, will guarantee the stability of the system. The criteria are usually overly conservative due to the fact that they are based on necessary as opposed to sufficient conditions. Kalman first introduced the Lyapunov "second method" in 1960 [56]. In his paper, Lyapunov's second method was described in detail, The presentation also included a discussion of the design of a control based on the method. Leitmann in 1979 [57] applied Lyapunov's second method to linear systems with bounded uncertainties. He developed a state feedback controller that guaranteed the global uniform asymptotic (Lyapunov) stability of the zero state in the presence of norm bounded uncertainties using the "matching condition" method. Petersen in 1987 [58] proposed a stabilization algorithm for a class of uncertain systems. In his paper, a definition is the so called "rank-1 uncertainty definition" was given, then a particular algebraic Riccati equation is derived to create a addition condition was used to created a constant state feedback control law. Barmish in 1988 [59] proposed a necessary and sufficient condition for the quadratic stabilizability of an uncertain system using Lyapunov's second method. Slotine in 1990 [60] suggested that a special Lyapunov function could be applied to verify the stability of a time-varying linear system. Brogan in 1991 [61] also discussed the stability problem for linear time-varying systems. He proposed the frozen coefficient method which can be used to verify stability for some linear time-varying systems. None of the techniques proposed to date provide a universal means of assuring the stability of nonautonomous system. The problem of stability for time-varying system remains open.

5.2 Problem Statement

Consider a bridge equipped with a semiactive actuator perturbed by a moving vehicle. The system is comprised of three subsystems; **a bridge girder** (the object to be controlled), **a vehicle** (the exogenous disturbance) moving across the bridge at a constant speed, and **a semiactive actuator** (the controller).

Figure 5.1 indicates the flow of energy for the closed loop system. The bridge and vehicle are a coupled system. The actuator is capable of storing and dissipating energy. If the service valve is fully closed, the actuator functions as a spring component; in that mode, the actuator is nondissapative. On the other hand, if the valve was fully opened, the actuator functions primarily as a fluid damper. Even when the valve is open, it is possible to compress the field; thus, providing a means for storing energy as well. The control design used here, however, demands that the valve be either fully closed or fully open. When the valve is fully open, the amount of fluid compression that occurs is negligible and can be, for all practical considerations, disregarded.

The semiactive control system is a combination of both. The bistate control therefore provides a dual natured passive device; an energy storage element or an energy dissipator. Past work has demonstrated that the semiactive control system can provide performance that is nearly equivalent to that provided by a fully active system, when the objective of the control is the mitigation of vibration.

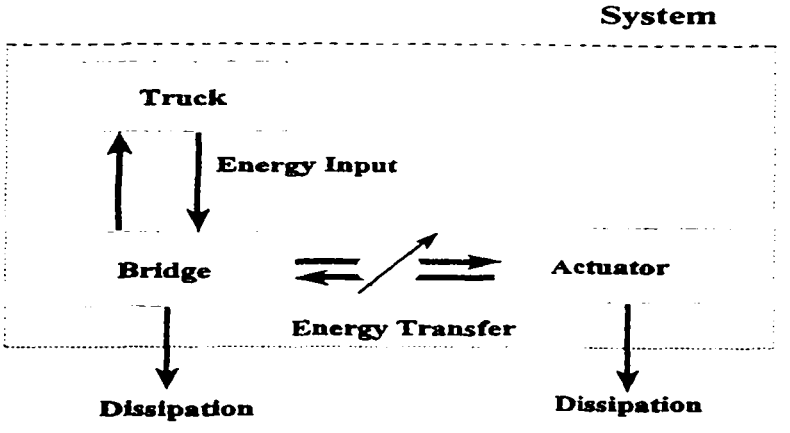

Figure 5.1 The system energy flow chart

The active system however requires power, while the power needed to actuate a semiactive system is much magnitudes less than the energy dissipated (or stored).

5.3 Robust Lyapunov Semiactive Controller Design

Recall that the state space form of the coupled bridge/vehicle model with a semiactive actuator is:

$$\dot{x} = \bar{A}(t)\,x + B\,u \tag{5.1}$$

where x is a vector of generalized coordinates of the bridge/vehicle coupled system. $\bar{A}(t)$ can be represented as the additive sum of a nominal (constant) system matrix $\bar{A}$ and a matrix of time-varying uncertainties, $\Delta\bar{A}(t)$, or:

$$\bar{A}(t) = \bar{A} - \Delta\bar{A}(t) \tag{5.2}$$

where

$$\bar{A} = \begin{bmatrix} 0 & I \\ -M^{-1}K & -M^{-1}C \end{bmatrix}, \qquad \Delta\bar{A}(t) = \begin{bmatrix} 0 & 0 \\ -M^{-1}\Delta K(t) & 0 \end{bmatrix} \tag{5.3}$$

and

$$\Delta K = \begin{bmatrix} k_{tire}\,\Psi(t)\,\Psi(t)^T & k_{tire}\,\Psi(t)\,\Phi(t)^T \\ -k_{tire}\,\Phi\,\Psi(t)^T & k_{tire}\,\Phi\,\Phi^T \end{bmatrix} \tag{5.4}$$

Recall that the nature of the uncertainties Equation (5.4), is associated with the stiffness coupling between the bridge and the truck, and the fact is that the truck's position is changing with time. The control input matrix **B** remains constant. The ISB actuator hydraulic equations can be combined with motion equations of the bridge. A more compact form can be obtained by combining ISB hydraulic dynamic equations with Equation (5.1) (refer to Equation 4.1-4.10) as:

$$\dot{\hat{z}} = A(t)\,\hat{z} + B\,g(\Delta P)A_v \tag{5.5}$$

where $\hat{z} = [x, \Delta P]$ and

$$A(t) = \begin{bmatrix} [0]_{m\times m} & [I]_{m\times m} & [0]_{m\times l} \\ [-M^{-1}K(t)]_{m\times m} & [-M^{-1}C]_{m\times m} & [hC_d A_p M_b^{-1}\Gamma]_{m\times l} \\ [0]_{1\times m} & [-\alpha A_p \hat{R}]_{1\times m} & [0]_{1\times l} \end{bmatrix} \quad B = \begin{bmatrix} [0]_{m\times l} \\ [0]_{m\times l} \\ -[hA_p]_{1\times l} \end{bmatrix} \qquad (5.6)$$

where **l** is the number of actuators and **m** is the order of the bridge/ vehicle model.

Some basic results on matrix algebra are reviewed next, because development will make extensive use of quadratic forms. The material presented here is an assigned representation of the work by Slotine. A positive definite symmetric matrix **Q**, can always be decomposed as:

$$Q = U^T \Lambda U \qquad (5.7)$$

where **U** is a matrix of eigenvectors that satisfies the unitary matrix relationship $U^T U = I$. Λ is a diagonal matrix containing the eigenvalues of the matrix **Q**. Let $\lambda_{\min}(Q)$ donate the smallest eigenvalue of **Q** and $\lambda_{\max}(Q)$, the largest. Then:

$$\lambda_{\min}(Q)\|z\|^2 \le z^T Q z \le \lambda_{\max}(Q)\|z\|^2 \qquad (5.8)$$

The preceding result is due to following three facts:

First:

$$z^T Q z = z^T U^T \Lambda U z = z^T \Lambda z, \quad \text{where} \quad Uz = y \qquad (5.9)$$

Second:

$$\lambda_{min}(Q)\, I \le \Lambda \le \lambda_{max}(Q)\, I \tag{5.10}$$

and Third:

$$y^T y = \|z\|^2 \tag{5.11}$$

The basic Lyapunov semiactive control design suggests that a positive definite matrix **Q** can be found to assure that $A^T Q + Q A \le 0$, which **A** is the nominal (non time varying) component of the system matrix. For the uncertain system with $A(t) = A + \Delta A(t)$, the robust controller design requires that **Q** should be selected to satisfy $A(t)^T Q + Q A(t) \le 0$ in order to stabilize the control system. The main Lyapunov stability results for non-autonomous systems can be summarized by the following theorem (Slotine [60]):

Theorem 5.1 If, for a given equilibrium state, there are exists a scaler function $V(x,t)$ with continuous partial derivatives such that: (1) $V(x,t)$ is positive definite; (2). $\dot{V}(x,t)$ is negative definite, then the equibrium state is asymptotically stable in the sense of Lyapunov.

The semiactive control system is guaranteed asymptotically stable if a set of **Q** >0 can be found, make V positive-definite and $\dot{V}$ negative definite in spite of the fact that modal uncertainties, $\Delta A(t)$, exist. In order to apply the Slotine theorem for a nonautonomous system, a Lyapunov function for the nominal (non time-varying) system is assumed:

$$V = \frac{1}{2} z^T Q z > 0 \tag{5.12}$$

Taking the time derivative of V, then:

$$\dot{V} = \frac{1}{2} z^T ((A + \Delta A)^T Q + Q(A + \Delta A^T)) z + z^T Q B g(\Delta P) A_v \tag{5.13}$$

Collecting terms, then:

$$\dot{V} = \frac{1}{2} z^T (A^T Q + QA) z + z^T Q B g(\Delta P) A_v + \frac{1}{2} z^T (\Delta A^T Q + Q \Delta A) z \tag{5.14}$$

where A_v is bounded by $0 < A_v < A_{vmax}$, and a suitable control law can be chosen to make $x^T Q B g(\Delta P) A_v \leq 0$ as:

$$z^T Q B g(\Delta P) \begin{cases} \geq 0, & A_v = 0 \\ < 0, & A_v = A_{vmax} \end{cases} \tag{5.15}$$

The preceding indicates that modal uncertainties do not affect the control law. The first item on the right side of Equation (5.13) is negative-definite by definition. An upper bound of V can be expressed as:

$$\dot{V} \leq -\frac{1}{2} \lambda_{min}(P) \|x\|^2 + \frac{1}{2} x^T (\Delta A_2^T Q + Q \Delta A_2) x \tag{5.16}$$

Noting that:

$$\|\Delta A^T Q + Q\Delta A\| \le \|\Delta A^T Q\| + \|Q\Delta A\| \le \|\Delta A\|^T \|Q\| + \|Q\| \|\Delta A\| \qquad (5.17)$$

The work here assumes that the pertubation of the system matrix is bounded:

$$\|\Delta A(t)\| \le \Delta A_{max} < \infty \qquad (5.18)$$

Combining this with Equation (5.16) produces the following bound on $\dot{V}$:

$$\dot{V} \le -\frac{1}{2}\lambda_{min}(P)\|x\|^2 + \lambda_{max}(Q)\,\Delta A_{max}\|x\|^2 \qquad (5.19)$$

Stability is therefore guaranteed, if the following condition is satisfied:

$$\Delta A_{max} \le 2\frac{\lambda_{max}(Q)}{\lambda_{min}(P)} \qquad (5.20)$$

Equation (5.20) provides a robust stability critiea for the Lyapunov semiactive controller when modal uncertainties exist.

Theorem 5.2 If condition (5.20) is satisfied, then, the control design described above for the bridge/vehicle coupled dynamics system (with time-varying norm bounded uncertainties) is stable.

The control design was shown to be straightforward. A_v is bounded by $0 < A_v < A_{vmax}$, and a suitable control law can be chosen to make $x^T Q B g(\Delta P) A_v \le 0$. The task was made particularly simple by the observation that the bistate control is always

stabilizing ($x^T Q B g(\Delta P) A_v \leq 0$) in Equation (5.13), no matter what control law is adopted to facilitate the service valve switch decision. The stability of the system depend on the self-tuning ability of the system to reject the modal uncertainties. If the **P** matrix is selected as a semi-definite and condition (5.20) is not satisfied, It means no guarantee of stability. On the other hand, if continuous vehicle disturbance exists in the system, a bounded input/bounded output stability should be concluded. The perturbated eigenvalues of the system should be examined.

5.4 Perturbation of Eigenvalues and Eigenvectors

Distributions of eigenvalues in the bridge/vehicle coupled dynamic systems with uncertainties and their relationship to the stability problem is the main topic in this section. The stability analysis of the closed loop system hinges upon the condition that the real part of every eigenvalue must be less than zero, or no eigenvalue has real part greater than or equal to zero for all time, for stability. A perturbation method is first introduced that make it possible to study on-line the essential impact that time dependent parameters have on the system dynamic character.

If the components of the matrix $\Delta A(t)$ are small relative to A, the perturbation method can be applied to predict the change of eigenvalues and eigenvactors $\Delta\lambda_i$ and $\Delta\phi_i$. Let $u^1, ..., u^n$ be eigenvectors corresponding to the eigenvalues $\lambda_1, ..., \lambda_n$ of matrix A. Assume $\lambda_i \neq \lambda_j$ for $i \neq j$. Let $v^1, ..., v^n$ be eigenvectors corresponding to the eigenvalues $\bar{\lambda}_1, ..., \bar{\lambda}_n$ of matrix A^*. Then:

$$(u^i, v^i) \neq 0, \quad (u^i, v^j) = 0 \quad for \quad i \neq j \tag{5.21}$$

The change of eigenvalues and eigenvectors can be expressed as

$$\Delta \lambda_j = \frac{((\Delta A) u^j, v^j)}{(u^j, v^j)} \qquad j = 1, 2, \ldots, n \tag{5.22}$$

for the changing of eigenvectors, one gets:

$$\Delta u^j = \sum_{k=1}^{n} \epsilon_{jk} u^k \qquad \epsilon_{kk} = 0 \tag{5.23}$$

where

$$\epsilon_{jk} = \frac{((\Delta A) u^j, v^k)}{(\lambda_j - \lambda_k)(u^k, v^k)} \qquad j \neq k \tag{5.24}$$

The eigenvalues and eigenvectors of the time-varying system can be evaluated on-line by applying Equations (5.22) and (5.23).

A commonly used stability analysis technique for time-varying systems is so called "frozen coefficient method"(Brogen [61]), in which all time-varying coefficients are fixed and the system stability is analyzed as if it were a constant coefficient system.

Theorem 5.3 If all the eigenvalues are "safely" within the stability region at all time points (all eigenvalues have negative real parts) and the coefficients and eigenvalues are not changing "too fast", then the time-varying system can be presumed stable.

This approach should be used with caution. To apply this theorem, it must first be established that all eigenvalues for the nominal system have negative real parts in complex plane. Next, the change rate of all eigenvalues and eigenvectors should be checked to ensure that they are "not changing too fast". It implies that changing rate of eigenvalues and eigenvectors should be much slower than that of the slowest mode of the system.

5.5 Simulation Results and Discussions

A 29 DOFs 122 m (400') long four-span single girder bridge FEM and a quarter vehicle model are adopted to investigate the robust stability of an ISB system. The quarter vehicle passes over the bridge at a speed of 60 m/h (26.66 m/s).

The time history of natural frequencies of the first five modes of the system is shown in Figure 5.2. The change rate of eigenvalues and eigenvectors depends on the vehicle speed. The natural frequency changing rate is 0.847 Hz ($\omega = \frac{Vel}{2 \times L}$, where Vel is the velocity of the vehicle and L is the length of the span), which is much slower than the lowest system natural frequency (2.5 Hz). It indicates that the changing rate of eigenvalues and eigenvectors is much slower than that of the smallest eigenvalues.

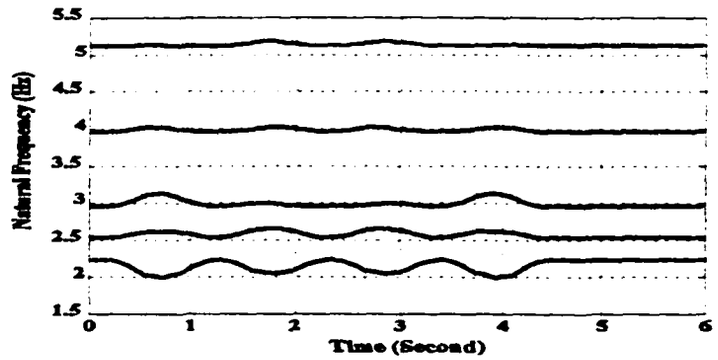

Figure 5.2 The first five modes natural frequencies time history of the bridge/vehicle coupled system

Figure 5.3 shows the variation of the first five eigenvalues (which have the smallest negative real parts) with respect to time. Since all the eigenvalues remain within the stability region at all time steps (all eigenvalues have negative real parts at all times), the time-varying system is assumed to be stable.

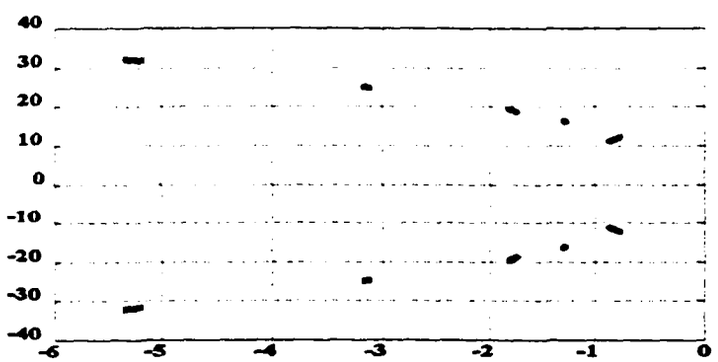

Figure 5.3 Eigenvalues changing with time in complex plane

5.5.1 Robust Semiactive Controller Design

Recall that if $A^T(t)Q + QA(t) \leq 0$, then the system is stable. The following choice of Q with appropriate values of β and α satisfy the inequality as:

$$Q = \begin{bmatrix} K & \beta M \\ \beta M & \alpha M \end{bmatrix} \tag{5.25}$$

Selecting $\alpha = 0.098$ and $\beta = 0.0045$, then the eigenvalues of $A^T(t)Q + QA(t)$ shown in Figures 5.4 and 5.5 are all negative implying, that the system is stable.

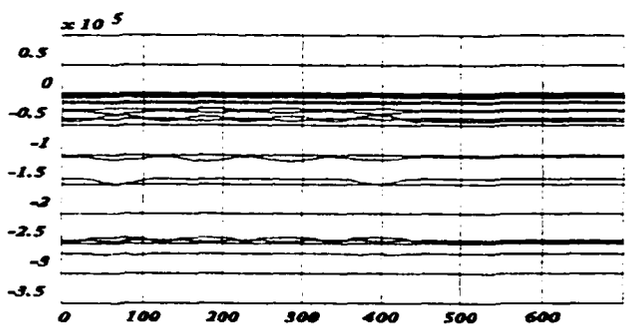

Figure 5.4 Eigenvalues of $A^T(t)Q + QA(t)$ changing with time

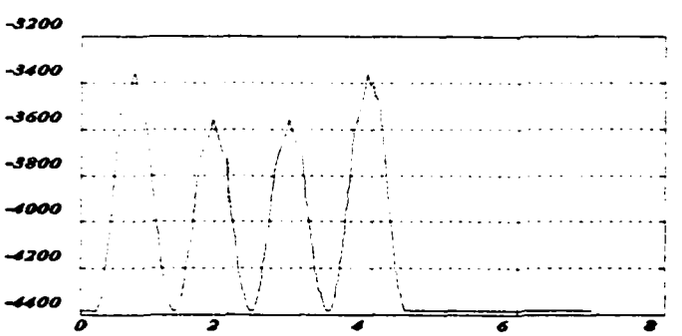

Figure 5.5 $-\lambda_{min}$ of $A^T(t)Q + QA(t)$ changing with time

5.5.2 Robustness of closed loop performance

It is important to investigate the control performance for varying vehicle characteristics and speeds. Figure 5.6 shows the control performance comparison when vehicle speed changes. Figure 5.7 depicts the response of the bridge when the chassis dynamics of the truck change radically. Here, the net weight of the truck is fixed, and the spring rate of the chassis is varied to produce the changing frequency content.

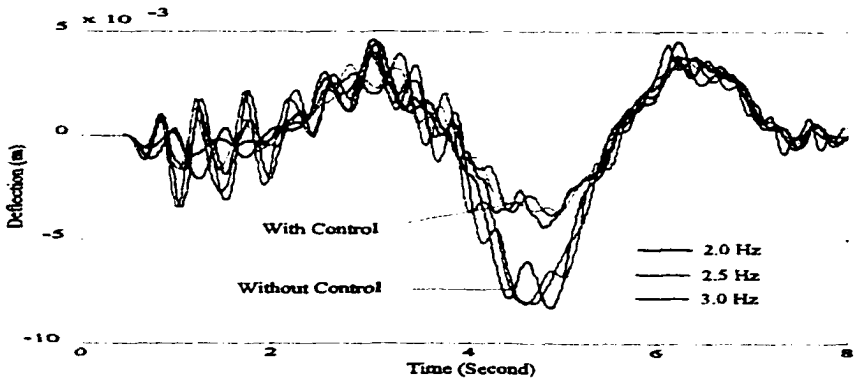

Figure 5.6 Control performance under different vehicle eigenvalues.

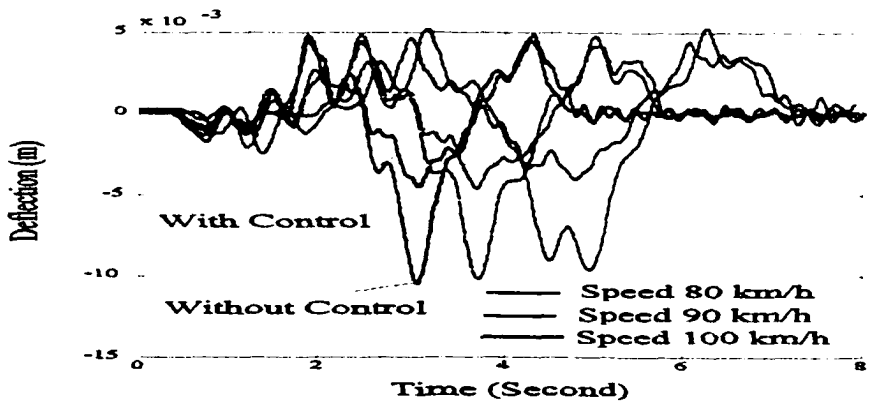

Figure 5.7 Control performance under different vehicle speed.

The simulation results show that the Parameter changes of vehicle disturbance do not affect the control performance.

5.6 Conclusions and Discussions

A practical method was presented to examine the stability of the controlled bridge/vehicle coupled nonautonomous system, which possesses arbitrary, time varying, but bounded uncertainties. A sufficient condition is formulated via matrix algebra to stabilize the semiactive control system. The following conclusion can be made based on these analysis:

(1) A semiactive control device is one that cannot inject mechanical energy into the controlled structures, but has properties that can be controlled to reduce the responses of the system by storing and dissipating system energy.

(2) The closed-loop performance of proposed semiactive control is robust, the variation of parameters (vehicle speed and natural frequency) do not significantly affect closed-loop performance.

CHAPTER SIX

ISB ON THE WALNUT CREEK BRIDGE: DESIGN AND FIELD TEST

6.1 Introduction

This chapter describes the results of the first full scale demonstration of a semiactive control to an in-service bridge. A semiactive controller for an ISB system was presented in Chapter Four. Numerical simulations of the ISB system indicated that a semiactive controller is very efficient for bridge stress reduction. In order to verify that apparent effectiveness, a full-scale control experiment was carried out at the Walnut Creek Bridge near Purcell, Oklahoma by the CSC team.

A brief review of the fundamental concept of the ISB system is first presented. The objectives of the experiment, the dynamic characteristics of the bridge and the ISB assembly, the experiment setup, and the results are also presented in this chapter. The field test results indicate a 52% reduction of the peak stress of the bridge with the ISB system and suggest that the ISB system can increase the safe life of the bridge by over 50 years.

6.2 Design of an ISB System

Once a reliable model of the bridge had been identified in Chapter Two, then the

control system design was accomplished next. The design process began with field tests to discover how the bridge responded to typical trucks. A wide variety of truck types, truck weights and traffic density patterns were included in the examination. Figure 6.1 depicts the frequency response of two accelerometers as a typical tractor-trailer passed over the bridge. The figure shows that the 1st, 2nd, 6th and 8th modes are bending modes, and the 3rd, 4th, 5th and 7th modes are torsion modes. Figure 6.1 indicates that the domain mode response for the particular test was the 5th modes (torsion). A large number of the tests suggest that the most often excited modes are the 1st, 2nd and 5th modes.

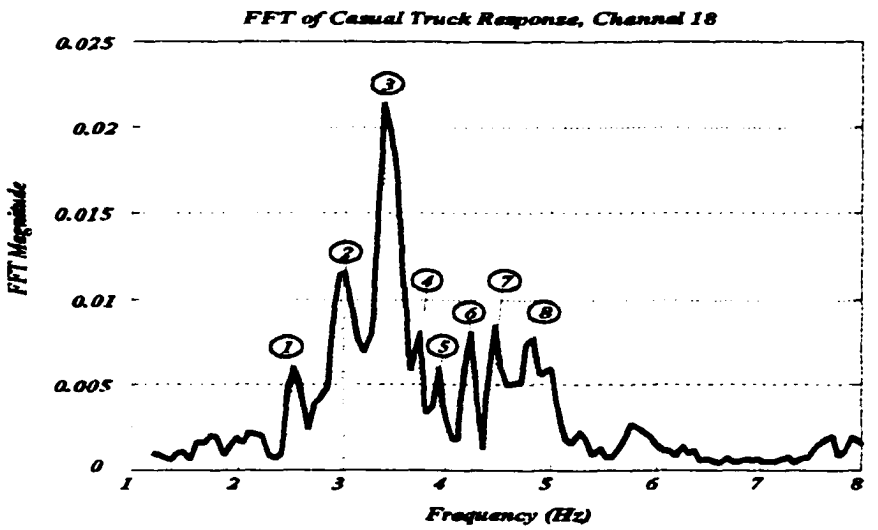

Figure 6.1 FFT of accelerometer at girder #5 (span #4), in response to the passage of a typical tractor-trailer traveling at 105 km/h

The material in Chapter Three made it clear that various combinations of modal response exist, depending on the type of trucks, their weights and the traffic pattern. The data confirm that the dominant response of the bridge was limited to those modes with

frequencies below 5 Hz. This observation established the required bandwidth of the controller hardware. Field testing also verified that a high percentage of the heavy trucks passing over the bridge are coupled dynamically with the bridge. The effect produces dynamic amplitudes that are often much higher than the static amplitudes (see Chapter Three). Figure 6.2 depicts measured deflections of the midpoint at the third span of girder #3 when four different trucks run over the bridge in the right lane at a speed of 105 km/h. The maximum vertical deflection induced by Heavy Truck 54.5 ton (120 klb) is 12 mm while relative displacement of two moment arm tips is 4 mm (assuming W=9.25 m, h=2.54 m). This observation established the required minimum actuator stroke of the controller hardware.

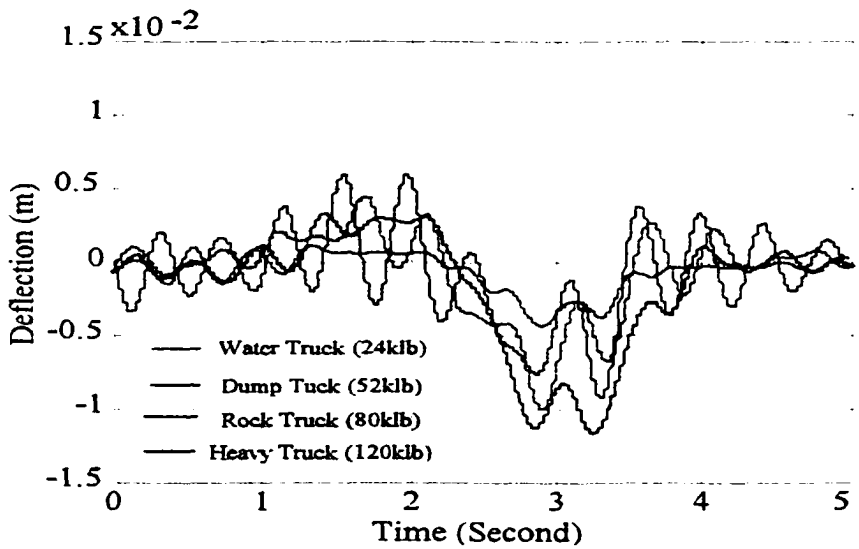

Figure 6.2 Test strain pot signal; girder #3, midpoint of span #3

Once the disturbance bandwidth was established, then the synthesis of the control

hardware design was begun. The design process relied in large part on intuitive initial decisions about the topology and the kinematic arrangement of the components. The basic mechanism employed is very similar (in principal) to the simple arrangement for an (active) moment inducing appendage that was proposed for a beam like structure by Abdel-Rohman and his coworkers [20].

In order to appreciate the design that was finally selected, one must understand the fundamental premise that underlies the concept of a semiactive intelligent stiffener for bridges. Those fundamentals have been presented in great detail in the previous chapter. In short, the ISB technology is intended to produce counter moments at the point of attachment in order to reduce deflection and to reduce the maximum stress that the girders experience during the passage of a heavy vehicle. In addition, the mechanism is intended to shed loads away from those parts of the girder that have experienced the largest stresses over the service life of the bridge (here, the center of the girder between the piers is where the maximum positive moment is experienced) to parts of the girder that have been subjected to much lower stress loads over the service life of the bridge. On the other hand, the local stress concertation at the point where the moment arms attached has to be taken into account in the design.

Once the basic kinematic design was established, then a design study was undertaken to determine the best possible combination of specific design parameters. Noting the configuration of the ISB, then a computer simulation program (see Chapter Four) was used to determine the most feasible design configuration. The study examined

the effectiveness and cost implications of the following design variables:

a) number of actuator assemblies and location on girders

b) distance between moment arms

c) hight of moment arms (from neutral axle of girders)

d) size of the actuator (diameter and stroke)

e) stiffness and weight of ISB assembly

f) number and location of sensors

e) bandwidth of control electronics

f) size of the control valve

g) fatigue life of the bridge and ISB components

The trade-off between cost and effectiveness was used to make a final decision. The final kinematic design of the system is shown in Figure 6.3. Three ISB assemblies were installed on girders #1, #3 and #5 in the third span (see Figure 6.3). Table 6.1 lists certain key parameters and dimensions for the components employed. The dimensions of the actuator cylinders and details of the moment arm assemblies are shown in Figure 6.4. The selected parameters of the control valve, hydraulic fluid and bypass pips are listed in Appendix III.

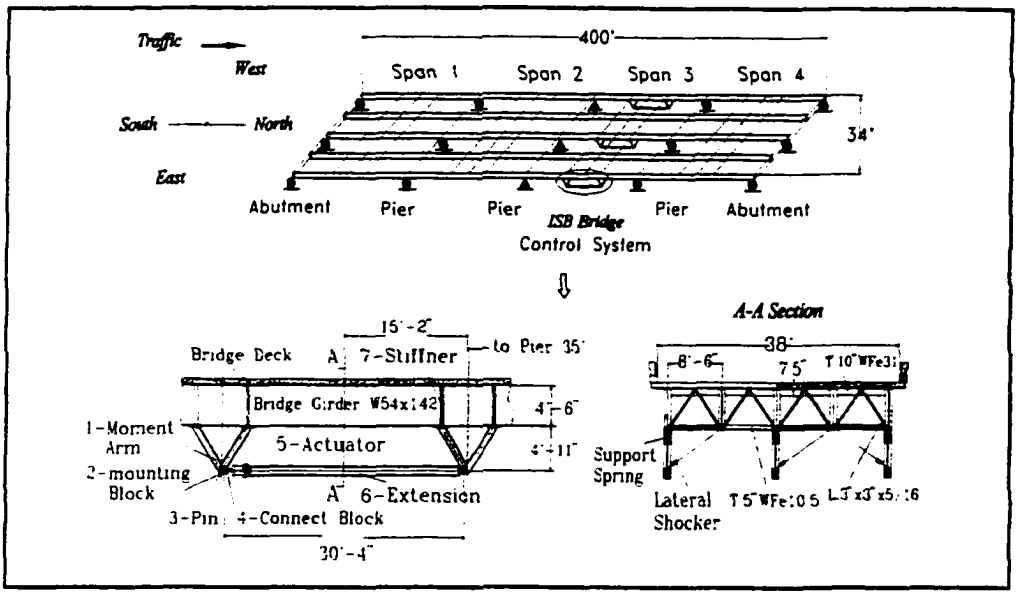

Fig. 6.3 The final ISB system setup on the I-35 Walnut Creek Bridge

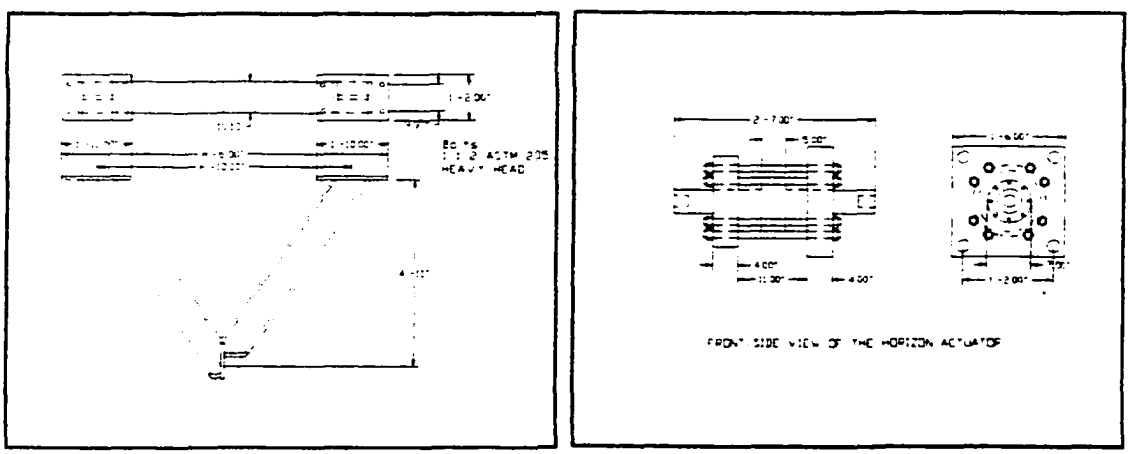

Figure 6.4 Design drawing of the moment arm and hydraulic actuator

Table 6.1 Structural Parts for the ISB Assemblies (See Figure 6.3)

Name of Elements		No.	Weight/Piece (kg)	Effective Stiffness (MPa)
1.	Moment Arm	6	448.2	41.42×10^3
2.	Mounting Block	12	14.0	
3.	Pin	6	7.3	
4.	Connect Block	6	19.0	
5.	Actuator (Typical)	1	280.6	
6.	Extension (Typical)	1	1742.4	25.473×10^3
7.	Stiffener	24	33.2	

6.3 Installation

The actuators and extension elements were assembled at the CSC on the OU campus. The installation on the bridge superstructure was accomplished by using monorails and block & tackle systems. First, holes were drilled in the girder to install web stiffeners. Then, holes were carefully drilled in the flange of one girder at a time. The effectiveness of the design relies, in part, on the ability of the ISB system to transmit forces at a specified moment in time. The installation required considerable care in the location and size of the holes drilled in the flanges. Tapered bolts and reamed holes were also used to guarantee a no-slip condition between the moment arm assembly and the girder that the moment arms were attached to. Next, the moment arms for the ISB assembly were hoisted into position and bolted. Following installation of the moment

arms, the actuator/extension assembly was trucked to the site. The assembly was then hooked to the monorail system, transported to its proper location, and hoisted into place. The process was repeated for each ISB assembly. Traffic was never impeded during the construction effort.

6.4 Control System Setup

Once the mechanical hardware was installed, the CSC team installed the computer systems and electronic components that were used to produce a intelligent semiactive control system.

6.4.1 System Configuration

The ISB assembly consists of a special hydraulic actuator that is outfitted with a motor-controlled valve. As Figure 6.5 shows, the control valve position is regulated by a DC-motor which was, in term, controlled by an Intel microcontroller 196 that was mounted near the actuator. The microcontroller receives the valve position command from the global controller and provides a closed loop control command to the DC motor. The position of the value was then transmitted back to the microcontroller via an encoder mounted on the valve motor, then automatically adjusted the value position to the desired final state.

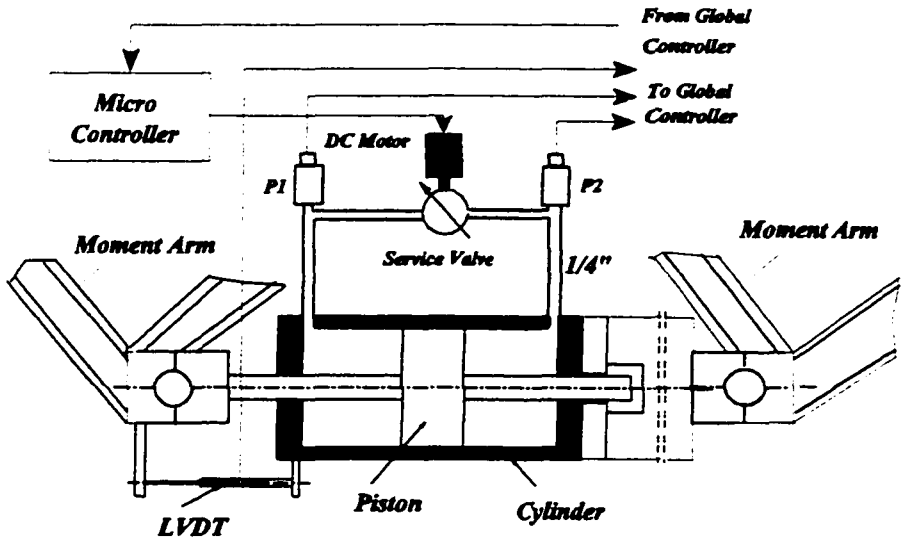

Figure 6.5 Kinematic assembly of an ISB actuator

A PC based multi-channel digital data acquisition and processing system was set up at the north end of the bridge. The control decisions for the ISB system were computed with that system. The PC was used to collect all the control sensor outputs. The new values of the valve orifice area (A_v) was computed at each update of the control step. The desired A_v commands were then transmitted to Intel 196 microcontroller. Figure 6.6 depicts the general framework of the semiactive feedback control system which was set up on the Walnut Creek Bridge.

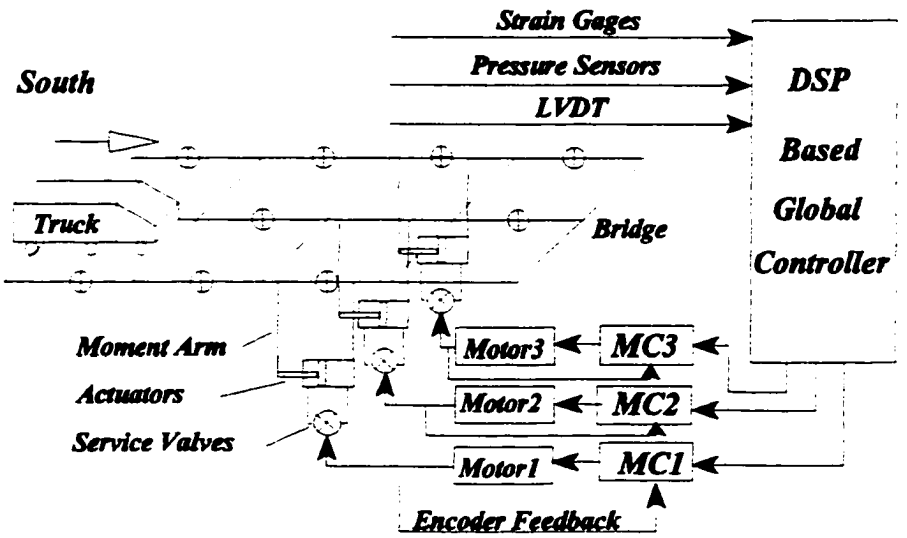

Figure 6.6 The control system layout; MC = micro controller

6.4.2 Sensors and Location

The closed loop operation of the ISB relies on the physical states of the bridge and of the hydraulic pressure in each of the actuators. That information is used at each time step to determine whether to open or close the bypass valve on each of the hydraulic actuators. Two groups of sensors are used: those associated with each of the actuators, and those associated with the bridge superstructure. Twelve strain gauges were mounted in each span midpoint of the east, center, and west girders as shown in Figure 6.6. A subset of those sensors were used as feedback outputs for the semiactive control system.

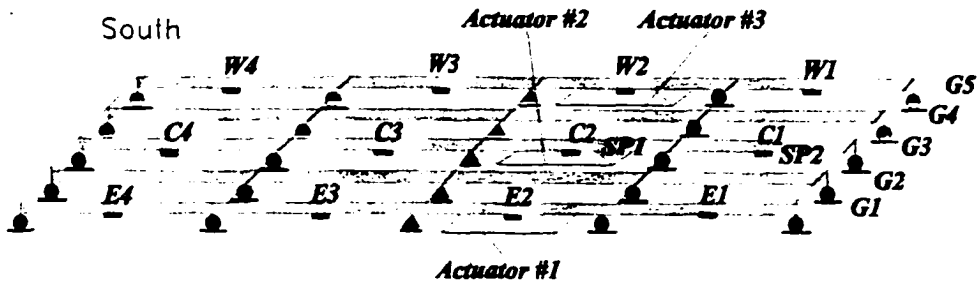

Figure 6.7 12 Strain gauges and two string pots locations

Each actuator was outfitted with two absolute pressure sensors and an LVDT to measure the stroke of the actuator piston. The stroke of a hydraulic piston for 36 ton (80 klb) truck load on is typically +3 mm.

6.4.3 Field Test of the Controller

The field tests provided insight into the selection of the best control logic for the system. The tests presented here rely on a Lyapunov bistate control logic (Chapter Four). The closed loop control relies on 11 measurements: the differential pressure at each actuator (3), the relative displacement of each actuator (measured with the LVDT) (3), and the five strain gauges at the bottom of the flange at the center of each of the three girders that the ISB system is attached to. Each of those measurements was weighed with a specific gain which is obtained from simulations. The weighed readings were then used to determine whether each valve should be open or closed at each point in time. The

control logic is depicted in Figure 6.9. The on-off or bistate control is a common characteristic of semiactive control systems that rely on saturation of the control to achieve a desired result.

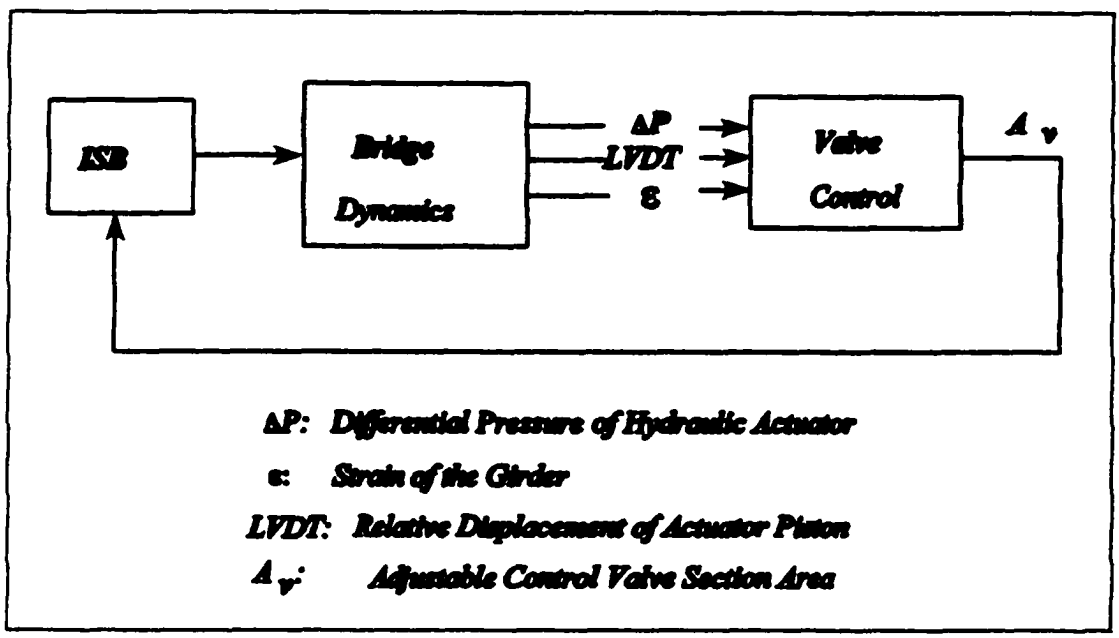

Figure 6.8 ISB control logic

It is necessary to setup a deadband to prevent high frequency switching of DC-motors and service valves. then, maximum dissipation is assured if A_v (the valve orifice) is selected by using the following bistate control law for all three actuators mounted on the Walnut Creek Bridge.

$$x^T q_r \, sign\,(\Delta P_r) \begin{cases} \geq +\epsilon, & A_{wr} = A_{wmin} \\ < -\epsilon, & A_{wr} = A_{wmax} \end{cases}, \quad r = 1,2,3 \qquad (6.1)$$

where the deadband ϵ was established via field tests.

The vector $\hat{q}_r$ establishes the weighing of different states to emphasize a particular control objective; here, the reduction of the nodal displacement amplitude at the center of the span is the objective of the control. The control law does not require full state feedback and some physical states which have no obvious contribution to control performance can be neglected. This is accomplished by setting the appropriate terms in the weighting vector $\hat{q}_r$ to zero.

6.4.4 Simulation Results of Controlled Response

In order to examine the performance of a full-scale control system, simulations were conducted using the Rock Truck model. Figure 6.9 depicts the comparison between controlled response and uncontrolled response of the three midpoints of east, center and west girders. The results indicate a 60% reduction of peak deflection at each test point. The differential pressure versus control command for the simulation is shown in Figure 6.10.

The gains ($\hat{q}_r$) used in the simulation were then utilized in an actual field test and was verified to be effective and robust for the field control tests.

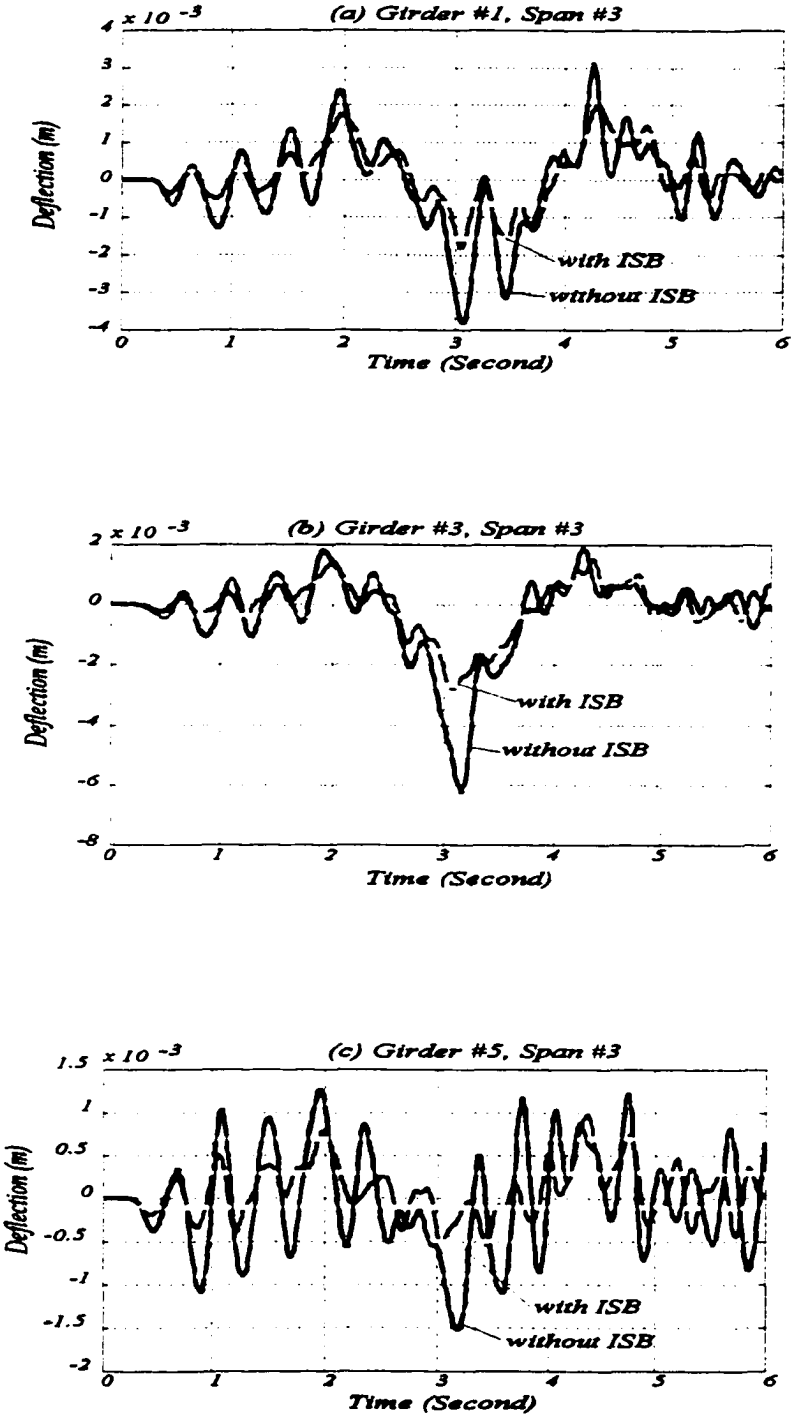

Figure 6.9 Simulated closed loop vs. open loop control performance, with the RT traveling in the right lane at 105 km/h

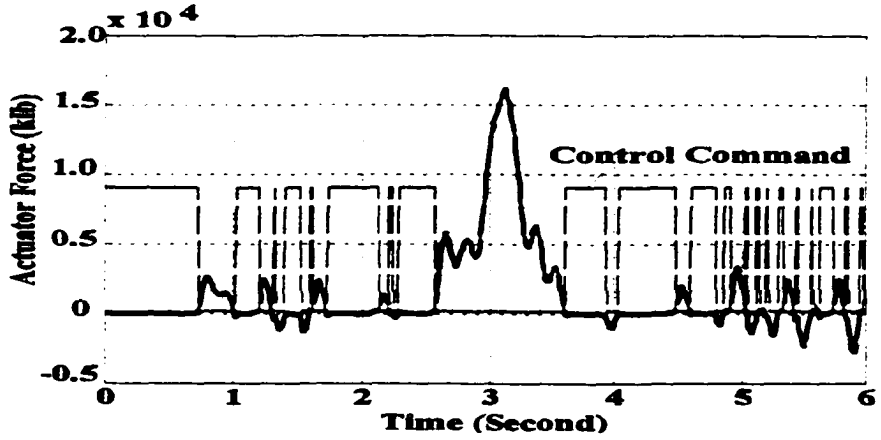

Figure 6.10 Simulated ISB control force output of the center actuator

6.4.5 Experimental C++ Program for Control Field Tests

A control program based on C++ was designed for the field test. The program (See Appendix IV) starts with a check of the offsets of each of the feedback signals. At each time step, the global controller receives the sensor outputs, the new values of the valve orifice area (A_v) were computed at each update step. The desired A_v commands were then transmitted to the Intel 196 microcontroller. The flow chart of the control program is shown in Figure 6.11.

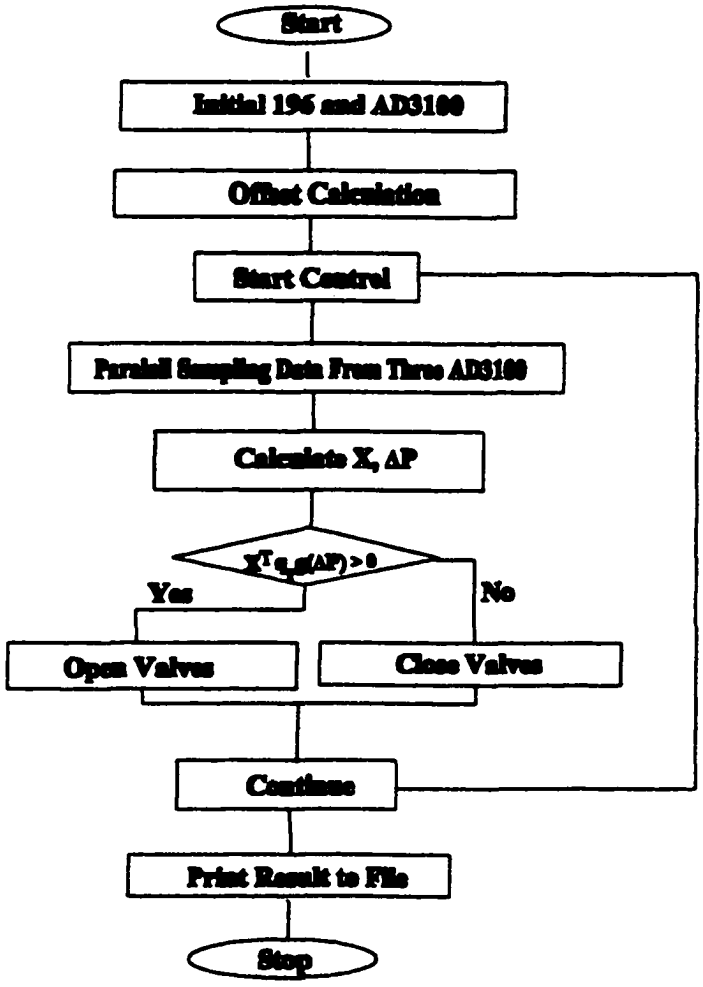

Figure 6.11 Flow chart of experimental control program

6.5 Semiactive Control Field Test Results

Four trucks were employed in the field test of the ISB system. They were: a Water Truck (weight 26.6 kips), a Dump Truck (weight 54.7 kips), a Rock Truck (weight 79.5 kips) and a Heavy Truck (weight 120 kips) (see Figure 6.12). The Water Truck and Rock Truck were equipped with accelerometers and LVDT for the purpose of truck modal identification and dynamic analysis.

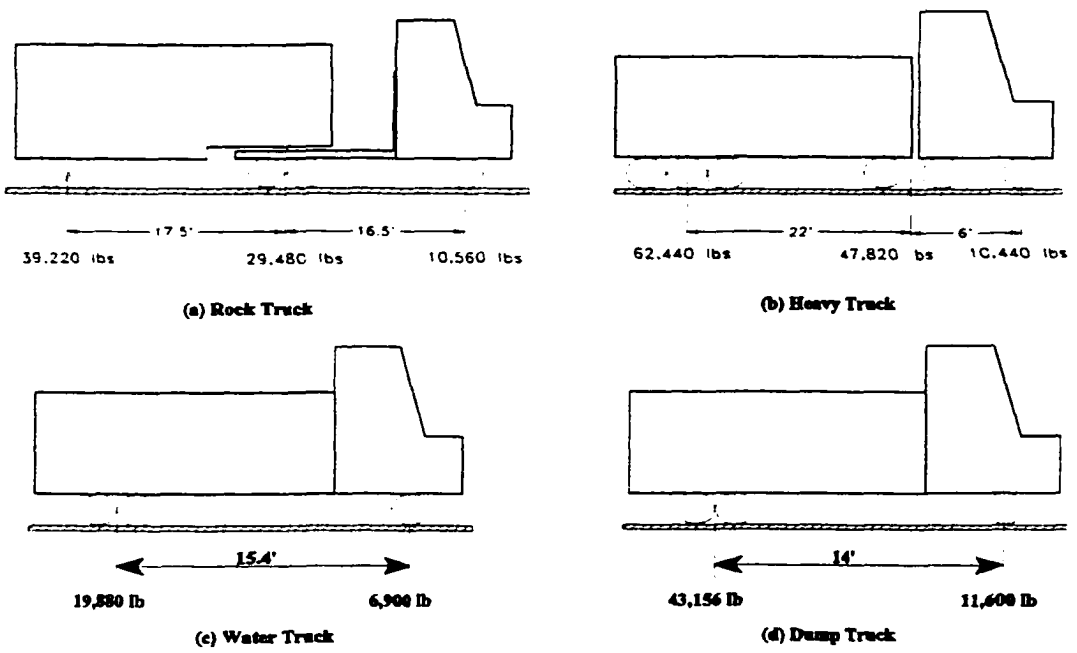

Figure 6.12 Four test trucks wheel load distribution and axle spacing

The first part of the tests was conducted to determine the difference in response produced when the ISB actuator valves were locked open. In that mode, the hydraulic

actuators function much like a simple passive damper. The second part of the tests was conducted to verify the performance of the Lyapunov control design. The tests also provide a means for iterative improving the control performance of the system.

6.5.1 ISB Passive Performance Test

The passive damper test discussed here was conducted in November, 1996. A RT was used in the test (see Chapter Three). The test was conducted to determine the passive (uncontrolled) performance of the ISB system versus the performance of the bridge prior to the installation of ISB system. Figure 6.13 depicts the time histories of strain gauges at the bottom flange of the three girders at the center of the third span where the ISB was mounted.

The truck was traveling at 105 km/h (65 m/h) in the test. Vehicles traveling behind the test truck slowed the following traffic down and made it possible to have the test truck cross the bridge without any other vehicles on the bridge. An inspection of the data indicates that when operated as a passive damper, the ISB does provide some reduction of the maximum stress for those girders that are not located near the wheel loads. The passive damper has very little effect on the stress induced in the girders that provide primary support. The conclusion is that passive dampers are ineffective as a means of extending service life.

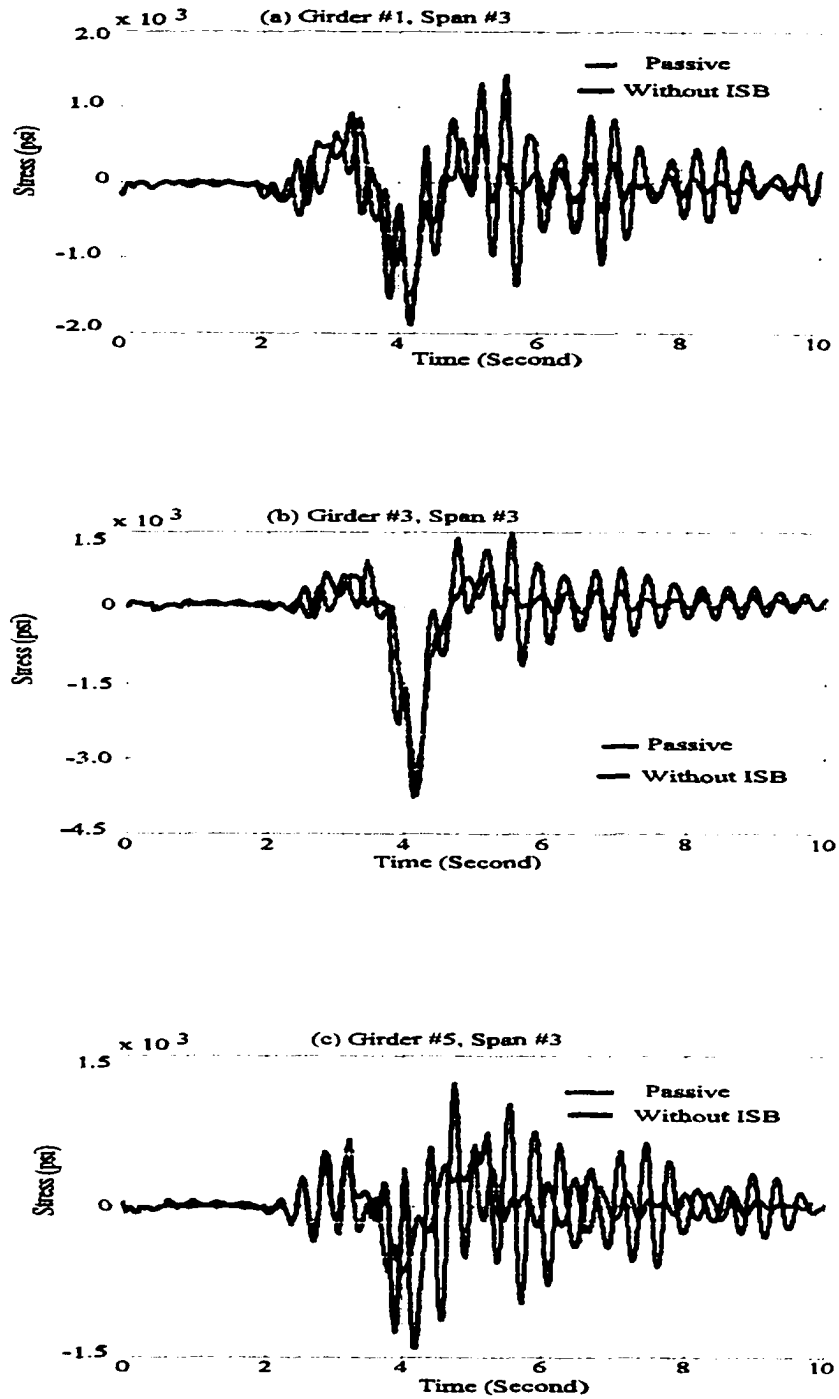

Figure 6.13 Stress response (a) when ISB was operated as passive damper, (b) before the ISB system was installed, (at span #3 bottom flange)

6.5.2 Controlled Response

Several field tests have been conducted at the bridge to examine the performance of the control system. The tests were also used to debug the design of the controller. The results of a test conducted in April, 1997 are reproduced here to demonstrate the closed loop performance of the ISB system.

The test included all four types of test trucks. Figures 6.14 indicates the controlled and uncontrolled bridge response for the Rock Truck. Figures 6.15 depicts the bridge stress response to the passage of the Heavy Truck with and without control. Figures 6.16 and Figure 6.17 provide the same comparison for the Dump Truck and Water Truck. All test trucks passed over the bridge in the right lane and at a speed of 105 km/h. The effectiveness of the ISB system is easily recognized in all these cases. The ISB can reduce the peak stress by 55%.

The time history of the differential pressure, the LVDT and the control command for the actuator mounted on girder #1 are shown in Figure 6.18 (1=open, o=closed) for the passage of the RT. The control command time history clearly indicates an added stiffness or damping results. A spectral analysis of the response of the bridge at the third span midpoint of girder #1 is shown in Figure 6.19, which was recorded when the RT passed over the bridge. The output of the strain gauge sensor was used in that analysis.

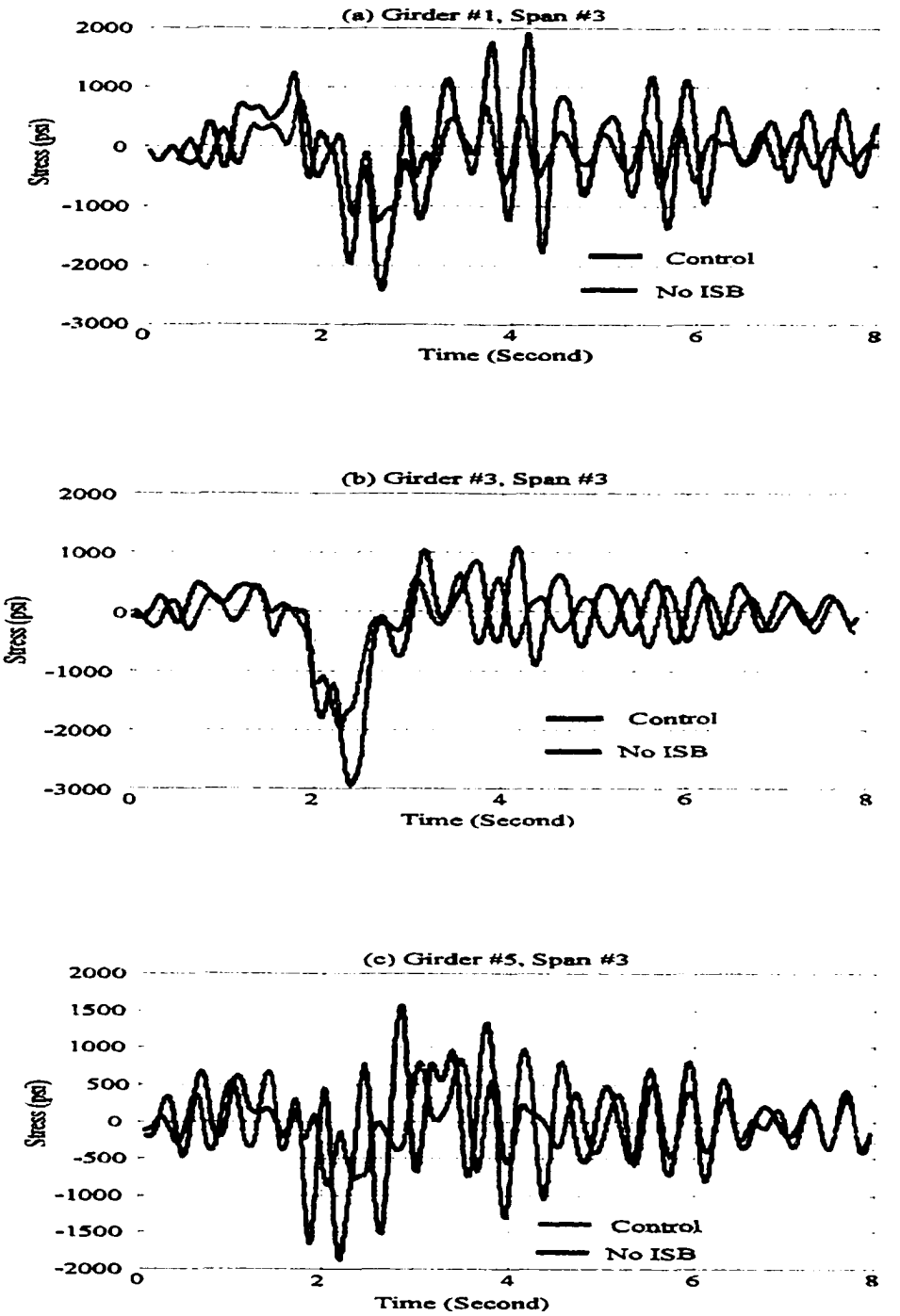

Figure 6.14 Close loop versus open loop control performance, RT traveling in the right lane at 105 km/h; a: girder #1, b: girder #3, c: girder #5.

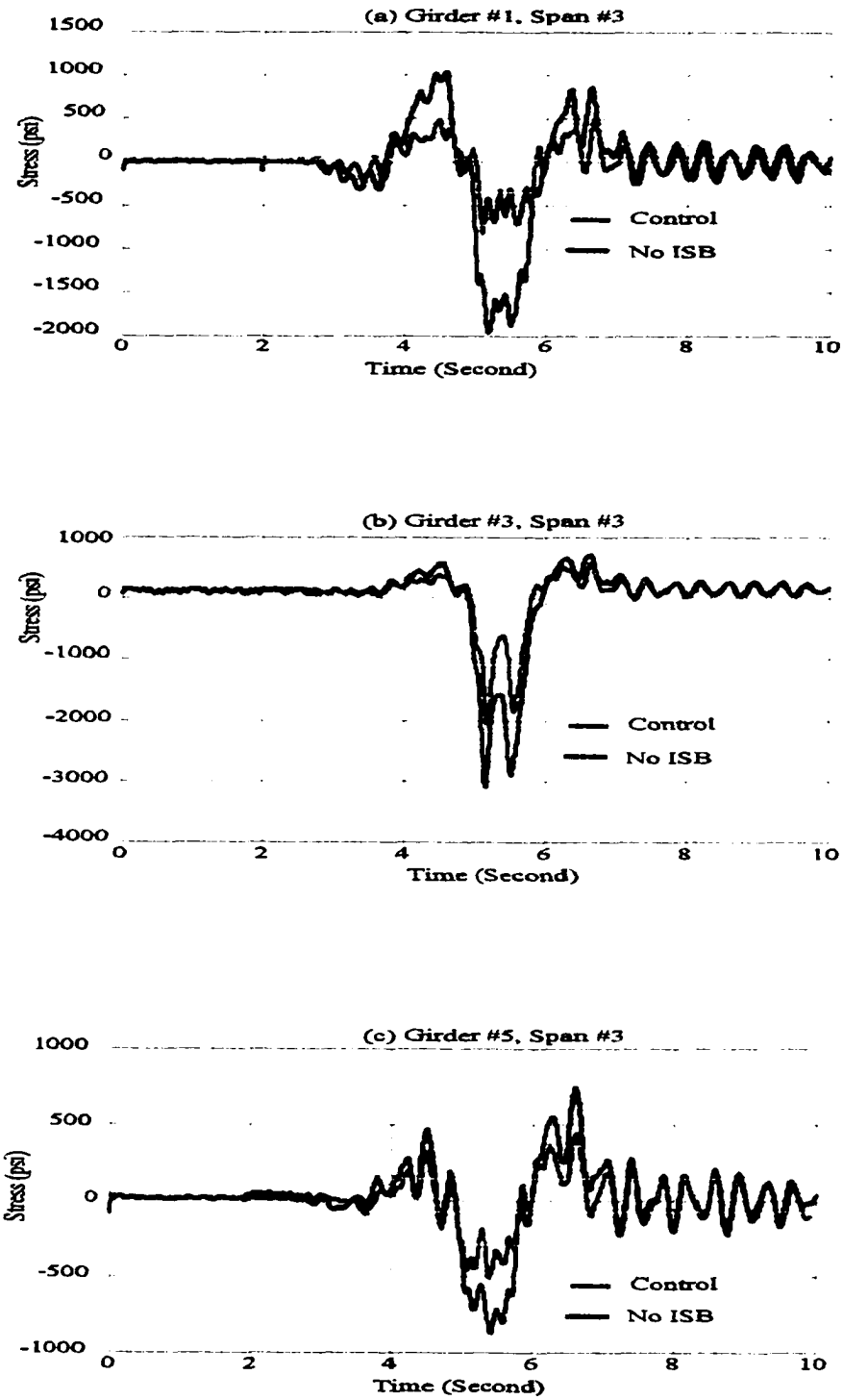

Figure 6.15 Close loop versus open loop control performance, HT traveling in the right lane at 105 km/h; girder #1, b:girder #3, c: girder #5.

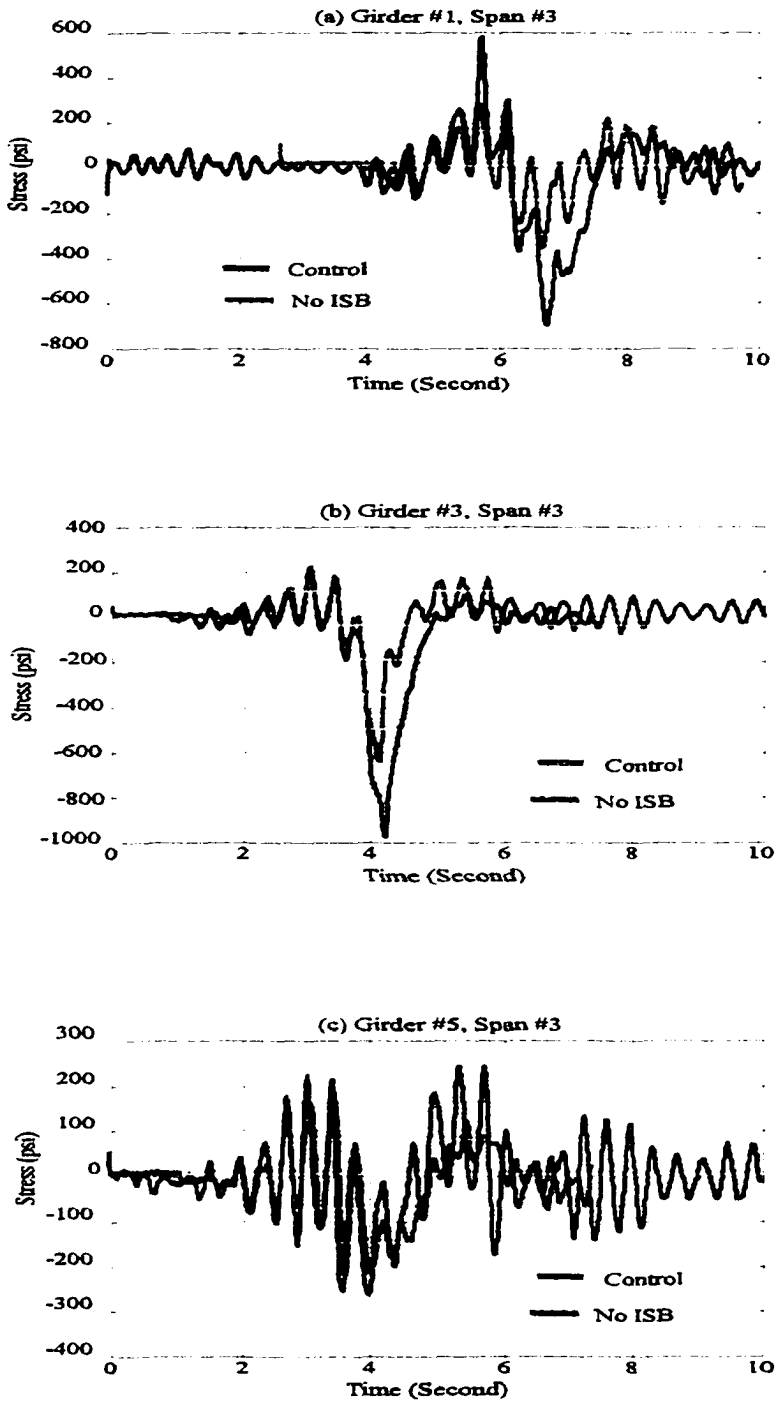

Figure 6.16 Close loop versus open loop control performance, WT traveling in the right lane at 105 km/h; girder #1, b:girder #3, c: girder #5.

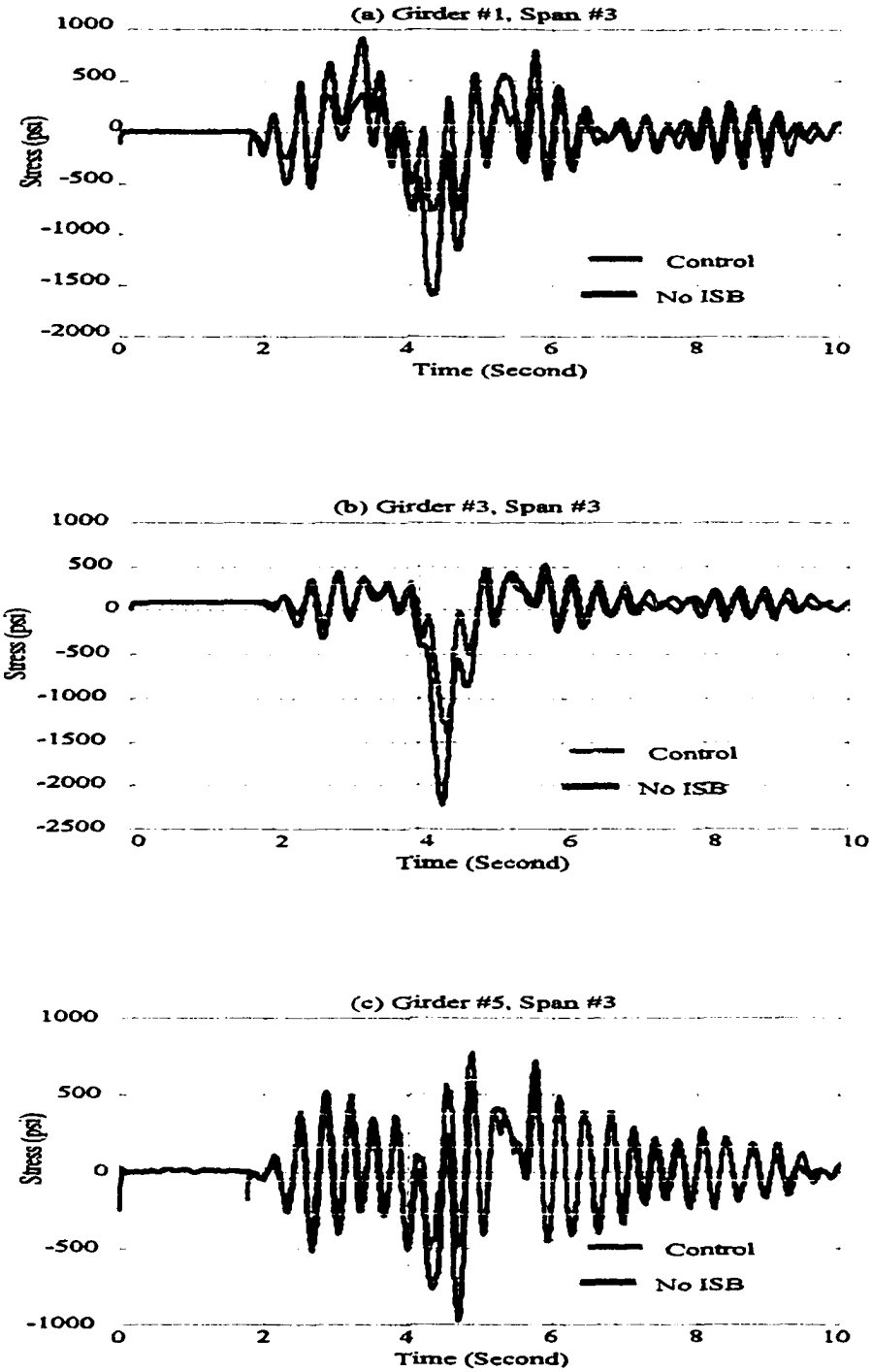

Figure 6.17 Close loop versus open loop control performance, DT traveling in the right lane at 105 km/h; girder #1, b:girder #3, c: girder #5.

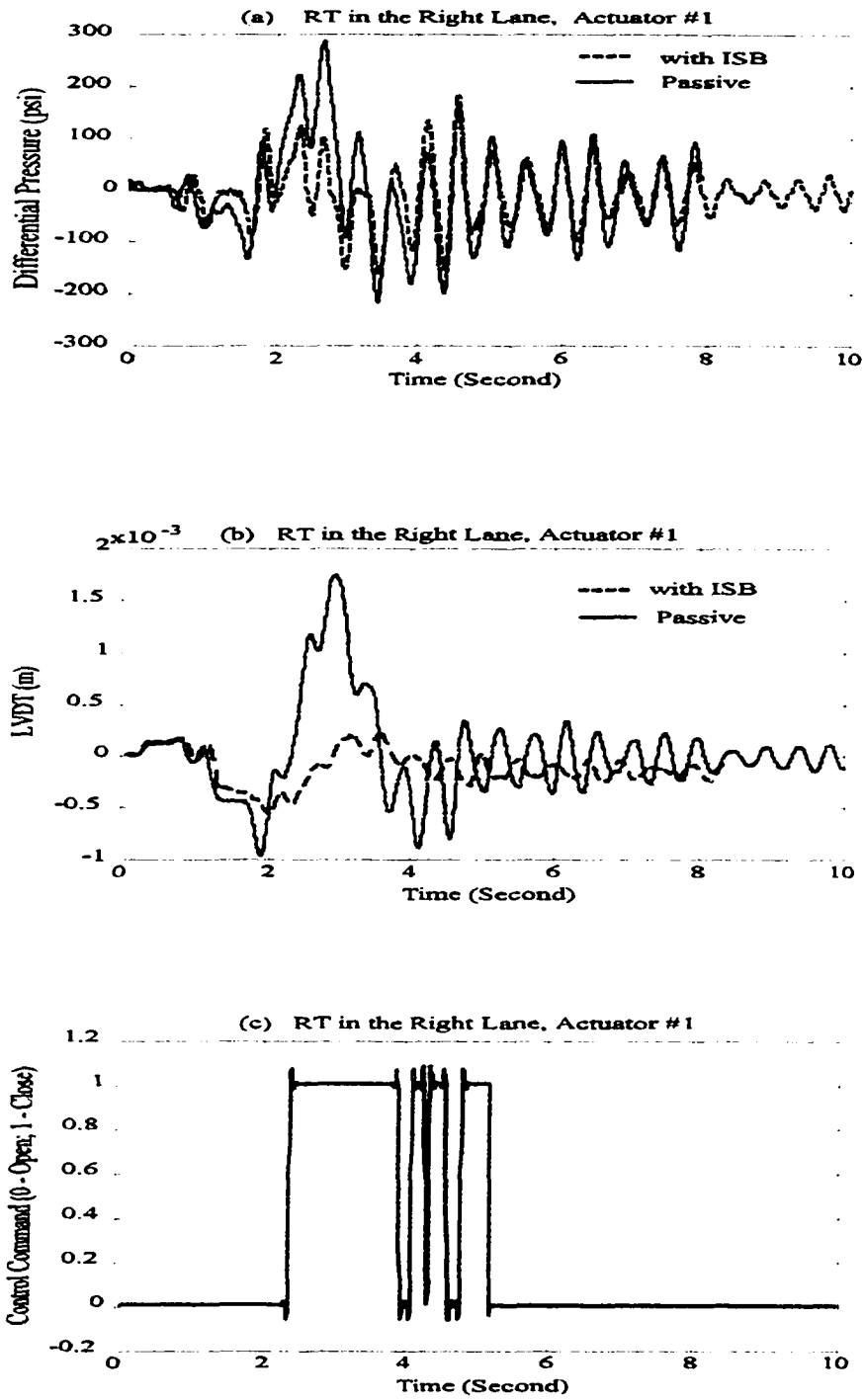

Figure 6.18 Actuator #1 performance, RT runs over the right lane passive vs. close loop, a) differential pressure; b) LVDT; c) control command

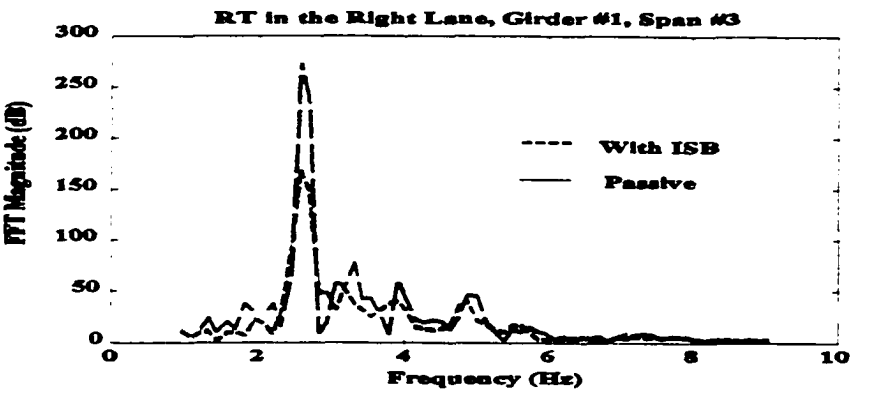

Figure 6.19 Frequency domain comparison of control performance, RT in the right lane; passive vs. close loop control

The comparison between controlled and uncontrolled maximum stresses at controlled span (span #3) for all four types of test trucks are listed in Appendix V.

6.6 Safe Life Predictions

The primary purpose of the ISB design was to afford a means of extending the remaining useful service life of the test bridge. The ISB accomplishes that goal by reducing the maximum deflection and maximum stress range that accompanies the passage of heavy trucks. The assessment of the effect that the ISB had on the remaining service life of the bridge was conducted by using a specific rule, Equation (4.17), prescribed for that purpose by NCHRP 299. Data obtained from the field measurements was used to make the determination of added fatigue life. Figure 6.20 depicts the maximum stress measured at the center of the girders when the RT crosses the bridge. The tests were conducted several times for various trucks traveling in each lane. The stress reduction that accompanies the use of the ISB is significant at the posted speed limit. The calculated differences of remaining safe life when the loaded rock truck

crossed the bridge is shown in Table 6.2. The differences are listed for the east girder (#1), the central girder (#3) and the west girder (#5). The minimum addition of safe life produced was 49.6 years. An almost identical result was observed when the loaded Rock Truck was employed in the test. The equation used to conduct the calculation is given in Table 6.2 along with the parameters of values that were employed in the calculations. The table indicates that prior to the installation of the ISB system, the code indicated negative safe life. A calculation of mean life with and without the ISB system also indicates a dramatic increase in useful life. That computation always produces much more optimistic projection of remaining life than does the estimate of safe life.

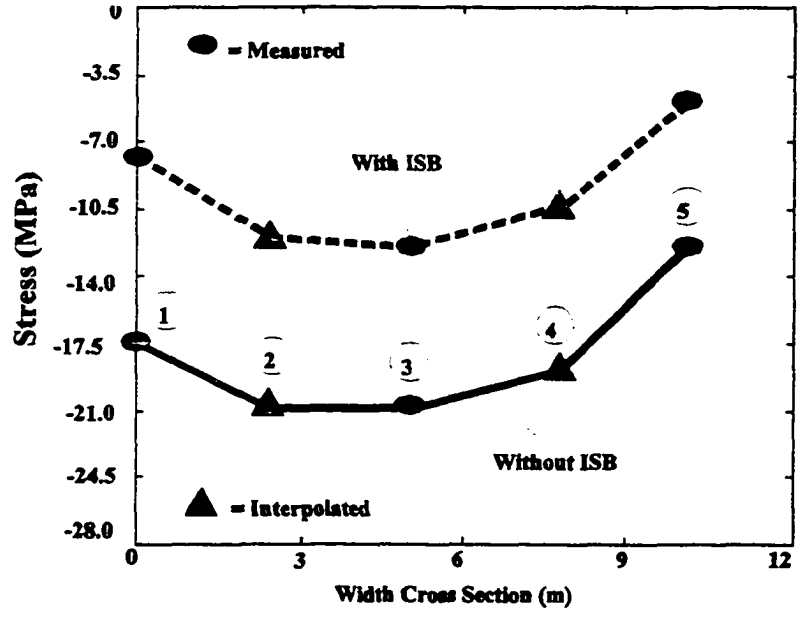

Figure 6.20 Maximum stress measured at span #3 mid-section, Rock Truck traveling in the right lane; girder numbered in circle

Table 6.2 Remaining Safe Life (Y_f) of the Walnut Creek Bridge from the Rock Truck Test (Year)

Span with ISB	East Girder	Center Girder	West Girder
No ISB	-12.4	-13.7	0.4
ISB Controlled	167.7	35.8	110.5
Life Extension	180.1	**49.5**	110.9

Note:

Safe Life (see NCHRP 299) : $$Y_f = \frac{f \times K \times 10^6}{T_a \times C \times (R_s \times S_{re})^3} - a;$$

f=1, K=12, Rs=1.35,C=1(Rainfall Count),

Ta=3000=Estimated Life Time Average Daily Truck Volume,

a=25 (Present Age of the Bridge),

Sre=Maximum Stress Range: (1) With ISB=1.54 x 10^7 N/m;

(2)Without ISB=3.41 x 10^7 N/m.

6.7 Summary

This chapter describes the results of the field testing of an intelligent bridge vibration mitigation system. To the author's knowledge, this test demonstrates for the first time the feasibility of a semiactive control system for highway bridges. The results

indicate that the concept is technically viable and the cost is minimal. The work also demonstrates that the control logic is very simple and fairly safe. The most important fact is that the ISB operates without pumping energy into the bridge. The ISB does not have any potential to destablize the system, while the performance is promised. The following observations are also offered: (1) The control algorithm based on Lyapunov's second method was shown here to be effective in mitigating the vibrations of a highway bridge that are induced by heavy truck traffic; (2) The semiactive control system provides much more vibration reduction than a passive damper; (3) The control design works for all variety of trucks, and (4) The trade-off design of the ISB system is verified to be successful.

CHAPTER SEVEN

AN INTELLIGENT VEHICLE/BRIDGE VIBRATION CONTROL SYSTEM

7.1 Introduction and Background

There is growing interest in the development of intelligent transportation systems. The previous chapters of this dissertation presented the prototype design and demonstration of an ISB system on an in-service bridge on I-35 in Oklahoma. The ISB provides one mean of bridge stress reduction system. The CSC team has also devoted an effort to the development of a truck-mounted control technology that, if implemented, could dramatically reduce a bridge vibration response to a truck passage. In Chapter Three, the research indicated that a large percentage of the heavy trucks that pass over bridges have chassis vibration modes that closely correspond to the fundamental modes of highway bridges. The simulation results also show that the near correspondence of truck chassis modes typically cause a significant increase in deflection and stress in the girders of the bridge. The useful service life of bridges may be shorter than first expected.

The objective of this chapter is to present a methodology that produces a general control design of an Intelligent Vehicle/Bridge System (IVBS). This chapter presents a proposed methodology for the development of a bridge/vehicle vibration control system. The system consists normal of a bridge outfitted with sensors, and a truck equipped with

a adjustable shock absorber. The investigate system will include telecommucation hardware to enable communication between the truck microcontroller and the bridge. The performance of prototype design of an IVBS is verified by numerical simulation. The results seem promising.

The number of works that explore the possibility of applying an automatically adjustable (active, semiactive) bridge/vehicle control to achieve bridge motion mitigation are few. Chung and Gennin (1978) [7] first suggested that a simple semiactive suspension system which controls the damping factor without requiring any power supply may be incorpoperated to reduced dynamic overloads. Green et al., (1995) [62] reported a theoretical study of bridge/vehicle interaction problem for short span bridges. Their analysis suggest that trucks equipped with leaf spring suspensions are more likely to interact with the short span bridges. Heywood [63] (The DIVINE Project, 1995) presented some experimental studies on the influence of vehicle suspensions on the dynamic response of short-span bridges. The experimental results show that the wheel hop mode of trucks strongly couples with the bridges that have fundamental modes in the same range as the truck chassis. The study demonstrated that maintaining smooth bridge entrance and deck profiles is very important. The vibration-induced stresses caused by trucks can be reduced substantially. The authors also suggested that wheel forces with axle hop frequencies need to be controlled for vehicles to be friendly to short-span bridges.

7.2 Prototype Design of an IVBS

The most general form of the proposed IVBS is shown in Figure 7.1. Both the bridge and the vehicle are outfitted with semiactive hydraulic actuators. One semiactive actuator is shown mounted on the center of the bridge. The other actuator is outfitted between truck axle and body. The physics that define both semiactive actuators was presented in Chapter Four. The truck is outfitted with various sensors and signal conditioners to monitor it's vibration and forward speed. It is assumed that all physical states of the system are fully observable.

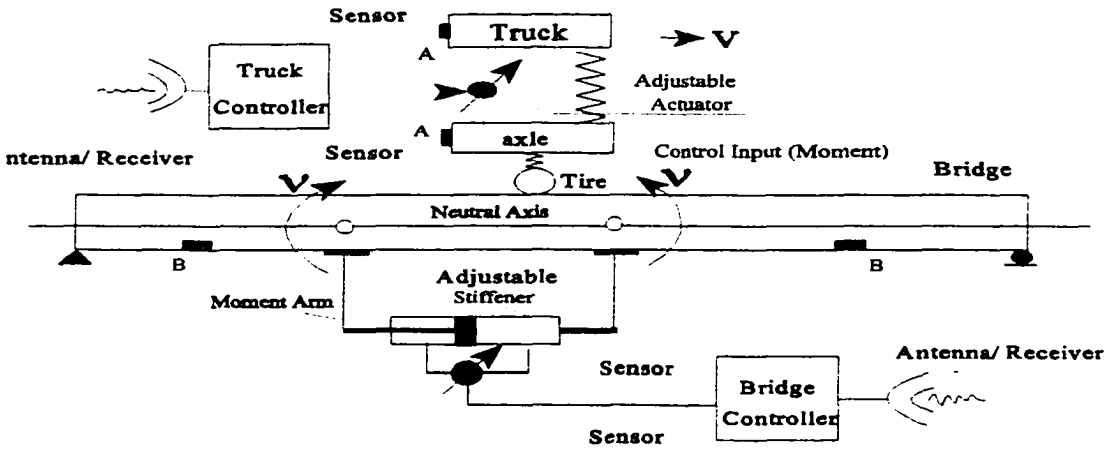

Figure 7.1 The IVBS layout

7.2.1 Modeling of the Bridge and Vehicle

The principles that underlie the IVBS control system design are best described first in terms of the control of a four-span bridge girder with a quarter vehicle representation of a truck passing over the bridge. A FEM of the bridge girder and a quarter vehicle model is used here to represent the bridge and truck (see Chapter Four).

Recall that the vehicle and the bridge are dynamically coupled, resulting in a nonautonomous system (see Chapter Three). The control design relied on a knowledge of the stability of the semiactive control system.

7.2.2 Control Design of the IVBS

The control algorithm is based on the Lyapunov control approach presented previously in Chapters Four and Five. The state space equations of motion of the bridge/vehicle system can be rewritten as:

$$\dot{z} = A(t)z + B_1 u + B_2 v \qquad (7.1)$$

where **A(t)** is the general time-varying plant matrix, z is vector of generalized coordinates of the bridge/vehicle coupled system, B_1 is a Boolean matrix that represents a mapping between generalized states and the control moment input of bridge; and B_2 is a second Boolean matrix that represents a mapping between generalized states and the control input of the truck suspension actuator. The control force created by semiactive

damper of the bridge is expressed as moment form:

$$u = h\, A_b\, \Delta P_b \tag{7.2}$$

where h is the distance between the neutral axis of steel girders and the tip of the moment arms. The control force created by the semiactive actuator between sprung and unsprung mass is in the form of:

$$v = A_t\, \Delta P_t \tag{7.3}$$

where A_t is the effective area of the truck hydraulic semiactive actuator. Combining bridge-vehicle coupled system equations with a hydraulic dynamic equation results in the following compact form:

$$\dot{\hat{z}} = A(t)\,\hat{z} + B_b\, g(\Delta P_b) A_{vb} + B_t\, g(\Delta P_t) A_{vt} \tag{7.4}$$

where

$$A(t) = \begin{bmatrix} [0]_{m\times m} & [I]_{m\times m} & [0]_{m\times l} & [0]_{m\times l} \\ [M^{-1}K(t)]_{m\times m} & [M^{-1}C]_{m\times m} & [h\,C_d A_{pb} M^{-1}\Gamma]_{m\times l} & [C_d A_{pt} M^{-1}\Pi]_{m\times l} \\ [0]_{1\times m} & [-\alpha\,\beta\, A_{pb}\hat{R}]_{1\times m} & [0]_{1\times l} & [0]_{1\times l} \\ [0]_{1\times m} & [0]_{1\times l} & [-\alpha\,\beta\, A_{pt}\hat{T}]_{1\times m} & [0]_{1\times l} \end{bmatrix} \tag{7.5}$$

and

$$B_b = \begin{bmatrix} [0]_{m\times 1} \\ [0]_{m\times 1} \\ -\alpha\ \beta\ A_{pb} \\ [0]_{m\times 1} \end{bmatrix} \qquad B_t = \begin{bmatrix} [0]_{m\times 1} \\ [0]_{m\times 1} \\ [0]_{m\times 1} \\ -\alpha\ \beta\ A_{pt} \end{bmatrix} \tag{7.6}$$

where **m** is the order of the bridge/vehicle model. Equation (7.4) provides the setting for a control design study.

The Lyapunov control design is employed again to produce a simple on off rule for the hydraulic actuator bypass valves. The global Lyapunov function of the form:

$$V = \frac{1}{2} z^T Q z \tag{7.7}$$

is selected. The first time derivative of V is:

$$\dot{V} = \frac{1}{2}\dot{Z}^T Q Z + \frac{1}{2} Z^T Q \dot{Z} \tag{7.8}$$

Substituting Equation (7.4) into Equation (7.8) yields

$$\dot{V} = \frac{1}{2} z^T (A(t)^T Q + Q A(t)) z + z^T Q (B_b g(\Delta P_b) A_{pb} + B_t g(\Delta P_t) A_{pt}) \tag{7.9}$$

We assume that a positive definite Q exists such that

$$A(t)^T Q + Q A(t) = -P \tag{7.10}$$

where, P is a positive definite matrix. $\dot{V}$ can be forced to be negative by choosing A_{pb} and

A_{vt} in the following way:

$$z^T Q B_b g(\Delta P_b) \begin{cases} \geq 0, & A_{vb} = 0 \\ < 0, & A_{vb} = A_{vmax} \end{cases} \tag{7.11}$$

and

$$z^T Q B_t g(\Delta P_t) \begin{cases} \geq 0, & A_{vt} = 0 \\ < 0, & A_{vt} = A_{vmax} \end{cases} \tag{7.12}$$

The control law, Equations (7.11) and (7.12) define a general Lyapunov bistate control law which provides the opportunity to maximize the reduction of the total energy of a general bridge/truck system. Noting that all the states of the bridge/vehicle coupled system were involved in control feedback output signals. It gives the option to achieve a best performance by tuning the weighting matrix Q, but it is not necessary to include those states because they make no contribution to control performance. Those states are eliminated by setting the corresponding terms in Q to zero. Figure 7.2 is a block diagram of the global bridge/truck control logic.

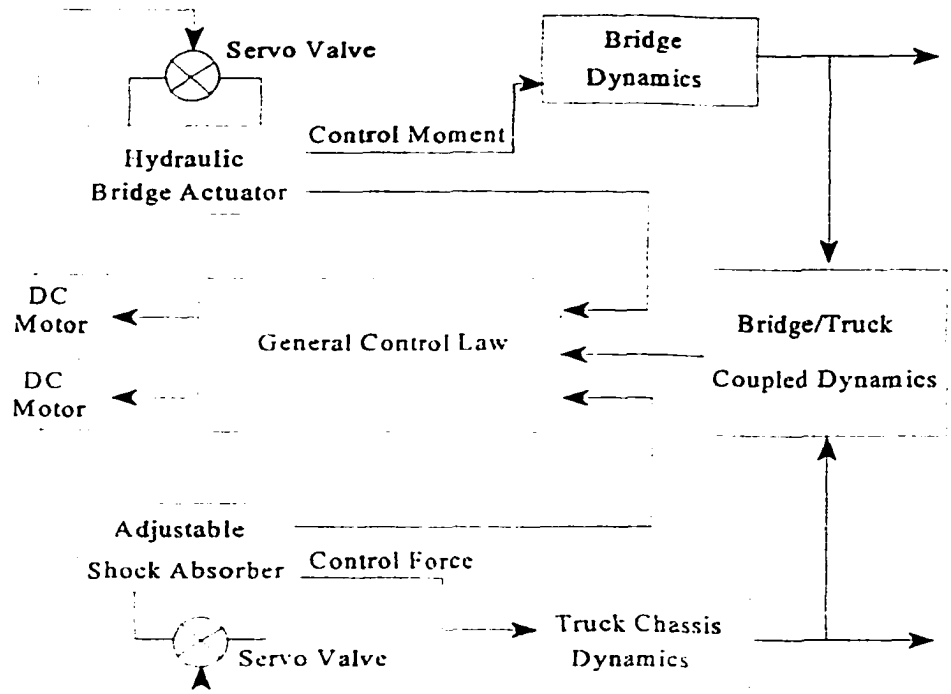

Figure 7.2 Block diagram of global bridge /truck control

7.3 Simulation Results

The expected performance of the IVBS design is portrayed first by simulating the response of a four span five girder bridge when a quarter vehicle passes over it at a constant speed (105 km hr). The FEM (56 DOF continuous girder) of the bridge and the quarter vehicle model are modeled as the same feature as in a previous chapter (Chapter Four). In the first control scheme, only the vehicle is equipped with automatically-adjustable suspension. The second control scheme includes the application of both the ISB and the truck's suspension. The objective of the control is to minimize the response vibration of the bridge

7.3.1 Bridge-Friendly Truck Suspension (BFTS)

The control scheme is defined as "local truck chassis control," which assumes that only the physical states of the chassis can be measured. The control design is based therefore on the dynamics of the truck and the control actuator mounted on the truck. The parameters of the semiactive actuator for the vehicle suspension are listed in Appendix III. The control gains are selected to minimize the variation of the tire force for its static value. The motion of the bridge is treated as an exogenous disturbance.

The response at the midpoint of the third span of the bridge at the bottom flange of the girder is shown in Figure 7.3. The first trace (blue line) in the figure depicts the response of the open loop of the system. The red trace indicates the controlled response using local control design. A comparison between controlled and uncontrolled response indicates a 30% reduction in peak deflection and a 35% reduction of RMS deflection. Figure 7.4 provides a comparison of the moment at the same point of the girder, and indicates a 40% reduction of maximum stress range (noting that $E = 1.96 \times 10^{11}\ (N/m^2)$, $I = 0.048\ (m^4)$, $\frac{1}{2}d = 0.7\ (m)$ for the girder, and the maximum moments without control and with control are $1.56 \times 10^6\ (N.m)$ and $0.96 \times 10^6\ (N.m)$, respectively, the maximum stress is $S_{max} = \frac{M_{max}y}{I} = 2.27 \times 10^7\ N/m^2$, 1.4×10^7, refer to Chapter Four).

The tire force comparison of the quarter vehicle is shown in Figure 7.5. The first trace (blue line) in the figure depicts the response prior to the installation of the semiactive automatically-adjustable suspension. The red trace indicates the controlled response. The comparison between controlled and uncontrolled responses shows 50%

amplitude reduction of the tire force. The truck suspension control command is shown in Figure 7.6.

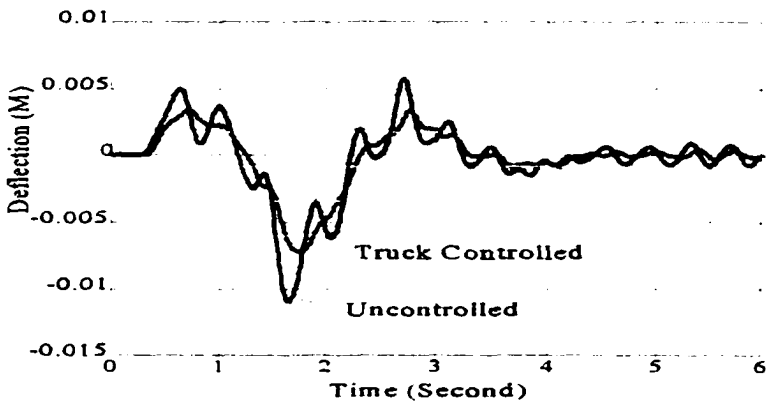

Figure 7.3 Dynamic response comparison at third span midpoint

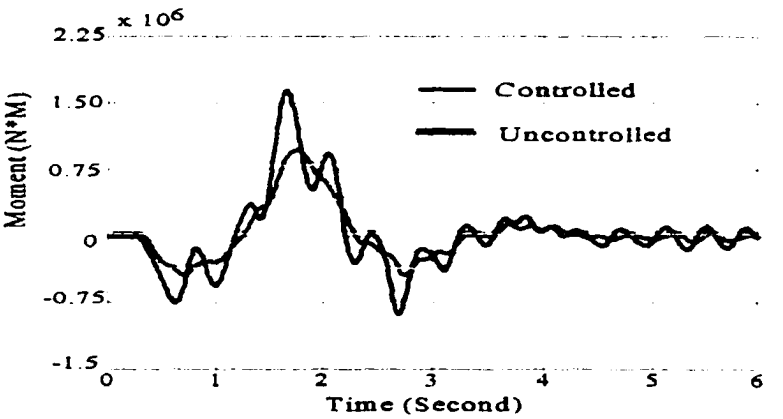

Figure 7.4 Moment time history at third span midpoint

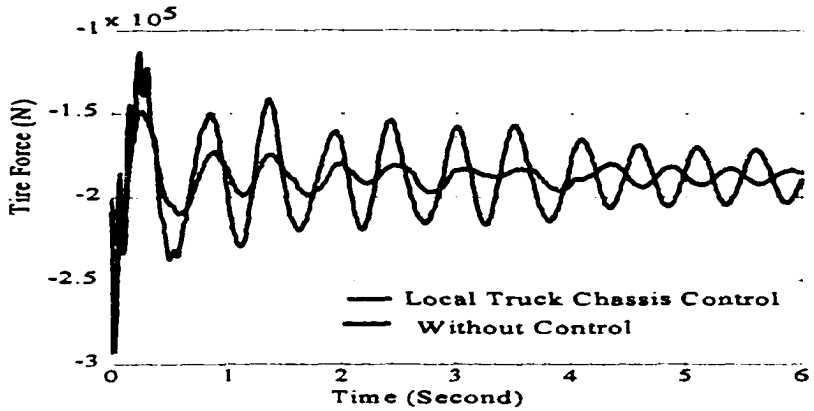

Figure 7.5 Tire force comparison: without control vs. local truck chassis control

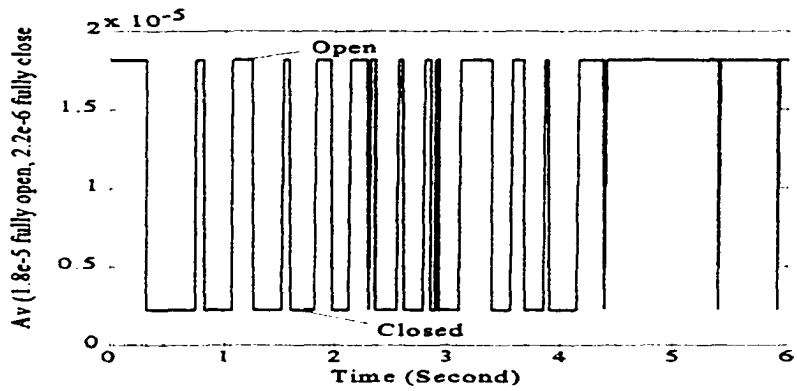

Figure 7.6 Control logic of local truck chassis controller

The second control scheme (global control) assumes that the bridge model and bridge states are available to the truck chassis computer while the truck is on the bridge. Figure 7.7 depicts a comparison between local and global truck chassis controls. The comparison indicates that the global control reduced the bridge vibration amplitude by

another 5%.

A comparison of the tire force for the local, global and no control schemes is shown in Figure 7.8. The global controller achieves 10% less tire force deviation than does the local controller.

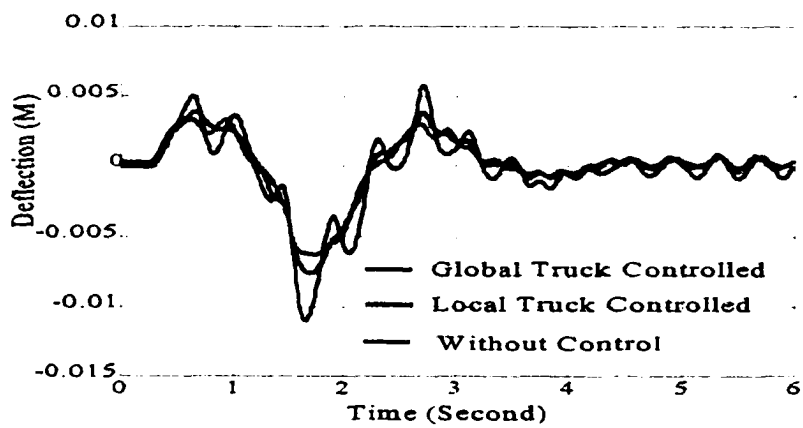

Figure 7.7 Deflection comparison between the local truck chassis control and the global truck chassis control

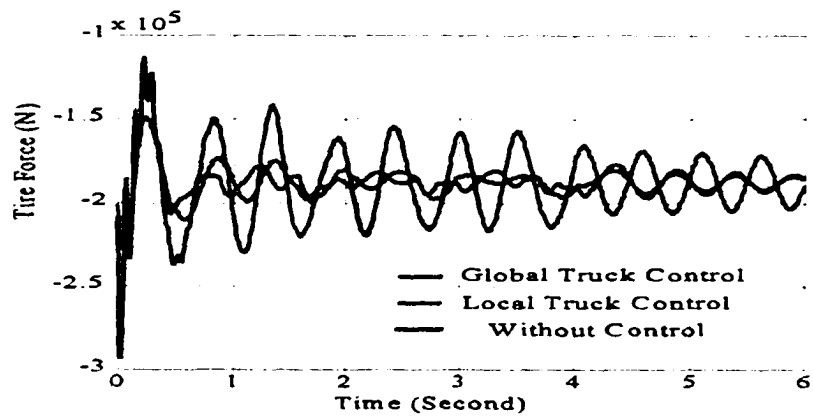

Figure 7.8 Tire force comparison a. Without Control, b. local truck chassis control, c. global truck chassis control

The differential pressure comparison of the hydraulic actuator is shown in Figure 7.9. The first trace (blue line) in the figure depicts the response of the local truck chassis control scheme. The red trace indicates the global truck chassis control scheme.

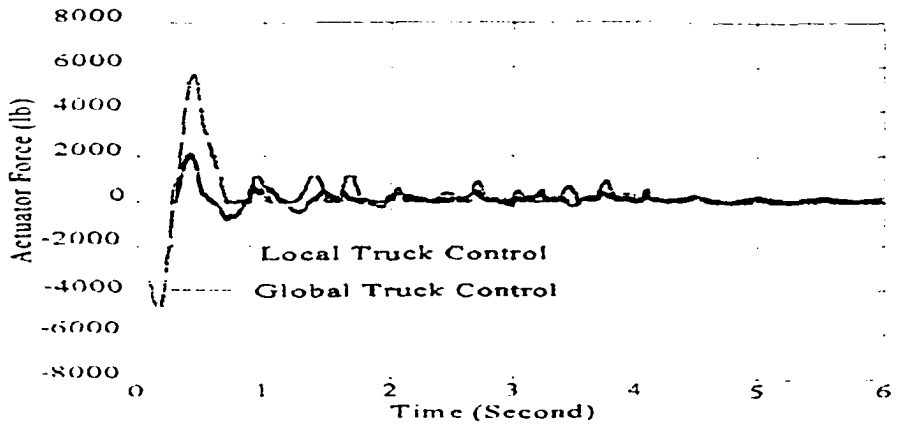

Figure 7.9 The actuator force comparison

7.3.2 Performance of the IVBS

The bridge and truck chassis actuators work together to produce a combination control performance in this case. The ISB control operates without a knowledge of the truck dynamics performance are carried out by locally control the the bridge. The responses of the midpoint of the bridge third span with and without ISB are shown in Figure 7.10. It is clearly shown that the ISB can provide about 60% deflection peak reduction compare to uncontrolled case. The performance of combined bridge/vehicle control scheme is shown in Figure 7.11. Only 4% more peak deflection is gained which assumes that the combined bridge/vehicle control does not improve the control

performance much.

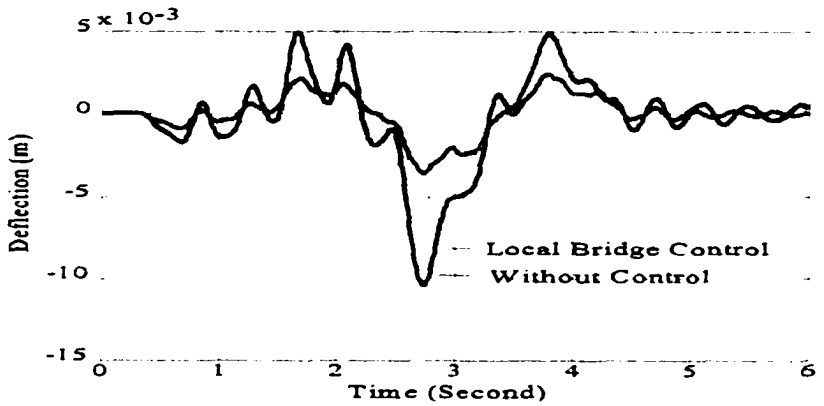

Figure 7.10 Performance Contrast of Semiactive Control, a. Without Control, b. Local Bridge Control

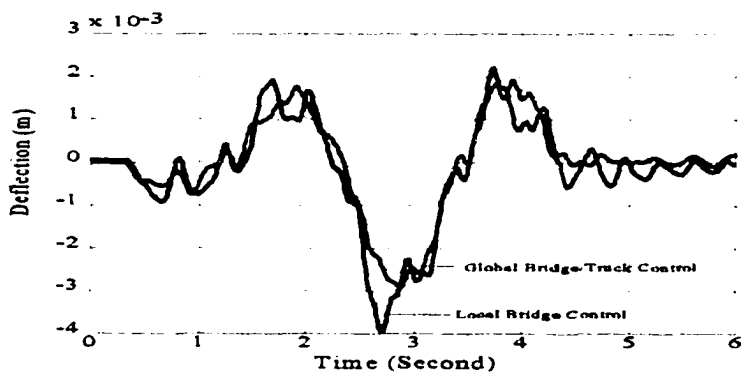

Figure 7.11 Performance Comparison of Different Semiactive Control Schemes, a. Local Bridge Control, b. Global Bridge/Truck Control

7.4 Conclusion and Recommendation

This chapter proposed a practical design method of an intelligent bridge/vehicle vibration mitigation control system. The global control algorithm was shown via simulation to be effective in reducing the vibration of a highway bridge. The study presented here indicates:

(1) The locally controlled truck suspension can reduce the bridge peak stress range by over 35%, while the dynamic impact wheel load can be reduced by 50%. The results suggest that an experiment to verify the design is warranted.

(2) The combined IVBS and ISB system produces very little additional benefit than that produced by the ISB controller

(3) Benefit of the IVBS will primarily effect those bridges not equipped with the ISB system. On the other hand, the most effective means of the extending the service life of a bridge is the ISB system.

CHAPTER EIGHT

CONCLUSIONS AND RECOMMENDATIONS

8.1 Conclusions

This dissertation has described methods for analysis, design and field test of a full-scale intelligent stiffener for bridges (ISB). The preliminary analysis and design method for the intelligent vehicle/bridge system (IVBS) are also included in the dissertation. The dissertation first introduced modal analysis, modal modification techniques which were used to conduct a high fidelity bridge model for dynamic analysis and control design. Then, the dissertation presented a tutorial on the methods used to design a semiactive vibration absorber (ISB) for application to bridges. A Lyapunov analysis was utilized to discover a feedback control rule. Field tests were conducted with several multi-axle trucks with calibrated loads. Open loop testing (without control) indicated that almost all the heavily-laden trucks produce impact levels in excess of the static load. The large impacts result from the fact that truck chassis vibrations couple strongly with bridge modal vibrations. Closed- loop testing confirmed the effectiveness of the ISB design. The semiactive system can typically reduce maximum stresses of the most heavily loaded girders by over 50%, producing a significant increase in the expected safe life of a bridge, adding at a minimum 50 years of additional life to the bridge. The work also demonstrated that the control logic is extremely simple and fairly safe, and that

the semiactive control system is demonstrated to be low cost and high performance.

The dissertation first introduced the modal reduction and modal test techniques. A quasi-static modal modification method was developed and applied to correct the analytical model of the Walnut Creek Bridge. An accurate and reduced order model was developed for bridge/vehicle dynamic analysis and control design purposes.

A bridge/vehicle coupled model was proposed. The model includes the coupling effect between the bridge and vehicle. The bridge/vehicle coupled model, which is nonautonomous, was then used to simulate the open loop response of the system. The comparison between simulation and test results indicated that the error between simulation and real test data is smaller than 5%, which assumes that the proposed coupling model can exactly predict the dynamic behavior of the bridge/vehicle interaction. The vehicle model represents the largest class of heavy truck suspension that often exhibits modal frequencies that are similar to the fundamental modes of many highway bridges. The near resonance between the vehicle and bridge result in large dynamic loads. These conclusion was then verified by field test results.

A Lyapunov analysis was utilized to determine a control law that regulates the service valve orifice between the fully open and fully closed positions. The effectiveness of the design and analysis were validated (via simulation and field test) by different types of trucks passing over the bridge. The simulation and field test results both show that the ISB system achieved a more than 50% reduction in deflection and stress under heavy traffic loads. The application of the design to a highway bridge could conceivably extend

the service life of a bridge by many years. According to the traditional calculation of the fatigue life of a bridge, an ISB system increases remain safe life of the bridge twice as much to a bridge with a passive damper. Furthermore, the control performance can be improved by tuning the control weighting matrix.

The robustness of the semiactive control system has been investigated to reject the modal uncertainties. The stability of the semiactive control system is guaranteed by Lyapunov stability theorem. The internal stability of a time-varying bridge/vehicle coupled system can be verified by modified frozen-coefficient method. The simulation study shows the modal uncertainties do not affect the performance of semiactive control system. The bistate control law which was based on Lyapunov stability theorem, was proved to work well.

The ISB system was field tested on an in-service interstate bridge. The field tests of the Walnut Creek Bridge was conducted to validate the hardware and control logic as well, and the dynamic model of the bridge vehicle coupled system. The system provides expected levels of control performance.

The dissertation also address the robustness of controlled bridge vehicle system to validate in truck fundamental frequencies and traveling speed.

The preliminary design and analysis of IVBS has been done to explore the feasibility of the smart truck suspension component of the intelligent bridge system we propose. The semiactive suspension control law based on Lyapunov bistate control algorithm which was applied in ISB system was involved in simulation study. A

preliminary analysis suggests that it is possible to reduce the deflection of the bridge approximately 35% when a truck is outfitted with controllable semiactive shock absorbers that are keyed to operate to avoid the resonance of the bridge. The 25% reduction of the peak stress range translates into a useful safe life extension of 25 years (mean life is extended over 50 years). The results do not support an increase in maximum truck weights.

8.2 Recommendations

Future work should explore a new design that will make it possible to use less sensors in the control algorithm. Thus, it is necessary to study the input-output model and estimator in future experiments. The system delay is another major factor that affect the performance of the semiactive control system. Future works need a in-depth study feedfoward or prediction control which will eliminate the disadvantage of system delay. The future work should also include a "tuck up" design of the ISB system, which is more challenging than the existing system. The new design will eliminate the moment arms, which will reduce the possibility of having floating debris damage the ISB assembly. The prototype design and effectness of the IVBS has been verified by numerical simulation. The simulation results indicated that the IVBS can dramatically increase the service life of heavy bridges. The prototype design of a IVBS system must be tested. The tests should be conducted by retrofitting heavy trucks with semiactive actuators. The semiactive controller must communicate with the bridge in order to achieve best performance. A

prediction or feedfoward control algorithm should be included to estimate the bridge response.

REFERENCES

[1] Housner, G. W., Bergman, L. A., Caughey, T. K., Chassiakos, A. G., Clus, R. O., Masri, S. F., Skelton, R. E., Soong, T. T., Spencer, B. F., and Yao, J. T. P. (1996). "Structure Control: Past, Present, and Future," *Journal of Engineering Mechanics*, 123, Special Issue #9, p 927.

[2] Kobori, T. (1996). "Future Direction on Research and Development of Seismic-Response-Controlled Structure," *Proc., First World Conf. on Struct. Control*, 19-31.

[3] Jeffcott, H. H. (1929). "On the Vibration of Beam under the Action of Moving Loads," *Philosophy Magazine*, 7(8), p 66

[4] Biggs, J. H., Suer, M. S., and Louw, J. M. (1955). "Vibration of Simple-Span Highway Bridge," *Transaction ASCE*, 124, pp 291-318

[5] Veletsos, A. S., and Huang, T. (1970). "Analysis of Dynamic Response of Highway Bridge," *Journal of Engineering Mechanics*, ASCE, 107(1), pp 229-246.

[6] Timoshenko, S. P., Young, D. H., and Weaver, W. (1974). " Vibration Problems in Engineering," 4th ed., John Wiley and Sons, Inc., New York, N. Y., 1974, pp 448-453.

[7] Chung, Y. T. and Genin, J. (1978). "Stability of a Vehicle on a Multispan Simply Supported Guideway," *Journal of Dynamic Systems, Measurement, and Control*, Dec., Vol 100, pp 326-332

[8] Schilling, C. G. (1984). " Stress Cycles for Fatigue Design of Steel Bridges," *Journal of Structural Engineering*, ASCE, Vol 110, pp 1222-1234.

[9] Hwang, R. C., and Nowak, R. C. (1991). " Simulation of Dynamic Load for

Bridges," *Journal of Structural Engineering*, ASCE, 117, pp 1413-1434.

[10] Kou, R. C., and Dewolf, R. C. (1997). " Vibrational Behavior of Continuous Span Highway Bridge-Influencing Variables," *Journal of Structural Engineering*, ASCE, 123, No.3, pp 333-344.

[11] Velestsos, A. S., and Huang, T. (1994). "Analysis of Dynamic Response of Highway Bridge," *Journal of Engineering Mechanics*, ASCE, 107(1), pp 229-246.

[12] Tiedeman, R. C., Albrecht, P., and Cayes, L. R. (1993). "Behavior of Two-Span Continuous Bridge under Truck Axle Loading," *Journal of Structural Engineering*, ASCE, 119, No.4, pp 1234-1250.

[13] Yang, F., and Fonder, G. A. (1996). " An Iterative Solution Method for Dynamic Response of Bridge-Vehicle Systems," *Journal of Earthquake Engineering and Structural Dynamics*, Mar. Vol. 25, pp 195-215.

[14] Senthilvasan, J., Brameld, R. C. and Thambiratnam, D. C. (1997). "Bridge-Vehicle Interaction in Curved Box Girder Bridges," *Journal of Microcomputers in Civil Engineering*, 12, pp 171-181.

[15] Yao, J. T. P. (1972). "Concept of Structural Control," *Journal of the Structural Divison*, ASCE, 98(7), pp 1567-1574.

[16] Yang, J. N., and Giannopoulos, F. (1978). "Dynamic Analysis and Active Control of Two Stayed-Cable Bridges," *Technical Report* No 2, NSF Grant No. ENG-76-2387, School of Engineering and Applied Science, George Washington University, Washington, D.C., Feb.

[17] Yang, J. N., and Giannopoulos, F. (1979). "Active Tendon Control of Slender Structure," *Journal of Engineering Mechanics Division*, ASCE, 104(EM3), Proceedings Paper 13836, pp 551-568.

[18] Achkire, Y. and Preumont, A. (1996). "Active Tendon Control of Cable-Stayed Bridges," *Earthquake Engineering and Structural Dynamics*, 25, pp 587-597.

[19] Adeli, H. and Saleh, A. (1997). "Optimal Control of Adaptive / Smart Bridge Structure," *Journal of Structure Engineering*, Feb., pp 330-351.

[20] Abdel-Roman, M., Quintin, V. H., and Leipholtz, H. H. (1980). "Optimal Control of Civil Engineering Structures," *Journal of Engineering Mechanics Division*, Proceedings of ASCE, 106(EM1), pp 57-73.

[21] Lin, Y. H., and Trethewey, M. W. (1993). "Active Vibration Suppression of Beam Structures Subjected to Moving Loads. A Feasibility Study Using Finite Elements," *Journal of Sound and Vibration*, 166(3), pp 383-395.

[22] Shelley, S. J., Aktan, A. E., and Frederick, N. (1993). "Active Vibration Control of a 250 Foot Span Steel Truss Highway Bridge," *Second IEEE Conference on Control Applications*, Vancouver, B.C., Sept., TA4, pp 34-40.

[23] Wu, Z., and Soong, T. T. (1996). " Modified Bang-Bang Control Law for Structural Control Implementation," *Journal of Engineering Mechanics*, ASCE, 122(8), pp 771-777.

[24] Das, A. K., and Dey, S. S. (1992). "Effects of Tuned Mass Dampers on Random Response of Bridges," *Journal of Computers and Structures*, Vol. 43, No. 4, pp 745-

750.

[25] Leitmann, G. (1994). "Semiactive Control for Vibration Attenuation," *Journal of Intelligent Material Systems and Structures*, 5, Nov., pp 652-670.

[26] Karnopp, D. C. and Crosby, M. J. (1973). "The Active Damper-a New Concept for Shock and Vibration Control," *43rd shock and Vibration Bulletin*, Part H, June.

[27] Soong, T. T. (1993). "Passive and Active Structure Vibration Control in Civil Engineering," New York, N.Y., Springer-Verlag.

[28] Spencer, B. F. Jr. (1995). "Experimental Verification of Acceleration Feedback Control Strategies for Seismic Protection," *Proc., Japan Soc. of Civil Engrg. 3rd Colloquium on Vibration Control of Structure*, Part A, pp 259-265.

[29] Symans, M. D., and Constantinuou, M. C. (1994). "Semiactive Fluid Viscous Dampers for Seismic Response Control,"*Proc., First World Conf. on Struct. Control*, Los Angles, CA, Aug. 3-5, FA2, pp 83-89.

[30] Feng, Q., and Shinozuka, M. (1990). "Use of a Variable Damper for Hybrid Control of Bridge Response under Earthquake," U. S. National Workshop on Structural Control Research Proceedings, October, Los Angeles, CA

[31] Hrovat, D., Barak, P., and Rabins, M. (1983). "Semiactive Versus Passive or Active Tuned Mass Dampers for Structural Control," *Journal of Engineering Mechanics*, ASCE, 109(3), pp 691-701.

[32] Hatada, T., and Smith, H. A. (1997)," Development and Application of Nonlinear Controller Using Variable Damping Devices," Proceedings of the American Control

Conference, Albuquerque, NM, June, pp 453-457.

[33] Patten, W. N., He, Q., He, J., and Hu, J. (1994a). "A New Algorithm of Semiactive Control for Suspension with Nonlinear Leaf Spring," *ASME Winter Annual Meeting*, Chicago, IL, pp 147-156.

[34] Patten, W., He, Q., Kou, C. C., Liu, L., and Sack, R. L. (1994b). "Suppression of Vehicle Induced Bridge Vibration Damper (SAVA)," *First World Conference on Structural Control*, Los Angles, CA, Aug. 3-5, FA2 pp 83-89.

[35] Patten, W., Sack, R. L., and He, Q. (1996). "A Controlled Semiactive Hydraulic Vibration Absorber for Bridges," *Journal of Structural Engineering*, ASCE. 122(2), pp 187-193.

[36] Patten, W. N., and Li, G. "Intelligent stress reduction for bridges," in review, *Journal of Engineering Mechanics*.

[37]Patten, W., Li, G., and Sun, J. "Field Test of an Intelligent Stiffener for Bridges at the I-35 Walnut Creek Bridge," in review, *Earthquake Engineering and Structural Dynamics*.

[38] Pang, J. (1996). "Experimental validation and modal analysis for a highway bridge," Ph. D. Thesis, University of Oklahoma, School of Aerospace and Mechanical Engineering, Norman, OK.

[39] Patten, W. N. (1997). " Semiactive vibration absorbers (SAVA) at the I-35 Walnut Creek Bridge," Final Report, No. 2125, FHWA, Oklahoma Department of Transportation, and the University of Oklahoma, OK.

[40] Sun, J., Pang, J., Song, G., and Patten, W. (1997). " Experimental Validation and Modal Analysis for a Highway Bridge," *ASME 199^ Design Engineering Technical Conferences*, Sept. 14-17, Sacramento, California. University of Oklahoma, DETC97/VIB-4251, 1-4 (97).

[41] Guyan, R. J. (1965). " Reduction of Stiffness and Mass Matrics." *AIAA Journal*, Vol. 3(2), pp 224-240.

[42] O' Callahan, J., (1989). " A procedure for an Improved Reduced System (IRS) Model," *7 th Intel. Model Analysis Conf.*, Las Vegas, Nevada, Feb.

[43] Pilkey, W. D. and Cohen, R. (1972). "System Identification of V Structure, Mathematical Models from Test Data." *American of Mechanical Engineers*, New York.

[44] Berman, A. (1978). "Mass Matrix Correction Using an Incomplete Set of Measured Modes." *AIAA Journal*, vol. 17, No. 10, October pp 1147-1148.

[45] Wei, F (1980). "Stiffness Matrix Correction From Incomplete Test Data," *AIAA Journal*, No.10, October, pp 1274-1275

[46] Collins, J. D., Hart, G. C (1974). "Statistical Identification of Structures," *AIAA Journal*, Vol. 12, NO.2, February, pp 185-191

[47] Snaayei, M. (1997). "Structural Model Updating Using Experimental Static Measurements," *Journal of Structural Engineering*, Vol 123, June, pp 792-798.

[48] Hajela, P., and Soeiro, F. J (1990). "Structural damge detection based on static and modal analysis." *AIAA Journal*, 28(9), pp 1147-1148

[49] Chen, J. C. (1979). "Direct Structural Parameter Identification by Modal Test

Result." *AIAA Paper*, 14(3), pp 83-0812.

[50] Zienkiewicz, O. C. (1977). "The Finite Element Method (Third Edition)," Maidenhead Berkshire, England: McGraw-Hill Book Company (UK).

[51] Patten, W. N., Mo, C. (1997). "A Primer on Design of Semiactive Vibration Absorbers (SAVA)." *Journal of Engineering Mechanics*, ASCE, 124 (1), pp 61-68.

[52] Dulay, I. K., Fureze, F., Harkey, G. and Lukacs, J. (1988). "Fundamentals of Hydraulic Power Transmission," *Studies in Mechanical Engineering*, 7, New York, NY: Elsevier Science.

[53] Mohler, R. R. (1991). "Nonlinear Systems," Englewood Cliffs, New Jersey: Prentice-Hall, Inc.

[54] Patten, W. N., and Sack, R. L. (1993). "Smiactive Hydraulic Structural Control." *Proceedings, International Work Shop on Structural Control*, Ed. G. W. Honsner and S. F. Marsi, Honolulu, Hawaii, August.

[55] Richardson H. H., and Wormley, D. N. (1974). "Transportation Vehicle/Beam-Elevated Guideway Dynamic Interactions A State-of-the-Art Review," *Journal of dynamic systems, measurement, and control*, June, pp 169-179.

[56] Kalman, R. (1960). "Control System Analysis and Design Via the "Second Method" of Lyapunov," *ASME Journal of Basic Engineering*, June, page 371~393.

[57] Leitmann, G. (1979). "Guaranteed Asymptotic Stability for Some Linear Systems with Bounded Uncertainties," *Journal of Dynamic System, Measurement, and Control*, Vol 101, September, pp 212~216

[58] Petersen, I. R. (1987). "A Stabilization Algorithm for a Class of Uncertain System," *Systems and Control Letters*, Vol. 8, pp 351–357.

[59] Barmish, B. R. (1988). "Necessary and Sufficient Conditions for Quadratic Stabilizability of an Uncertain System", *Journal of Optimization Theory and Applications*, Vol. 46, No. 4, August, pp 1023-1038.

[60] Slotine, J. E. (1991). "Applied Nonlinear Control." Englewood Cliffs, New Jersey 07632, Prentice-Hall, Inc.

[61] Brogan, W. L. (1991). "Modern Control Theory." Upper Saddle River, New Jersey 07485, Prentice-Hall, Inc.

[62]Green, R. J. (1995). "Dynamic Response of Highway Bridges to Heavy Vehicle Loads: Theory and Experimental Validation." *Journal of Sound and Vibration*, Vol. 170(1), pp 51-78.

[63] Heywood, R. J. (1995). "Short-Span Bridge Friendly Suspensions-Research Element 6 of The OECD DIVINE Project." Queensland University of Technology, Australia.

Appendix I Parameters of a Typetcal Quarter Vehicle Model

Symbols	Unit	Value
m_1	kg	4600
m_2	kg	19560
ω_1	Hz	2.12
ω_2	Hz	10.25
K_1	N/m	6330000
K_2	N/m	4700000
C_1	N.sec/m	37000
C_2	N.sec/m	7000

Appendix II Parameters of the Tractor-Trailer Model (RT)

Symbols	Unit	Value	Symbos	Unit	Value
m_1	kg	250	K_6	N/m	1.58e+6
m_2	kg	544	K_7	N/m	1.58e+6
m_3	kg	500	K_8	N/m	3.15e+6
m_4	kg	794	C_1	N/sec/m	6.13e+3
J_{G5}	kg m^2	5.26e+3	C_2	N/sec/m	8.75e+3
J_{G6}	kg m^2	6.3e+4	C_3	N/sec/m	8.75e+3
K_1	N/m	2.63e+5	C_4	N/sec/m	1.75e+3
K_2	N/m	3.68e+5	C_5	N/sec/m	8.75e+3
K_3	N/m	3.68e+5	C_6	N/sec/m	1.75e+3
K_4	N/m	2.36e+5	C_7	N/sec/m	1.75e+3
K_5	N/m	7.88e+5	C_8	N/sec/m	3.5e+3

Appedix III Parameters for an ISB Assembly

A	0.084	m^2
E	1.96×10^{11}	N/m^2
I	0.048	m^4
W	12.2	m
h	2.54	m
A_p	4.013×10^{-2}	m^2
A_{xmax}	$1.394 \cdot 10^{-1}$	m^2
A_{xmin}	0.00	m^2
C_d	0.82 (0.52)	
ρ	$8.83 \cdot 10^{-2}$	kg/m^2
α	$1.14 \cdot 10^{11}$	N.m
β	$8.7 \cdot 10^{7}$	N.m

Appendix IV Control Program for Field Test

```
*****************************************************************
*****************   Included head files   *****************************

#include <stdio.h>
#include <stdlib.h>
#include <bios.h>
#include <dos.h>
#include <alloc.h>
#include <conio.h>
#include <string.h>
#include <ctype.h>
#include <time.h>
#include <math.h>
#include <iostream.h>
#include "c:\ad3100\ad3100.h"
#include "c:\ad3100\ad3100.inc"

*****************   Define varables   *****************************

#define NumOfPoint 2500                    * define number of sample data*/
#define Sample_Rate 250 /40000             * desine sampling rate*/
#define BASE 0x300                         * serial Port number 1 */
#define COM 0
#define DIV_LO 0x300
#define DIV_HI 0x301                       * Divisor latch LO, Hi *
#define LINE_CTRL 0x303                    * Line control register *
#define LINE_STATUS 0x305
#define RS232 0x14                    * RS-232 serial port interrupt number *
#define DATAR 0x100                   * data ready bit in status word *
#define TRUE 1

*****************   Included subprogram   *************************

void adc(float []);
void initadc1(void);
void initadc2(void);
void initadc3(void);

char receive(void);
int ready(void);
```

```
void init(void);
void send(unsigned int c);
void SaveData(void);
void mode_con(float,float,float,float,float,float,float,float,float);

unsigned int valve1_open = 0x09D;
unsigned int valve2_open = 0x05D;
unsigned int valve3_open = 0x0AD;
unsigned int valve1_close = 0x09B;
unsigned int valve2_close = 0x05B;
unsigned int valve3_close = 0x0AB;

unsigned int kp = 0x066;
unsigned int init196_num3 = 0x0A5;
unsigned int init196_num2 = 0x055;
unsigned int init196_num1 = 0x095;
int comm0=0;
int comm1=0;
int comm2=0;
float max1=0.5;
float max2=0.5;
int close1=0;
int close2=0;

**********          Define sample data  ****************************
float far ch1[NumOfPoint];
float far ch2[NumOfPoint];
float far ch3[NumOfPoint];
float far ch4[NumOfPoint];
float far ch5[NumOfPoint];
float far ch6[NumOfPoint];
float far ch7[NumOfPoint];
float far ch8[NumOfPoint];
float far ch9[NumOfPoint];
float far ch10[NumOfPoint];
float far ch11[NumOfPoint];
float far ch12[NumOfPoint];
float far ch13[NumOfPoint];
float far ch14[NumOfPoint];
float far ch15[NumOfPoint];
float far ch16[NumOfPoint];
float far ch17[NumOfPoint];
```

```
float far ch18[NumOfPoint] ;
float far ch19[NumOfPoint] ;
float far ch20[NumOfPoint] ;
float far ch21[NumOfPoint] ;
float far ch22[NumOfPoint] ;
float far ch23[NumOfPoint] ;
float far ch24[NumOfPoint] ;
float far ch25[NumOfPoint] ;
float far ch26[NumOfPoint] ;
float far ch27[NumOfPoint] ;

****************** Main Program ******************************
void main(void)
{
        long int i,j,k,l,m;
        float start,end,time;
        float x[8];
        float z[24]={0.0,0.0,0.0,0.0,0.0,0.0,0.0,0.0,0.0,0.0,0.0,0.0,
                     0,0.0,0.0,0.0,0.0,0.0,0.0,0.0,0.0,0.0,0.0,0.0};
        float y[24];

        init();                         /* initilize serial port *
        initadc1();                     /* initilize No 1 AD3100 *
        delay(5);
        initadc2();                     /* initilize No 2 AD3100 */
        delay(5);
        initadc3();                     * initilize No 3 AD3100) *
        delay(5);

        clrscr();

        for(i=0;i<100;i++)    /* initilize signal offeset *
        {
        SetBoardParameters(512, 20.0);
        adc(x);
                z[0]=z[0]+x[0];
                z[1]=z[1]+x[1];
                z[2]=z[2]+x[2];
                z[3]=z[3]+x[3];
                z[4]=z[4]+x[4];
                z[5]=z[5]+x[5];
                z[6]=z[6]+x[6];
```

```
            z[7]=z[7]+x[7];
  SetBoardParameters(640, 20.0);
  adc(x);
            z[8]=z[8]+x[0];
            z[9]=z[9]+x[1];
            z[10]=z[10]+x[2];
            z[11]=z[11]+x[3];
            z[12]=z[12]+x[4];
            z[13]=z[13]+x[5];
            z[14]=z[14]+x[6];
            z[15]=z[15]+x[7];

 SetBoardParameters(800, 20.0);
  adc(x);
            z[16]=z[16]+x[0];
            z[17]=z[17]+x[1];
            z[18]=z[18]+x[2];
            z[19]=z[19]+x[3];
            z[20]=z[20]+x[4];
            z[21]=z[21]+x[5];
            z[22]=z[22]+x[6];
            z[23]=z[23]+x[7];

            }
  for(k=0; k<24; k++)
  {z[k]=z[k]/100.0;}


  gotoxy(5, 5);                          /* print the data in volts */
  printf("%7.4f %7.4f %7.4f %7.4f %7.4f %7.4f %7.4f %7.4f
 %7.4f\n",z[0],z[1],z[2],z[3],z[4],z[5],z[6],z[7],z[8]);

  printf("Are you ready to run?:\n");
 printf("Enter any key:");

 getchar();
 clrscr();
 gotoxy(15,10);
 printf("Sampling... Sampling... Sampling...\n");
 start_clock();

******************  Control Process Circle  **************************
```

```
for(i=1; i <= NumOfPoint;i++)
{
        while (ClockDone(2,2) == 0) {}
SetBoardParameters(512, 20.0);  /* set first AD board adress */
adc(x);                                 /*sampling data */
        ch1[i]=-(x[0]-z[0]);
        ch2[i]=-(x[1]-z[1]);
        ch3[i]=x[2]-z[2];
        ch4[i]=-(x[3]-z[3]);
        ch5[i]=-(x[4]-z[4]);
        ch6[i]=-(x[5]-z[5]);
        ch7[i]=(x[6]-z[6]);
        ch8[i]=-(x[7]-z[7]);


SetBoardParameters(640, 20.0);  /* set second AD board adress */
adc(x);                                 /*sampling data */

        ch10[i]=x[0]-z[8];
        ch11[i]=x[1]-z[9];
        ch12[i]=x[2]-z[10];
        ch13[i]=-(x[3]-z[11]);
        ch22[i]=-(x[4]-z[12]);
        ch23[i]=x[5]-z[13];
        ch24[i]=x[6]-z[14];
        ch9[i]=x[7]-z[15];

SetBoardParameters(800, 20.0);  /* set third AD board adress */
adc(x);                                 /*sampling data */

        ch14[i]=x[0]-z[16];
        ch15[i]=-(x[1]-z[17]);
        ch16[i]=x[2]-z[18];
        ch17[i]=-(x[3]-z[19]);
        ch18[i]=x[4]-z[20];
        ch19[i]=-(x[5]-z[21]);
        ch20[i]=-(x[6]-z[22]);
        ch21[i]=x[7]-z[23];
 *Call Control logic Subrountine */
mode_con(ch1[i],ch2[i],ch3[i],ch4[i],ch5[i],ch6[i],ch7[i],ch8[i],ch13[i]);

        ch22[i]=comm0;
```

```
                ch23[i]=comm1;
                ch24[i]=comm2;
        while (ClockDone(2,2) == 1) {}
        }
                end=clock();
                time = (end-start)/CLK_TCK;
                clrscr();
                printf("\n\t Time taken = %f ",time);   * end control process *
                send(valve2_open);
                delay(2);
                send(valve1_open);
                delay(2);
                send(valve3_open);
                delay(2);
                SaveData();                     /* print data to output file *

 }

 void init()
 {   outp(LINE_CTRL,0x80);
        outp(DIV_LO, 0x03);     //Baud rate approx 38K.
        outp(DIV_HI, 0x00);
        outp(LINE_CTRL,0x03);
 }

/* send character to the serial port *
 void send(unsigned int ch)
 {
        outp(LINE_CTRL, 0x03);          * Enable Port1 to transmitt *
        outp(BASE, ch);
 }

/* get the serial port ready status *
 ready()
 {
        return (inp(LINE_STATUS));
 }

/* get character from the serial port *
        char receive()
 {      char ch;
        outp(LINE_CTRL, 0x03);          * Enable Port1 to transmitt *
```

```
    ch=inp(BASE);
    return(ch);
}

void initadc1(void)                    /* initialize first AD board */
{
SetBoardParameters(512, 20.0);
SetUserClock(Sample_Rate);
ClearBoard();
ClearFiFo();
SetPacerClock(200000L);
SetGain(1);
SetTriggerType(MULTI_INT_TRIG);
SetBurstChannels(8);
SetScanType(BURST);
SetChannel(0);
}
void initadc2(void)                    /* initialize second AD board */
{
 SetBoardParameters(640, 20.0);
 SetUserClock(Sample_Rate);
 ClearBoard();
 ClearFiFo();
 SetPacerClock(200000L);
 SetGain(1);
 SetTriggerType(MULTI_INT_TRIG);
 SetBurstChannels(8);
 SetScanType(BURST);
 SetChannel(0);
}

void initadc3(void)                    * initialize third AD board *
{
SetBoardParameters(800, 20.0);
SetUserClock(Sample_Rate);
ClearBoard();
ClearFiFo();
SetPacerClock(200000L);
SetGain(1);
SetTriggerType(MULTI_INT_TRIG);
SetBurstChannels(8);
SetScanType(BURST);
```

```
        SetChannel(0);
}

/******************  Control Algorithm  ****************************/
******************  Control command  ****************************
void mode_con(float p1,float p2,float l1,float p3,float p4,float l2,float p5,float
                    p6,float l3)
  {
       int jj;
       float det[3];
       float door[3];
       float rator[3];
      for (jj=0; jj<3; jj++)
       {       det[jj]=0.0;
       }
              det[0]=(p1-p2)*l1;
              det[1]=(p3-p4)*l2;
              det[2]=(p5-p6)*l3;
              if(l1 <= -0.02 || rator[0] == 1.0){
               send(valve2_close);
               rator[0] = 1.0;}
              else {
                  send(valve2_open);
                  }
               delay(1);

              if(l1 >= -0.02 && rator[0] == 1.0){
                  send(valve1_close);}
              else {
                  send(valve1_open);
                  }
                delay(1);
              if(l3 >= -0.02 && rator[1] == 1.0){
                  send(valve3_close);
                  rator[1] = 1.0;}
                else {
                  send(valve3_open);
                  }
                delay(1);
}
```

```
void adc(float x[8])
 {
        int channel,l;
        float t;
                for(l=0; l<8; l++)
                {x[l]=0.0;}
       StartConversion();
       while (BurstDone( ) == 0);
       while (DataInFiFo( ) == 1)
          {
              for(channel = 0 ; channel< 8 ; channel++)
                {
                 x[channel]=DigitalToReal(ReadFiFo( ));
                }
          }
 }
******************  Print data to file  ***************************
void SaveData(void)
{
int k;
FILE *outpf;
char buffer[16],*fname;
buffer[0] = 14;
printf("\n\n\tEnter output filename : ");
fname = cgets(buffer);
if((outpf = fopen(fname,"w"))==NULL)
        {
        printf("\n\n\tCannot open file.\n");
        exit(1);
        }
printf("\n\n\tWriting data to filename : %s", fname);
for(k=0;k<NumOfPoint;k++)
         {
        fprintf(outpf,"%f %f %f %
```

Appendix V Field Test Results

Test Trucks	Sensors (Strain Gauges) And Truck Location					
	E2 Left Lane	E2 Right Lane	C2 Left Lane	C2 Right Lane	W2 Left Lane	W2 Right Lane
WaterTruck(26k) A. without control B. with ISB	555 (430)	1500 (730)	790 (620)	1434 (1044)	1348 (1010)	700 (580)
Dump Truck(55k) A. without control B. with ISB	2280 (1800)	3000 (1497)	2350 (1850)	3283 (2450)	3395 (2610)	1930 (1600)
Rock Truck(80k) A. without control B. with ISB	1378 (810)	3000 (1509)	2237 (1560)	3431 (2400)	3187 (2028)	1960 (1505)
HeavyTruck(120 k) A. without control B. with ISB	not tested	3506 (1504)	not tested	4585 (3350)	not tested	1853 (1280)

IMAGE EVALUATION TEST TARGET (QA-3)

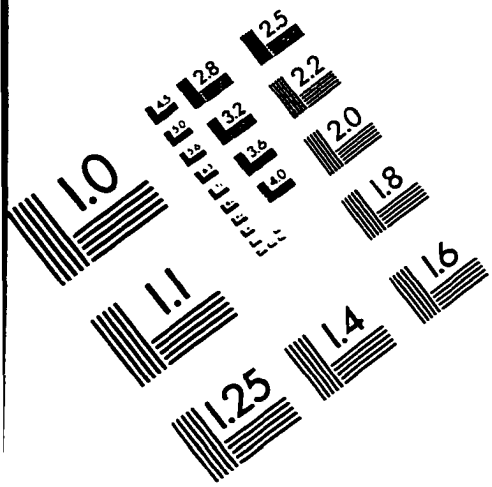

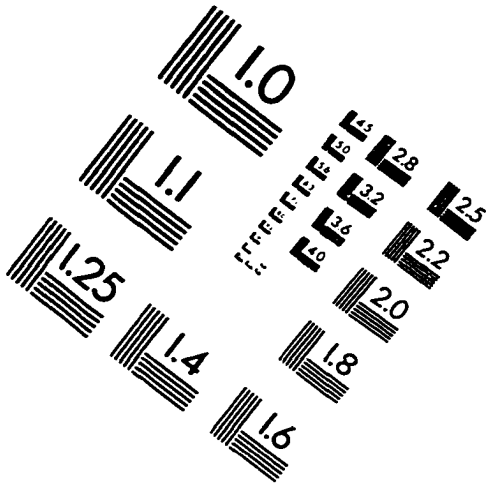

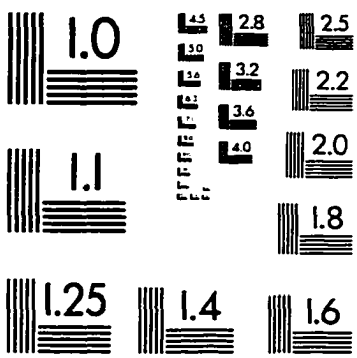

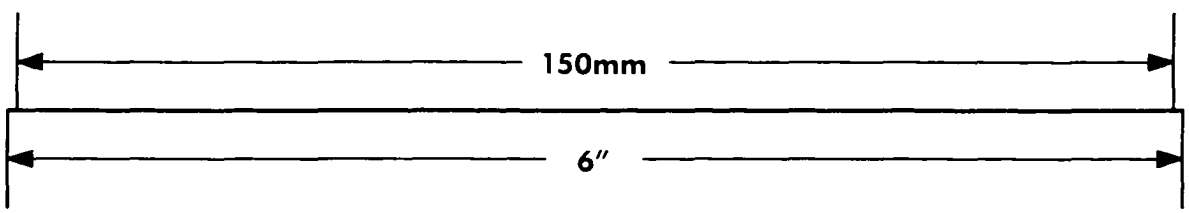

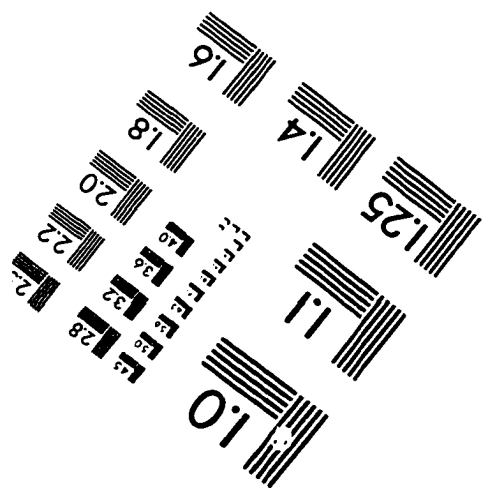

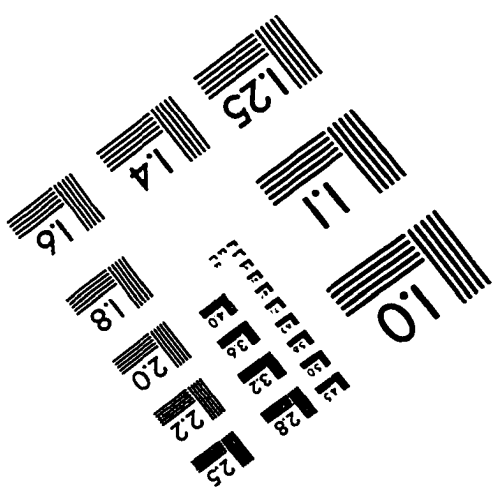

APPLIED IMAGE, Inc
1653 East Main Street
Rochester, NY 14609 USA
Phone: 716/482-0300
Fax: 716/288-5989

© 1993, Applied Image, Inc., All Rights Reserved